

UCLA

UCLA Electronic Theses and Dissertations

Title

High-Performance Water Filtration Membranes using Surface Modification and New Materials

Permalink

<https://escholarship.org/uc/item/072373wv>

Author

Huang, Xinwei

Publication Date

2016

Peer reviewed|Thesis/dissertation

UNIVERSITY OF CALIFORNIA

Los Angeles

High-Performance Water Filtration Membranes using
Surface Modification and New Materials

A dissertation submitted in partial satisfaction of the
requirements for the degree of Doctor of Philosophy
in Chemistry

by

Xinwei Huang

2016

ABSTRACT OF THE DISSERTATION

Los Angeles

High-Performance Water Filtration Membranes using Surface Modification and New Materials

by

Xinwei Huang

Doctor of Philosophy in Chemistry

University of California, Los Angeles, 2016

Professor Richard B. Kaner, Chair

Water scarcity is one of the most critical challenges faced by mankind and it is only getting worse due to source pollution and rising population. There is critical need for the development of water filtration membranes in order to treat polluted water and turn water from non-potable sources such as waste water and ocean water into freshwater for human consumption and agricultural irrigation. Filtration Membranes are generally classified into four categories: microfiltration (MF), ultrafiltration (UF), nanofiltration (NF) and reverse osmosis (RO), with decreasing pore size for rejecting different sized substances. Commercial filtration membranes are able to provide decent flux and rejection for their targeted applications. However, most of them suffer from fouling issues when the microorganisms and organic matter such as proteins and polysaccharides

in the water source deposit onto the membrane surface, impeding the permeation of water and lowering the flux. Therefore, it is of high demand to develop membranes that are anti-fouling. Foulants such as protein particles adhere to the membrane surface via hydrophobic interactions. In order to minimize such effects, a typical way is to increase the hydrophilicity of the membrane by surface modification or by utilizing hydrophilic membrane materials. Foulants also tend to get trapped in the open “pores” on a rough membrane surface with ridges and valleys. It is then expected that a smoother membrane surface tend to lessen such effects. Incorporating antimicrobial properties into the membrane is also an effective way to reduce fouling as this inhibits the growth of microorganisms on the membrane surfaces. New materials are also used to fabricate membranes with improved performance. Conducting polymers have recently been discovered as a new category of membrane-making materials that are hydrophilic and low-fouling. A new type of polyaniline derivative has been used to fabricate UF membranes that demonstrate chlorine resistance and anti-fouling properties. Nanostructured polyanilines are highly processable and possess unique properties that can be used in the membrane field as well as many other applications such as sensors, electrochromic devices, supercapacitors and antistatic coatings with enhanced performance, as described in a review section at the end of this thesis.

The dissertation of Xinwei Huang is approved

Xiangfeng Duan

Shaily Mahendra

Richard B. Kaner, Chair

University of California, Los Angeles

2016

This dissertation is dedicated to my parents, Yanyin Liu and Yuliang Huang
for their unconditional love.

TABLE OF CONTENTS

Chapter 1

Introduction to Water Filtration Membranes

1.1 Introduction

1.2 Membrane Materials and Fabrication

1.3 Current Drawbacks

1.4 Surface Modifications and New Materials utilization

1.5 Conclusion

1.6 References

Chapter 2

Low-Fouling Antibacterial Reverse Osmosis Membranes via Surface Grafting of Graphene Oxide

2.1 Introduction

2.2 Synthesis of Azide Functionalized Graphene Oxide and Characterization

2.3 Membrane Surface Modification

2.4 Results

2.5 Conclusion

2.6 References

Chapter 3

pH-Responsive Polyethersulfone Ultrafiltration Membrane with Low Bio-Fouling and Low Protein-Fouling

3.1 Introduction

3.2 Synthesis of Azide Functionalized Tetraaniline and Characterization

3.3 Membrane Surface Modification

3.4 Results

3.5 Conclusion

3.6 References

Chapter 4

Novel Chlorine Resistant Low-fouling Ultrafiltration Membrane Based on a Hydrophilic Polyaniline Derivative

4.1 Introduction

4.2 N-substituted Polyaniline

4.3 Membrane Fabrication

4.4 Chlorine Tolerance comparison

4.5 Degradation Mechanism

4.6 Antifouling properties

4.7 Conclusion

4.8 References

Chapter 5

Polyaniline Nanofibers: Broadening Applications for Conducting Polymers

5.1 Introduction

5.2 Sensors

5.2.1 Gas Vapor Sensors

5.2.2 Biological Sensors

5.3 Printable Electronics

5.4 Electro-Optical Applications

5.4.1 Electrochromics

5.4.2 Photovoltaics

5.5 Actuators

5.6 Supercapacitors

5.7 Protective Applications

5.7.1 Electrostatic Dissipation

5.7.2 Electromagnetic Interference (EMI) Shielding

5.8 Inorganic Nanocomposite Applications

5.9 Other Applications

5.9.1 Corrosion protection

5.9.2 Biocomposites

5.9.3 Filtration Membranes

5.10 References

LIST OF FIGURES

Chapter 1

Introduction to Water Filtration Membranes

Figure 1.1 Chemical structures of common MF and UF membrane materials.

Figure 1.2 Cross-sectional SEM images of UF membranes showing the typical asymmetric morphology with dense top layer on porous support layer.

Figure 1.3 Schematic illustration for the synthesis of polyamide for NF/RO applications.

Figure 1.4 Chemical structure for perfluorophenyl azide (X=halogen, OR or NR)

Figure 1.5 Schematic diagram illustrating sodium alginate adhesion to PFPA unmodified and modified PES UF membranes.

Figure 1.6 Target PFPA-derivatives and general synthesis route.

Figure 1.7 Synthesis routes for the three PFPA compounds.

Figure 1.8 Change in contact angle for PES membranes modified using zwitterion PFPA(+/-) with different concentrations.

Figure 1.9 Microscopic images of PES membrane surface modified using different concentrations of zwitterion PFPA(+/-) solution. The BSA rejection of each membranes are also shown as comparison purpose.

Figure 1.10 Short and long term fouling study of the unmodified and modified membranes

Figure 1.11 Synthesis of SPANi from polyaniline (PANi) and it can dedoped in base to be processed into a solution.

Figure 1.12 Captive bubble contact angle images of (a) pure PS membrane; (b) 1% SPANi membrane; (c) 5% SPANi membrane and (d) 10% SPANi membrane.

Figure 1.13 Flux decline and recovery results for PS membranes containing 0, 1, 5, 10% SPANi after being exposed to BSA feed sotlution.

Chapter 2

Low-Fouling Antibacterial Reverse Osmosis Membranes via Surface Grafting of Graphene Oxide

Figure 2.1 Schematic illustration for the azidation process on graphene oxide (GO).

Figure 2.2 FT-TR spectra of GO and AGO.

Figure 2.3 AFM height analysis of AGO shows that AGO exhibits a planar morphology with an average thickness of 1.15 nm (inset).

Figure 2.4 Schematic illustration of the modification of commercial polyamide RO membrane using UV activated AGO.

Figure 2.5. After GO grafting on the polyamide RO membrane surface, (a) the water contact angle decreased from 85° to 45° and (b) the average surface roughness decreased from 44.3 nm to 29.0 nm based on a $5\ \mu\text{m} \times 5\ \mu\text{m}$ analyzed area.

Figure 2.6 Long-term BSA fouling test on the control and modified membranes showing the differences in flux decline. Inset pictures are the membranes with BSA fouling layer covering the surface at the end of the fouling test.

Figure 2.7 (top) Fluorescence and SEM images showing the percentages and condition of *E. coli* cells on membrane surfaces after contact for 24 hours; (bottom) quantitative analysis of live (blue) and dead (red) cell percentages on both membrane surfaces.

Chapter 3

PH-Responsive Polyethersulfone Ultrafiltration Membrane with Low Bio-Fouling and Low Protein-Fouling

Figure 3.1: Figure 3.1 Synthesis route for PFPA-TANi molecule.

Figure 3.2 ^{19}F -NMR spectra for the starting material, first step reaction product and final product as well as the molecular weight of the two products measured by ESI mass spectroscopy.

Figure 3.3 Modification scheme of commercial PES UF membrane using PFPA-TANi ethanol solution.

Figure 3.4 (a) Pictures of unmodified PES membrane (left), PES membrane modified with 2 mM PFPA-TANi solution (middle) and modified PES membrane doped with HCl;

(b) PFPA-TANi doping/dedoping chemistry illustration.

Figure 3.5 Contact angle images of (a) unmodified PES membrane, (b) PES membrane modified with 0.1 mM PFPA-TANi ethanol solution and (c) PES membrane modified with 2 mM PFPA-TANi ethanol solution using the captive bubble technique setup as shown in (d).

Figure 3.6 Bar and pie chart showing the live/dead bacteria density difference on the modified PES membranes and those modified using 0.1 mM and 2 mM PFPA-TANi solutions.

Figure 3.7 Cross-flow system illustration. (1. Feed tank; 2,11. Pump; 3,9. Valve; 4. Flow meter; 5,8,10. Pressure gauge; 6. Cross-flow cell; 7. Electronic balance.)

Figure 3.8 Normalized TMP change for unmodified PES membrane and 2 mM PFPA-TANi modified PES membrane during three BSA fouling stages.

Figure 3.9 Proposed mechanism for the fouling-release ability of TANi grafted PES membrane.

Figure 3.10 Zeta potential plot of TANi material at various pH.

Chapter 4

Novel Chlorine Resistant Low-fouling Ultrafiltration Membrane Based on a Hydrophilic Polyaniline Derivative

Figure 4.1 A polyamide unit with a secondary amine (a) is more susceptible to chlorine attack than that consisting of tertiary amine (b).

Figure 4.2 The polymer structures of (a) n-PANi and (b) PANi.

Figure 4.3 Polymerization scheme for n-PANi.

Figure 4.4 (a) Gelling of PANi is caused by intermolecular hydrogen bonding. (b) 4-MP inhibits PANi from gelling by taking up some of the hydrogen bonding sites.

Figure 4.5 SEM images of (a) a PANi membrane and (b) an n-PANi membrane surface at 3,000× magnification, (c) an n-PANi membrane surface at 100,000× magnification and (d) its black-white picture after conversion using Image J software. Cross-sectional images of (e) pristine PANi membrane, (f) PANi membrane after chlorine exposure, (g) pristine n-PANi membrane and (h) n-PANi membrane after chlorine exposure at 600× magnification. Surface images of (i)

pristine PANi membrane, (j) PANi membrane after chlorine exposure, (k) pristine n-PANi membrane and (l) n-PANi membrane after chlorine exposure at 600× magnification.

Figure 4.6 Photos of PANi and n-PANi membranes before and after being soaked in 250 ppm free chlorine for 2 days.

Figure 4.7 FT-IR spectra of membranes before and after being soaked in bleach containing 250 ppm free chlorine. The small peak at 875 cm^{-1} for n-PANi pristine membrane is due to the chloride counterion on doped n-PANi membrane. After n-PANi membrane is soaked in basic sodium hypochlorite solution, n-PANi is dedoped, demonstrated by the disappearance of the chloride counterion peak.

Figure 4.8 UV-Vis spectra of membranes before and after being soaked in bleach containing 250 ppm of free chlorine.

Figure 4.9 (a) NMR spectra of I. pristine PANi membrane; II. PANi membrane soaked in 250 ppm free chlorine for 2 days; III. pristine n-PANi membrane; IV. n-PANi soaked in 250 ppm free chlorine for 2 days and (b) a schematic representation of the PANi/4-MP/NMP complex formed by hydrogen bondings.

Figure 4.10 Contact angles of n-PANi and PANi membranes and their *E. coli* adhesion test microscopic images.

Figure 4.11 Flux decline and recovery results for membranes fouled by 1.5 g/L BSA solution before being washed with DI water.

Chapter 5

Polyaniline Nanofibers: Broadening Applications for Conducting Polymers

Figure 5.1 (a) Each of the five polyaniline oxidation states shown on top can be interconverted by either oxidation (removal of electrons) or reduction (addition of electrons) as indicated. (b) The undoped emeraldine base, can be doped with an acid to yield the conductive emeraldine salt structure as shown on the bottom.

Figure 5.2 The as-synthesized polyaniline with uniform nanofiber morphology (left) can be readily dispersed in water at an appropriate pH (right). Reproduced with permission from ref. 3. Copyright 2005 Royal Society of Chemistry.

Figure 5.3 A gap electrode configuration (top left) and an interdigitated electrode configuration (top right) are used to measure resistance changes. The lower image shows the configuration of a surface acoustic wave device.

Figure 5.4 A Dimatix printer (top) was used to print an image of Jimi Hendrix (bottom) using a carbon nanotube polyaniline composite ink. Reproduced with permission from ref. 5. Copyright 2007 Royal Society of Chemistry.

Figure 5.5 Image of a polyaniline nanowire film at different potential (top) and a schematic showing an integrated energy storage smart window device system. Reproduced with permission from ref. 70. Copyright 2012 Royal Society of Chemistry.

Figure 5.6 Core-shell model of polyaniline for charge storage influenced by the diffusion of dopants. Reproduced with permission from ref. 104. Copyright 2009 Elsevier Ltd.

Figure 5.7 Schematic 3D hierarchical porous polyaniline nanofiber sponge/graphene foam composite electrode (a) showing the pore size ranges for each structure, as analyzed from SEM images of (b) a graphene foam and (c) a polyaniline sponge. Reproduced with permission from ref. 115. Copyright 2016 Elsevier Ltd.

Figure 5.8 TEM images of autoreduced gold nanoparticles with (a) <1 , (b) 2, (c) 6, (d) >20 nm and (e) gold sheets grown on polyaniline nanofibers. Reproduced with permission from ref. 137. Copyright 2011 American Chemical Society.

LIST OF TABLES

Chapter 2

Low-Fouling Antibacterial Reverse Osmosis Membranes via Surface Grafting of Graphene Oxide

Table 2.1 XPS Surface Composition Analysis for AGO Powder and RO membranes

Chapter 3

PH-Responsive Polyethersulfone Ultrafiltration Membrane with Low Bio-Fouling and Low Protein-Fouling

Table 3.1 Fluorescence images and percentages of *E-coli* cells on the unmodified PES membranes and membranes modified using 0.1 mM and 2 mM PFPA-TANi solutions.

Table 3.2 Starting TMP difference after each cleaning step compared to the previous fouling stage.

Chapter 4

Novel Chlorine Resistant Low-fouling Ultrafiltration Membrane Based on a Hydrophilic Polyaniline Derivative

Table 4.1 Permeability and BSA Rejection of Membranes Before and After being Soaked in 250 ppm Free Chlorine

Table 4.2 The FT-IR Benzenoid (B) and Quinoid (Q) Peak Positions and Intensity Ratios for N-PANi Membranes

Table 4.3 The Benzenoid (B) and Quinoid (Q) Peak Positions and Ratios for N-PANi and Pure PANi Membranes

Chapter 5

Polyaniline Nanofibers: Broadening Applications for Conducting Polymers

Table 5.1 Reported Properties of Polyaniline

ACKNOWLEDGEMENTS

First, I would like to dedicate my deepest gratitude to my supervisor Richard B. Kaner. Thank you for choosing me as the CSST program summer undergraduate researcher in 2011 and later accepting my application to pursue a PhD degree in Kaner Lab. You have been such a kind, humble and understanding person and have always given full support for my research in UCLA. My appreciation also goes to Professor Eric Hoek from Civil and Environmental Engineering department who has been my collaborator throughout my entire PhD. Thank you for being a great mentor and giving me feedbacks on the problems that I encountered.

I would also need to thank the students that I have collaborated with in the various research projects that I was involved in: Jimmy Temple, Jinwen Wang, Kris Marsh, Catalina Marambio-Jones, Mavis Wong, Robert Jordan, Dukwoo Jun and above all, Brian McVerry, who has always been a great mentor and role model for me. Thank you Brian for all your wisdom words. I also really appreciate all the training and guidance from the various equipment managers in UCLA. Thank all of you for teaching me how to use SEM, AFM, ESI mass spec and so on. Many thanks to the rest of the Kaner group members as well for creating such a friendly atmosphere for me to be submerged in.

Last but certainly not least I need to thank many people that I met who has made my 4 years of living in Los Angeles fun and enjoyable. Kyle Jiang who has been my gym partner and best friend. Thank you for your unlimited humor which makes me laugh every day; Chris Norlin who has been my tennis buddy and great friend over the years; Chencai Wang and Zhongyue Yang for all the fun times at UCLA; Yufu Kuo, Angus Sun and Julian Huang for all the fun parties that you invited me to.

VITA

- 2008-2012 Bachelor of Science
 Materials Science and engineering
 Zhejiang University
 Hangzhou, China
- 2011 summer Cross-disciplinary Science and Technology program
 University of California, Los Angeles
 Los Angeles, California
- 2012-present Research Assistant
 Department of Chemistry and Biochemistry
 University of California, Los Angeles
 Los Angeles, California
- 2012-present Teaching Assistant
 Department of Chemistry and Biochemistry
 University of California, Los Angeles
 Los Angeles, California

PUBLICATIONS AND PATENT

Huang, X.; McVerry, B. T.; Marambio-Jones, C.; Wong, M. C. Y.; Hoek, E. M. V.; Kaner, R. B.; Novel Chlorine Resistant Low-fouling Ultrafiltration Membrane Based on a Hydrophilic Polyaniline Derivative, *Journal of Materials Chemistry A*, 2015, 3, 8725-8733.

Huang, X.; Marsh, K. L.; McVerry, B. T.; Hoek, E. M. V.; Kaner, R. B.; Low-Fouling Antibacterial Reverse Osmosis Membrane via Surface Anchoring of Graphene Oxide, *ACS Applied Materials & Interfaces*, 2016, 8, 14334-14338.

Baker, C. O.; **Huang, X.**; Nelson, W.; Kaner, R. B.; Polyaniline Nanofibers: Broadening Applications for Conducting Polymers, *Chemical Society Reviews*, submitted.

McVerry, B. T.; Temple, J. A. T.; **Huang, X.**; Marsh, K. L.; Hoek, E. M. V.; Kaner, R. B.; Fabrication of Low-fouling Ultrafiltration Membranes Using a Hydrophilic, Self-Doping Polyaniline Additive, *Chemistry of Materials*, 2013, 25, 3597-3602.

McVerry, B. T.; Jun, D.; Jordan, R.; **Huang, X.**; Marsh, K. L.; Hoek, E. M. V.; Kaner, R. B.; Novel Small Molecule Perfluorophenylazide Coatings for Fouling-Resistant Membrane Bioreactors, submitted.

Huang, X.; McVerry, B. T.; Hoek, E. M. V.; Mahendra, S.; Kaner, R. B.; Polyaniline-Based Chlorine Resistant Hydrophilic Filtration Membranes, International Patent Serial No. PCT/US15/024635, filed on Apr. 7th, 2015.

Chapter 1. Introduction to Water Filtration Membranes

1.1 Introduction

Filtration membrane processes are effective separation techniques with a wide variety of applications, from the food/beverage/pharmaceutical/medical industries to water purification. During operation, water constituent mixtures (source) are pumped against the active side of the membrane surface, producing permeate and retentate (the waste stream).¹ Due to the size exclusion and electrostatic repulsion effects of the membrane, different components in the feed stream pass through the membrane at different speeds. The more permeable/small species will be dominant in the permeate, while the less permeable/large particles get rejected and go into the retentate.

Four main types of pressure-driven filtration membranes exist in the current market: microfiltration (MF), ultrafiltration (UF), nanofiltration (NF) and reverse osmosis (RO). They are classified based on their distinctive pore size and ability to reject different sized matter. MF membranes have the largest pore size with an average of ~100 nm and are generally used to reject relatively large particles, sediments, algae, bacteria, etc. UF membranes are tighter. Their average pore size of ~10 nm makes them great candidates for small colloids and protein rejection. They can be used in food-processing and the pharmaceutical industry for purifying and concentrating solutions of macromolecules such as proteins, polysaccharides and drugs. They are also used for blood dialysis. NF membranes have pore sizes of only 1 nm or less and are normally positively or negatively charged, making them suitable for softening water by rejecting divalent ions such as Ca^{2+} and Mg^{2+} . RO membranes are considered nonporous and used to reject monovalent salts such as NaCl. They are used in the desalination process, which produces freshwater from

seawater as well as specific inorganic contaminants (arsenic, fluoride, nitrate, nitrite, selenium and synthetic organics) removal.

1.2 Membrane Materials and Fabrication

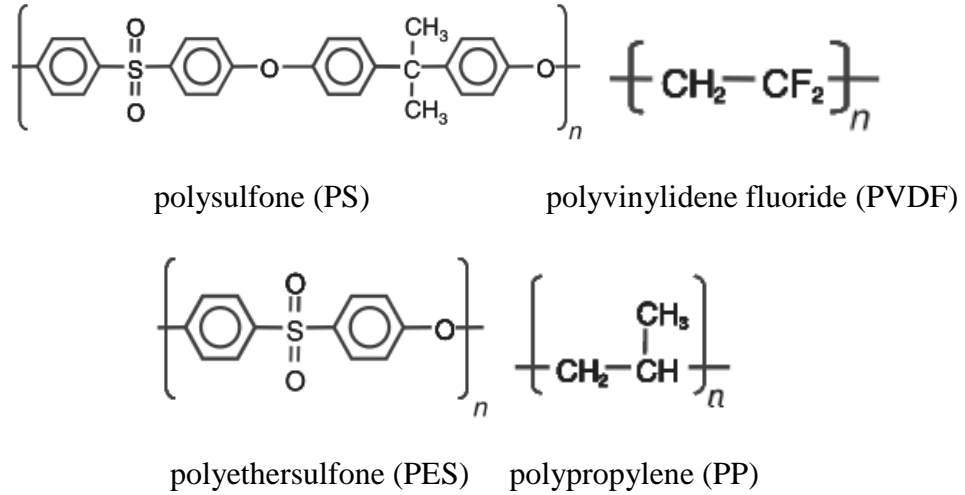


Figure 1.1 Chemical structures of common MF and UF membrane materials.

MF and UF membranes are normally made of polymers such as polysulfone (PS), polyethersulfone (PES), polyvinylidene fluoride (PVDF), polypropylene (PP). MF membranes have homogeneous morphology with consistent pore size throughout their depth. In comparison, UF membranes have an asymmetric structure with a thin dense active layer on top of a highly porous support layer (Figure 1.2). The dense active layer is effective at maintaining the desired rejection, while the porous bottom layer provides support without adding too much impedance to the permeation of water.

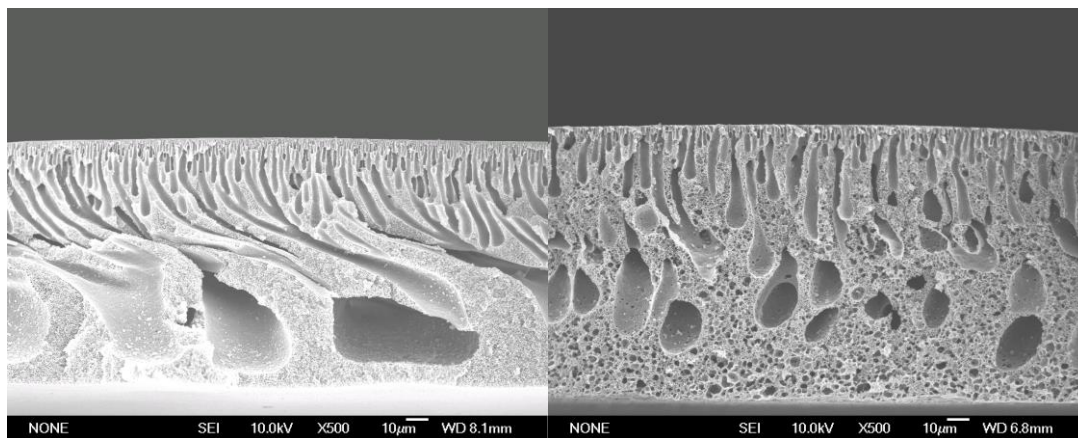


Figure 1.2 Cross-sectional SEM images of UF membranes showing the typical asymmetric morphology with a dense top layer on a porous support layer.

Such asymmetric structure is achieved via a phase-inversion method. The polymer material is dissolved in an organic solvent first to form a homogeneous casting solution before casting onto a nonwoven polyester support using a casting blade. The polymer film and support were then immersed into a non-solvent coagulation bath that is mostly water. This is where phase-inversion takes place. As the organic solvent is fully miscible with water, the organic solvent and water will diffuse into each other rapidly while the polymer precipitates out and solidifies.² Such solvent-non-solvent exchange can be directly visualized under a microscope and the polymer membrane can be formed within seconds.³

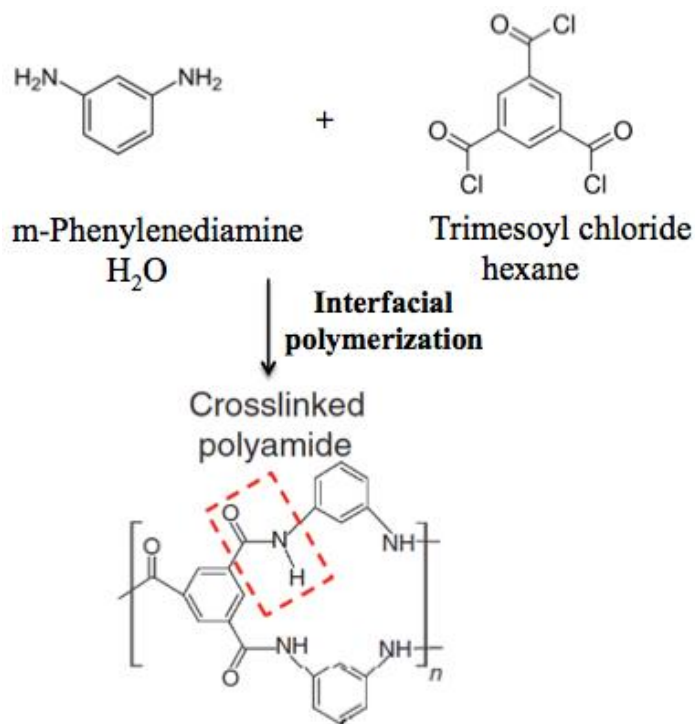


Figure 1.3 Schematic illustration for the synthesis of polyamide for NF/RO applications.

The active layer of NF and RO membranes are typically made of cross-linked polyamide (Figure 1.3) material. It is fabricated through the interfacial polymerization between two monomers, m-phenylenediamine and trimesoyl chloride on a UF membrane support. Because m-phenylenediamine dissolves in water and trimesoyl chloride dissolves in hexane, which is not miscible with water, the reaction only occurs at the interfacial layer of the two solvents, forming a thin ~100 nm active layer that is cross-linked and nonporous. This dense layer has just the right structure and chemical property to allow the permeation of water to be two orders of magnitude faster than the permeation of salts, achieving the separation of salt ions from water. The underlying UF membrane acts as a mechanic support for the thin active layer. There's no apparent distinction

between RO and NF membranes. The NF membrane can sometimes be viewed as a “loose” RO membrane for low-pressure applications.

Before the commercialization of polyamide material, cellulose acetate was mostly used for RO applications. However, cellulose acetate suffers from a series of issues that limit the potential of this material. Cellulose acetate is not tolerant to temperatures above 30°C and tends to hydrolyze when the pH is below 3 or above 8. Also, cellulose acetate is highly susceptible to biological and chlorine degradation. In comparison, polyamide materials are chemically more durable over a wide pH range from 2-12 and nearly immune to bacterial degradation. Despite the merits of polyamide materials, there are still critical issues that require attention.

1.3 Current Drawbacks

Polyamide material itself is hydrophobic. The microorganisms and natural organic matter such as proteins and polysaccharides can easily deposit onto the RO membrane surfaces via hydrophobic interactions. This will impede the permeation of water and lower the membrane flux. Moreover, interfacial polymerization produces rather rough membrane surface with ridges and valleys that can act as potential sites that trap microorganisms and protein particles. Such process in which naturally occurring matter in the feed source adheres to membrane surfaces, which then block the pores and water flow, is referred to as membrane fouling. This is the one of the most serious issues that lowers productivity and hinders the commercial scaling of filtration membranes.

Fouling is also a common problem with MF/UF membranes. Depending on the different polymer materials used to fabricate the MF/UF membranes, they will have

different fouling tendencies. PES is one of the more hydrophilic materials, while PVDF is fairly hydrophobic. Therefore, PVDF membranes generally exhibit a higher fouling propensity compared to PES membranes.

Other than fouling, chlorine susceptibility is also a big issue with commercial membranes. When a membrane gets fouled by microorganisms, the common practice in industry is to use chlorine (bleach) solution to disinfect the membrane and restore the membrane flux. Such chlorine cleaning is highly effective in recovering the reduced flux with inexpensive chemicals. On the other hand, however, chlorine is a potent oxidant and can deteriorate a variety of functional groups/chemical structures. Polyamide, for instance, is highly susceptible to chlorine.⁴ The aromatic rings bonded to the amide groups are highly electron rich and can be easily attacked by chlorine radicals. The N-H group in the amide linkages can also be converted to N-Cl group by N-halogenation. The resulting N-chloroamide then undergoes hydrolysis that causes chain scission with amine being oxidized to quinone. At the same time, the N-chloroamide can undergo intermolecular rearrangement (also called Orton rearrangement) which produces chloro-substituted benzene rings that can also hydrolyze, resulting in chain scission which leads to the failure of polyamide membranes causing decreased salt rejection after chlorine cleaning.⁵ Besides the widely recognized and studies chlorine tolerance issue for RO membranes, UF membranes also have problems when it comes to chlorine cleaning. Chlorine is shown to cause leaching out of poly(vinyl pyrrolidone), a common membrane additive for increasing membrane hydrophilicity.⁷ Chlorine cleaning of PES membranes actually cause more severe fouling afterwards and leads to polymer chain scission and loss in mechanical strength, as exhibited by deterioration of membrane integrity.⁷

1.4 Surface Modifications and New Materials Utilization

Various attempts have been carried out to fabricate chlorine resistant RO membranes using new materials. Polyamides with nitrogen atoms substituted with alkyl and aryl groups were demonstrated to have no chemical reaction with chlorine.^{8,9} However, membranes fabricated using polyamide bearing tertiary amine groups do not have comparable permeability/rejection performance. Interfacially polymerized polyimides have been reported to create chlorine resistant RO membranes.¹⁰ However, the curing of polyimides require temperatures above 200°C which will melt the polysulfone support. Although chlorine damage is a big issue in the membrane industry, very little research has successfully made an impact in fabricating chlorine resistant RO membranes that are scalable and cost-effective without compromising their intrinsic membrane performance, i.e., flux and rejection.

Most of the current research in this field has been focused on making anti-fouling membranes and there has been numerous methods, including surface modification, blending hydrophilic materials and novel material utilization which will each be described in the following discussion. Hydrophilic membranes tend to resist fouling due to the thin layer of water molecules spontaneously formed on hydrophilic membrane surfaces acting as physical barriers that prevent the attachment of foulants.

As commercial membrane materials are generally chemically inert in order to remain stable under natural water environment, they do not possess many reactive functional groups that can be used for modification. Membrane surface modification methods typically include physical adsorption such as layer-by-layer deposition as well

as covalent grafting using carbodiimide activation, radical-initiated graft polymerization, plasma activation, chemical vapor deposition and atomic layer deposition in order to attach hydrophilic polymer chains/materials onto the membrane surface. Physically adsorbed hydrophilic materials are potentially unstable and can detach at extreme pH/ionic strength in the presence of water flow shear forces. The commonly used chemically modified method involves an exotic environment with complex reaction steps that are not cost effective or scalable for industrial implementation.

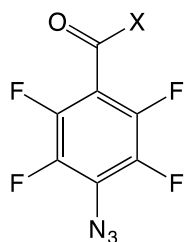


Figure 1.4 Chemical structure of perfluorophenyl azide (X = halogen, OR or NR).

As a new approach, our research group started utilizing highly versatile perfluorophenyl azide (PFPA) (Figure 1.4) as an effective modifying agent for a variety of membrane materials.¹¹ The azide functional group in the PFPA material is UV-sensitive and readily decomposes into nitrogen gas and nitrene singlet when exposed under UV light. The resultant nitrene singlet is highly reactive and can covalently bond to chemical groups such as alkyl groups, C=C, and amine groups. Membrane materials usually have abundant aromatic groups with unsaturated C=C bonds for the reaction to occur. The acyl group on the other end of the PFPA molecule can be easily modified with other hydrophilic functional materials. Therefore, PFPA agents bearing hydrophilic chains can be easily grafted onto membrane surfaces via azide photochemistry.

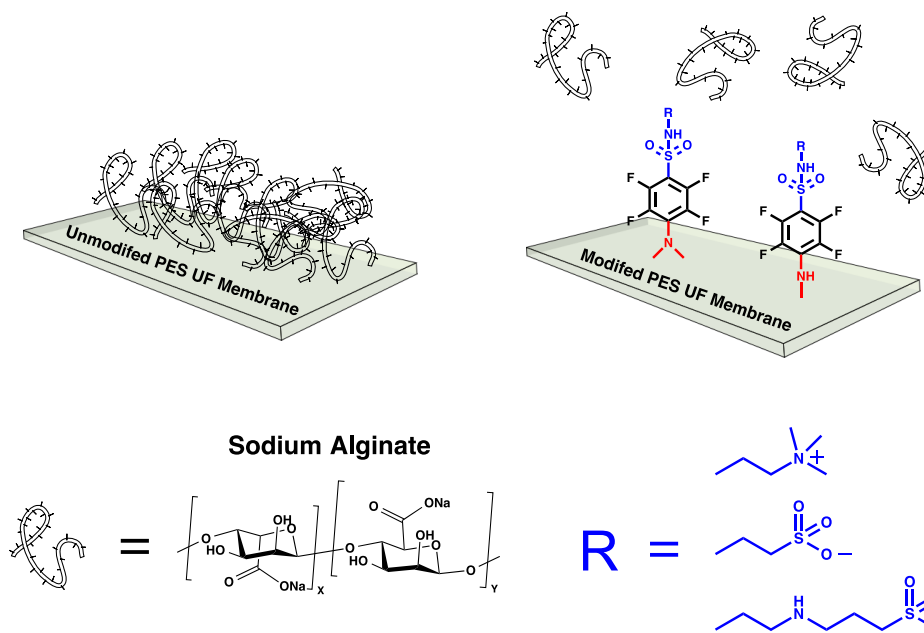


Figure 1.5 Schematic diagram illustrating sodium alginate adhesion to PFPA unmodified and modified PES UF membranes.

One example of this is our demonstration of using PFPA hydrophilic small molecules to modify commercial PES membranes, making it more antifouling against sodium alginate, a common foulant in natural water sources (Figure 1.5). The chemical structures of the three PFPA small molecules are shown in Figure 1.6. They each possess different charged groups with positive charges for PFPA(+), negative charges for PFPA(-) and both positive and negative charges for the zwitterionic PFPA(+). PES membranes modified using these three compounds are characterized using contact angle measurements to see the change in hydrophilicity after modification. The fouling propensity test can also be carried out in a cross-flow system.

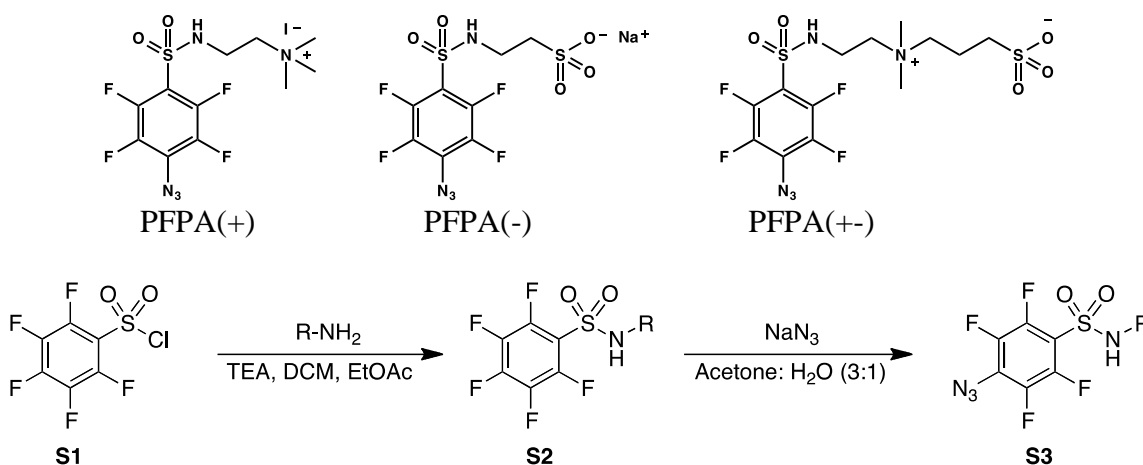
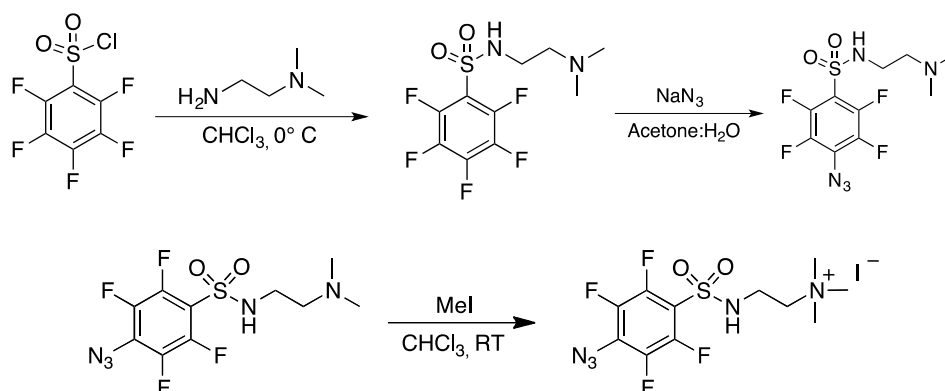


Figure 1.6 Target PFPA-derivatives and a general synthesis route.

The three PFPA compounds were synthesized with the starting material pentafluorobenzene sulfonamide chloride (S1). Its sulfonamide group can react with an appropriate amine compound and form pentafluorobenzene sulfonamide (S2). S2 can then react with sodium azide overnight to produce the PFPA final product. The detailed synthesis steps for all three PFPA compounds can be seen in Figure 1.7. These charged PFPA compounds are water soluble and can be made into 0.1 mM aqueous solutions. Commercial PES membranes can then be dipped into the PFPA solutions followed by exposure to UV light for one minute. Membranes can then be thoroughly rinsed with DI water and the modification is complete.



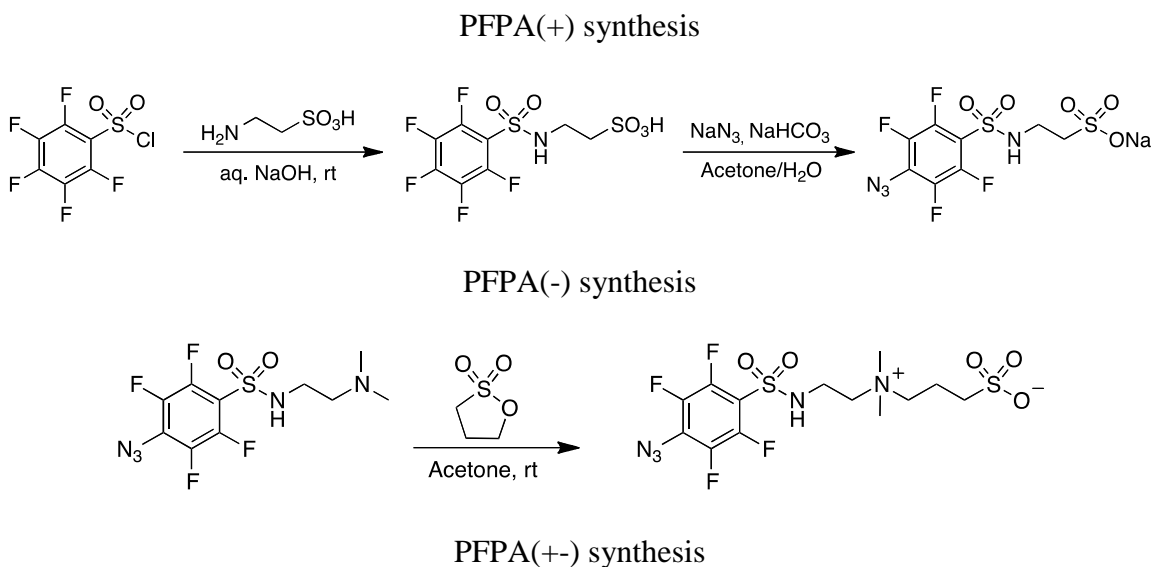
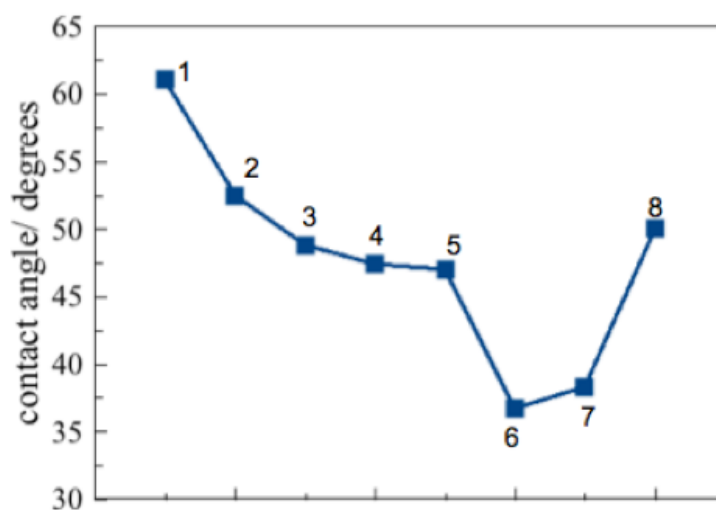
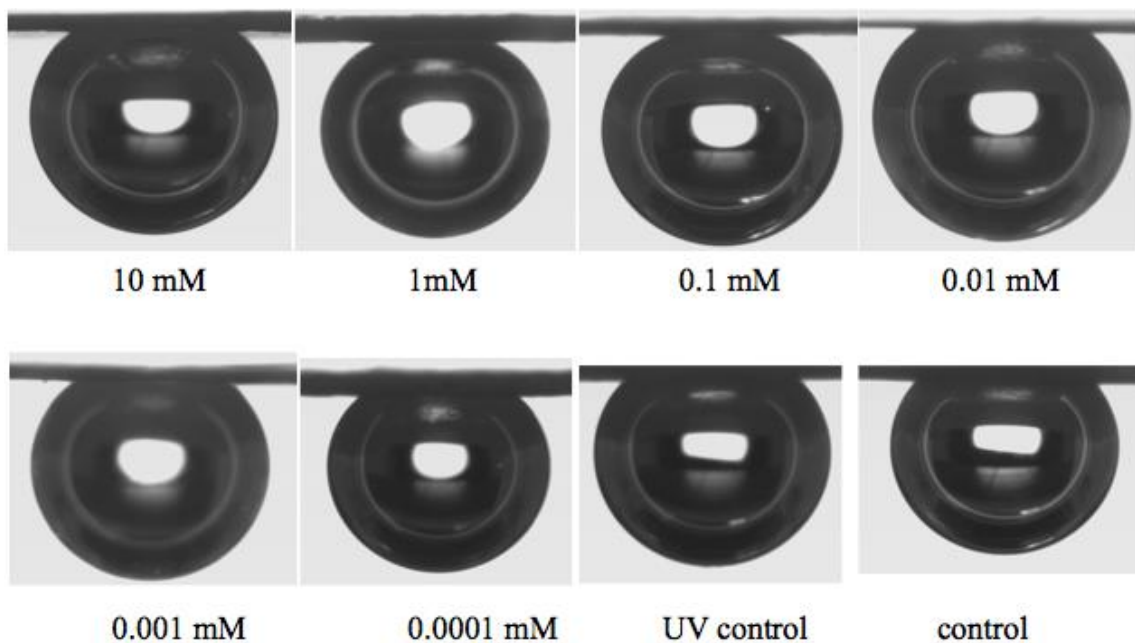


Figure 1.7 Synthesis routes for three PFPA compounds.

Contact angles measured for all the modified PES membranes were lower than the unmodified PES membranes with the zwitterion PFPA(+/-) modified PES membrane exhibiting the lowest contact angle of 36° compared to 61° for the unmodified PES, demonstrating much improved hydrophilicity. The effect of the PFPA solution concentration on the modified membrane hydrophilicity was also studied. The concentration of the zwitterion PFPA(+/-) solution was changed to different orders of magnitude before UV exposure and contact angle measurements. Figure 1.8 demonstrates that a 0.1 mM concentration seems to be the optimal concentration for this application as it leads to the lowest contact angle value. As a control a UV membrane was modified using UV light only without the PFPA solution.



1: PES control 61.0 ± 1.9	5: 0.01 mM 47.0 ± 0.8
2: PES UV control 52.4 ± 0.3	6: 0.1 mM 36.7 ± 0.7
3: 0.0001 mM 48.8 ± 3.4	7: 1 mM 38.3 ± 0.6
4: 0.001 mM 47.4 ± 0.2	8: 10 mM 50.0 ± 2.1

Figure 1.8 Change in contact angle for PES membranes modified using a zwitterion PFPA(+/-) with different concentrations.

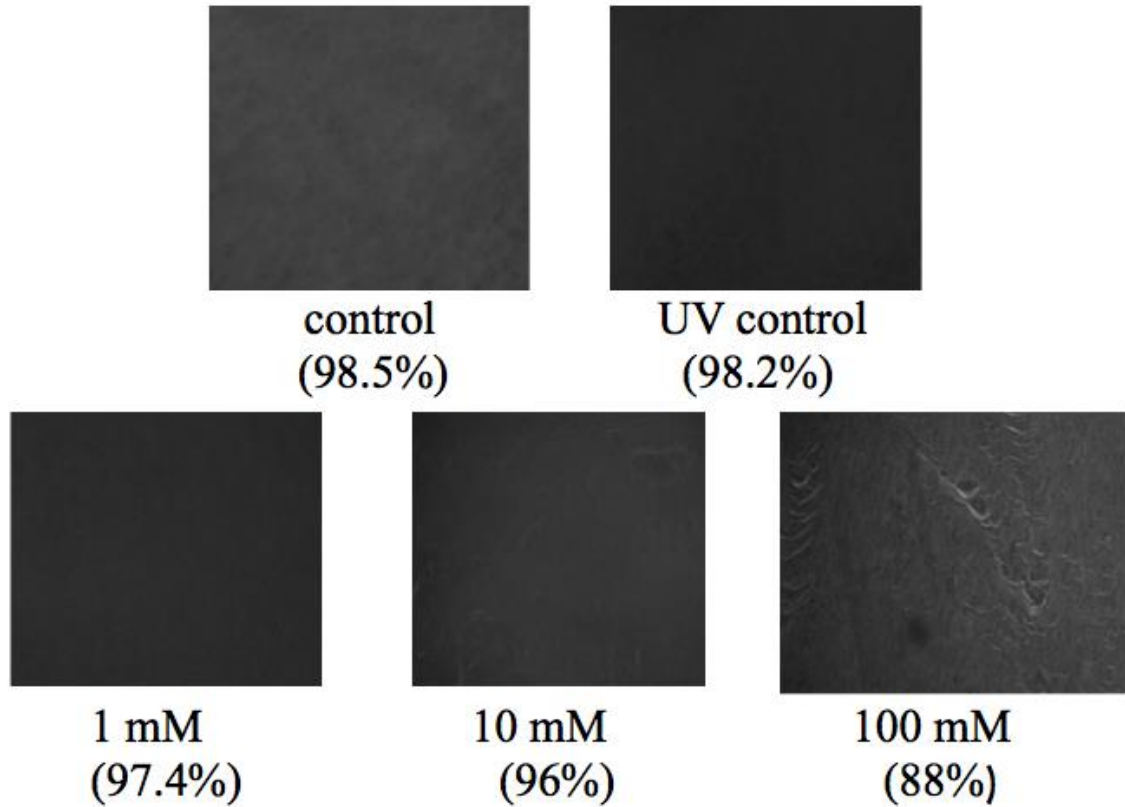


Figure 1.9 Microscopic images of PES membrane surfaces modified using different concentrations of zwitterion PFPA(+/-) solution. The BSA rejection of each membrane is shown for comparison purposes.

It is speculated that concentrations lower than 0.1 mM will only be able to attach a very limited amount of zwitterion molecules on the PES membrane, while concentrations much higher than 0.1 mM will dissolve some polyethersulfone polymer chains away, leaving only a small amount of zwitterion molecules on the membrane. This hypothesis is based on the microscopic images of the modified membrane surfaces (Figure 1.9) that show noticeable holes and defects, likely from the damage caused by the modification as PFPA molecules are highly soluble in water and polymer chains in UF membranes are not cross-linked with each other. BSA (bovine serum albumin, protein) rejection values show that membranes modified with high concentrations of zwitterion

molecules indeed suffer from damage with lower rejection compared to an unmodified control membrane.

In order to evaluate the fouling resistance of the modified membranes, a lab-built cross-flow apparatus was used to monitor the dynamic change of trans-membrane pressure (TMP) in the presence of sodium alginate solution as a model foulant. Sodium alginate, which has a strong attractive force to the polyethersulfone membrane surface, is a common polysaccharide-based extracellular polymeric substance (EPS) secreted by microorganisms that facilitates initial attachment of microbes to membrane surfaces and provides the framework in biofilm formation. Once the SA is anchored to the membrane surface, other foulants can readily attach to the polysaccharide and rapidly foul the membrane. Membranes are compacted first with DI water at 16 psi. Once stable, permeate flux is adjusted manually to 3.2 mL/min with a peristaltic pump. After 10 min of stable flux, feed can be switched to sodium alginate solution and TMP can be monitored throughout the fouling test. After 90 min of the fouling test, the feed can be switched back to DI water for 5 min. This step is known as water cleaning. Afterwards, the feed source can be switched to the foulant solution again while monitoring the TMP change during the second fouling stage. The TMP was calculated automatically throughout the cross-flow fouling test via the following equation:

$$\text{TMP} = (P_{\text{in}} - P_{\text{ret}})/2 - P_{\text{perm}}$$

where P_{in} is the inlet pressure and P_{ret} are the pressure at the feed side and the retentate side of the membrane, respectively, and P_{perm} is the pressure on the permeate side of the membrane. When the membrane gets fouled, the flux at the

permeate side will decrease which leads to a decrease in P_{perm} . This way the TMP value will increase. Therefore, the faster that the TMP increases, the higher the fouling there is on the membrane surface.

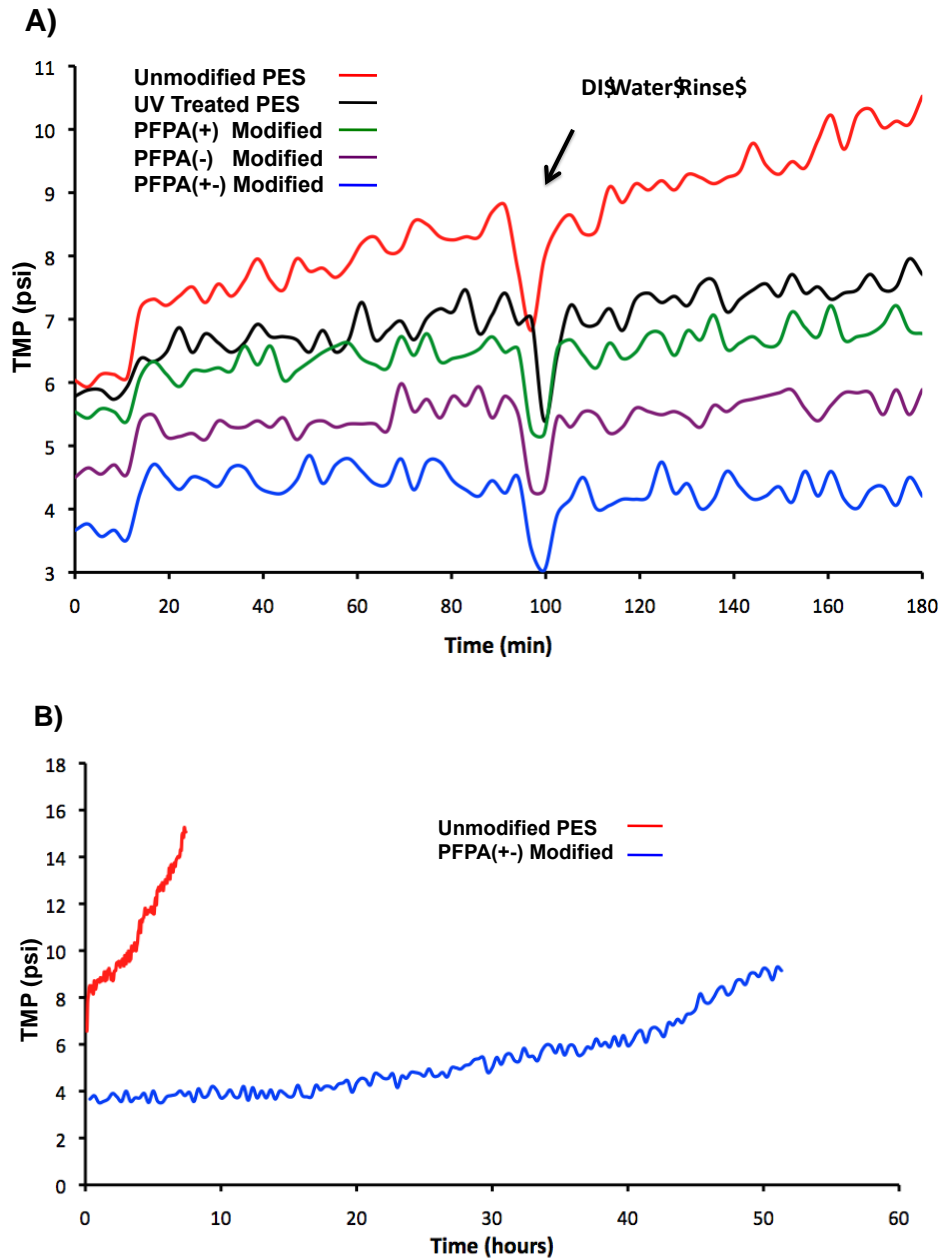


Figure 1.10 A short- and a long-term fouling study of the unmodified and modified membranes.

Figure 1.10 (A) shows that the commercial PES membrane possesses a greater initial and second stage fouling rate compared to the modified membranes. The second stage fouling is presumably higher than the initial stage due to unsuccessful rinsing of the foulant layer from the surface of the membrane, enabling additional sodium alginate particles to attach. Among the modified membranes, the zwitterion PFPA(+/-) coated membrane demonstrates the greatest anti-fouling ability, with a 0 fouling rate for the 3 hour comparative study. Zwitterionic surface monolayers¹² and polymers¹³⁻¹⁵ have shown to possess ultra-low fouling properties under static conditions. When the sodium alginate solution is initially introduced, the TMP immediately increases due to the rapid change in concentration of sodium alginate. However, due to the contribution of repulsion of the membrane surfaces and the cross-flow velocity of the retentate, the particles are removed at a faster rate than the membrane is fouled. Over a longer duration of time, the modified membrane begins to foul, as observed in a long-term fouling study shown in Figure 1.10 (B). When running the cross-flow experiment for >2 days, there is only a ~4 psi change in the TMP. In comparison, the same long-term cross-flow experiment was conducted with the unmodified PES membrane. Because the TMP reaches the inlet pressure, there is no permeation through the membrane and the experiment was stopped.

In addition to imparting anti-fouling ability to the membrane surfaces, the PFPA grafting treatment also increases the permeability of the membrane. The modified membranes all demonstrate greater permeability than the unmodified

membranes, with the PES-PFPA(+/-) modified membrane exhibiting a water permeability 169% greater than the unmodified PES membrane. The increased permeability is likely caused by some of the PES polymer at the membrane surface being dissolved away. Aromatic polyethersulfones are known to undergo photolysis into lower molecular weight species when exposed to UV irradiation.¹⁶ In other words, PFPA molecules can be easily synthesized and produced in large quantities. They can be dissolved in an environmentally benign solvent such as water for the rapid modification of commercial membrane surfaces under UV exposure. Such modification is successful resulting in increased water permeability, negligible changes in sodium alginate rejection and greatly enhanced long-term fouling resistance.

PFPA chemistry can be rather versatile as one can synthesize different PFPA compounds bearing different functional groups for membrane modification. The application of azide chemistry for scalable membranes is further explored in later chapters.

Blending hydrophilic/antibacterial materials with commercial membrane making materials during the fabrication process is another effective way to increase the hydrophilicity/bacteriacidal ability of membranes. For example, sulfonated polyaniline (SPANi) can be blended into PS UF membranes to enhance the hydrophilicity and fouling resistance.

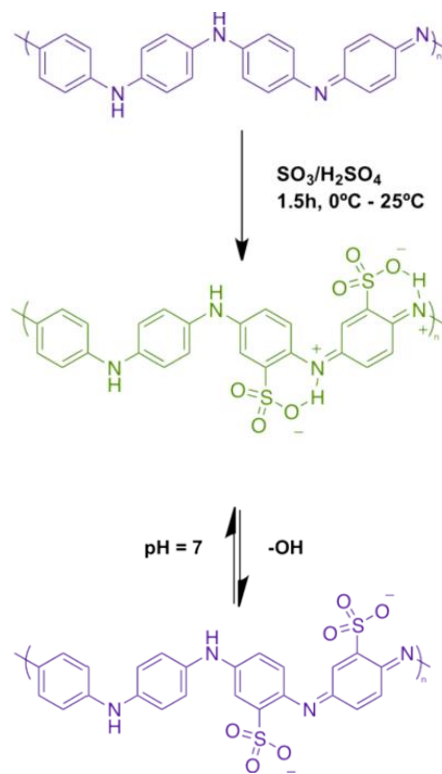


Figure 1.11 Synthesis of SPANi from polyaniline (PANi) that can be dedoped to create the base form, which can be processed into a solution.

SPANi is a unique self-doped conducting polymer. It's very hydrophilic due to the zwitterionic positively and negatively charged groups on the polymer backbone. SPANi can be synthesized through a reaction between PANi and fuming sulfuric acid. The resultant SPANi can dissolve in strong base and can be easily blended into a polysulfone/N-methylpyrrolidone (NMP) casting solution at different weight percentages. From Figure 1.12, it is clear that with a higher percentage of SPANi blending, the contact angle decreases, showing improved hydrophilicity.

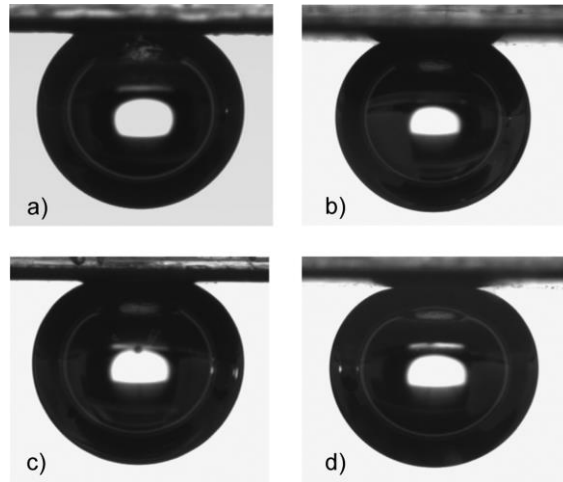


Figure 1.12 Captive bubble contact angle images of (a) a pure PS membrane; (b) a 1% SPANi membrane; (c) a 5% SPANi membrane and (d) a 10% SPANi membrane.

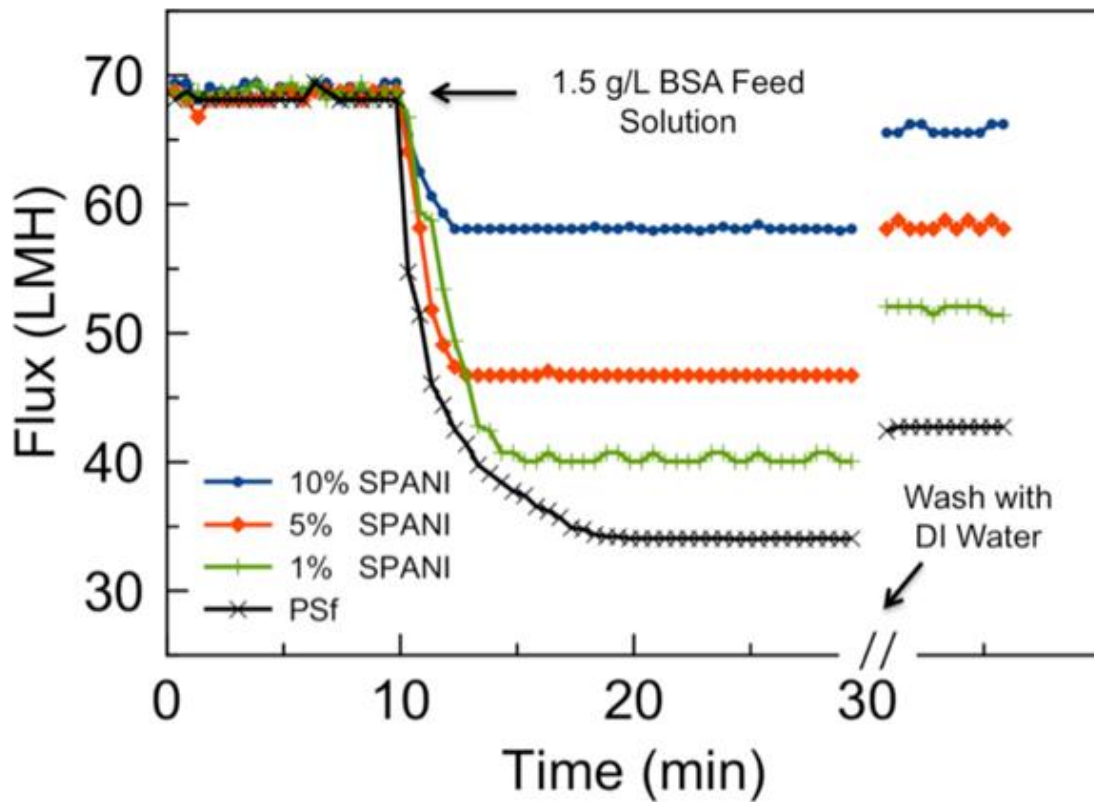


Figure 1.13 Flux decline and recovery results for PS membranes containing 0, 1, 5, 10% SPANi after being exposed to a BSA feed solution.

To evaluate the effects of the enhanced hydrophilicity on fouling properties, flux decline and recovery testing was performed using BSA as a model organic foulant in a

cross-flow system. When the membranes were exposed to a BSA solution, the flux decreased immediately. (Figure 1.13) The pure PS membrane lost about half of its original flux, while the SPANi blended membranes exhibited less flux decline with higher SPANi content. The 10% SPANi membrane only lost 16% of flux and was able to recover 95% of its flux after a simple wash flushing step.

1.5 Conclusions

Filtration membranes are becoming more and more crucial to our everyday lives. Despite the various commercial products available out there, continuous efforts are needed in order to design and formulate better membranes that are antifouling and chlorine resistant. In later chapters, more research on membrane surface modification methods using azide photochemistry will be discussed. A novel chlorine resistant UF membrane fabricated using a polyaniline derivative will also be described. In the end, a review on the various applications of nanostructured polyaniline will be given to show the importance of nanostructured conducting polymers in fields other than membranes.

1.6 References

- 1 J. C. Crittenden, R. R. Trussell, D. W. Hand, K. J. Howe and G. Tchobanoglous, *Water Treatment: Principles and Design*, John Wiley & Sons, Inc., Hoboken, New Jersey, 2nd edn, 2005.
- 2 Guillen, G. R.; Pan, Y.; Li, M.; Hoek, E. M. V.; *Industrial & Engineering Chemistry Research*, 2011, 50, 3798-3817.
- 3 Guillen, G. R.; Ramon, G. Z.; Kavehpour, H. P.; Kaner, R. B.; Hoek, E. M. V.; *Journal of Membrane Science*, 2013, 431, 212-220.
- 4 Kawaguchi, T.; Tamura, H.; *Journal of applied Polymer Science*, 1984, 29, 3359-3367.
- 5 Shin, D. H.; Kim, N.; Lee, Y. T.; *Journal of Membrane Science*, 2011, 376, 302-311.
- 6 Wienk, I. M.; Meuleman, E. E. B.; Borneman, Z.; Boomgaard, V. D.; Smolders, C. A.; *Journal of Polymer Science: Part A: Polymer Chemistry*, 1995, 33, 49-54.
- 7 Arkhangelsky, E.; Kuzmenko, D.; Gitis, V.; *Journal of Membrane Science*, 2007, 305, 176-184.
- 8 Glater, J.; Hong, S.; Elimelech, M.; *Desalination*, 1994, 95, 325-345.
- 9 Shintani, T.; Matsuyama, H.; Kurata, N.; *Desalination*, 2007, 207, 340-348.
- 10 Hong, S.; Kim, I.; Tak, T.; Kwon, Y.; *Desalination*, 2013, 309, 18-26.
- 11 Liu, L.; Yan, M.; *Accounts of Chemical Research*, 2010, 43, 1434-1443.
- 12 Holmlin, R. E.; Chen, X.; Chapman, R. G.; Takayama, S.; Whitesides, G. M.; *Langmuir*, 2001, 17, 2841-2850.
- 13 Jiang, S.; Cao, Z. *Adv. Mater.* 2010, 22, 920-932.
- 14 Yang, R.; Jang, H.; Stocker, R.; Gleason, K. K. *Adv. Mater.* 2014, 26, 1711-1718.
- 15 Mi, L.; Jiang, S. *Angew. Chemie Int. Ed.* 2014, 53, 1746-1754.
- 16 Yamagishi, H.; Crivello, J. V; Belfort, G. J. *Memb. Sci.* 1995, 105, 237-247.

Chapter 2. Low-Fouling Antibacterial Reverse Osmosis Membranes via Surface Grafting of Graphene Oxide

2.1 Introduction

The dwindling of reliable freshwater supplies is one of our most severe problems exacerbated by rising population and source contamination.^{1,2,3} Although there have been improved efforts in water conservation, infrastructure repair, and allocation, these approaches are only effective in making better use of existing resources.² With the increasing need for more freshwater, it is imperative to find alternative sources to meet future demand. Membrane desalination can produce a sustainable supply of freshwater from both seawater and brackish water utilizing reverse osmosis (RO) membranes. The thin-film membranes reject salts from the feed solution and continuously produce a freshwater effluent for use. State-of-the-art, interfacially polymerized RO membranes provide high permeability and high rejection with relatively low manufacturing costs.^{2,3} Despite their outstanding transport and selectivity, their susceptibility to fouling remains one of the most problematic issues due to reduced performance and increased energy consumption.^{4,5} Fouling occurs when proteins, microorganisms, and inorganic materials accumulate on membrane surfaces and increase their resistance to water permeation.^{6,7} Of these, biofouling caused by the deposition and growth of microorganisms, is the most difficult to prevent.^{5,7-9} Once microorganisms irreversibly attach to the surfaces of a membrane, they can proliferate rapidly in the presence of nutrients, creating microcolonies that produce extracellular polymeric substances (EPS) which eventually lead to the formation of biofilms on the membrane surface. Unfortunately, chlorine-based

disinfecting agents that are generally used to control biofouling are not suitable for cleaning RO membranes due to chlorine degradation of polyamide-based polymers.¹⁰

Methods that have been investigated to introduce anti-adhesion/anti-microbial properties to polyamide RO membranes include the surface coating of hydrophilic functional materials¹¹⁻¹⁶ and the incorporation of biocidal materials^{8,19,20,22} directly onto the polymer surfaces. A hydrophilic surface will form a hydration layer that hinders the hydrophobic interactions between the membrane surfaces and the foulants, preventing the initial attachment of foulants on the membranes.¹⁹ However, a majority of the modification methods are not practical or scalable and therefore are unlikely to be of commercial importance. Physically applied coatings, for example, can be easily removed during membrane operation and only produce short-term anti-fouling effects.⁷ Layer-by-layer (LBL) coatings of oppositely-charged materials tend to disintegrate under high/low pH and/or high ionic strength²⁰ which are common environments found during RO applications. Covalent tethering of hydrophilic materials maintains the stability of the modification layer; however, these modifications typically require exotic synthetic conditions such as radical-initiated polymerization¹⁹, plasma¹⁵, or carbodiimide activation,^{8,11,12} which have only been demonstrated on a laboratory scale. Such processes tend not to be amenable to the high-rate roll-to-roll manufacturing process used for commercial RO membranes.²³ Furthermore, the grafting layer often reduces the permeability of the membranes by adding resistance to the passage of water through the membrane.^{12,13,15,21} The modification of RO membranes with biocidal materials can increase their antimicrobial properties and biofouling resistance. However, commonly used materials such as silver nanoparticles will slowly leach out of the membrane,

spreading toxic nanoparticles into the environment, while losing antimicrobial activity over time.⁸ Therefore, a facile, scalable process is needed to produce antifouling RO membranes in order to improve the productivity of membrane-based desalination.

Graphene oxide (GO) can be grafted onto commercial polyamide RO membranes to promote anti-fouling and anti-adhesion properties. GO is a hydrophilic, one-atom-thick two-dimensional structure^{11,22} that possesses antimicrobial properties^{8,22}. Previous research has examined applying the outstanding properties of GO in the RO membrane field through the incorporation of GO into the polyamide active layer^{17,18}, LBL coating of GO dispersions¹¹ and covalent surface bonding of GO using carbodiimide activation^{8,16,22}. The covalent surface bonding method appears to be the best method because it allows full utilization of GO material¹⁸ and is more environmentally stable²⁰.

2.2 Synthesis of Azide Functionalized Graphene Oxide and Characterization

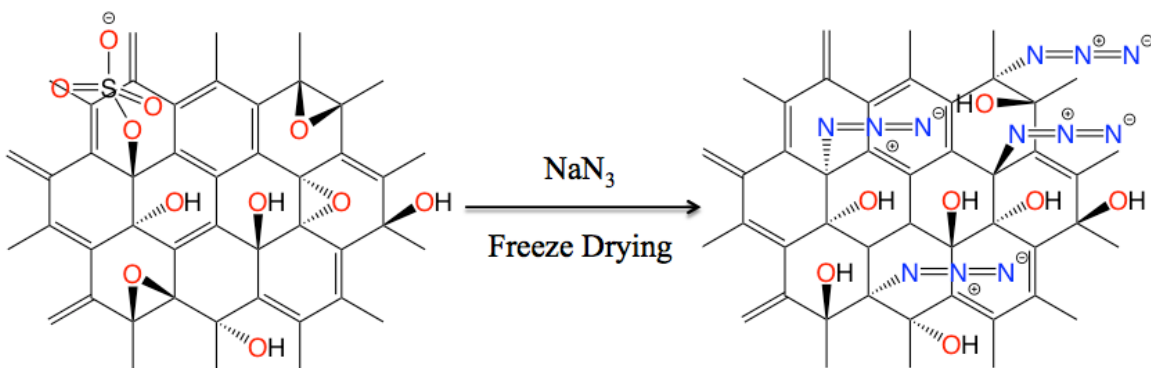


Figure 2.1 Schematic illustration of the azidation process of graphene oxide (GO).

Azide-functionalized GO (AGO) was employed to modify commercial RO membranes due to the unique photochemistry of azide groups. Upon photoactivation, AGO produces a highly reactive singlet nitrene intermediate that reacts with the abundant

aromatic rings found within the polyamide membrane active layer.^{25,26} AGO is synthesized according to the route developed by Eigler, *et al.*²⁴ Sodium azide was added into an aqueous dispersion of GO followed by freeze-drying (Figure 2.1). The solid-state azidation reaction takes place during the drying in which azide groups substitute for the sulfonate and epoxide groups. The as-synthesized product was purified by centrifugation in water. FT-IR spectra (Figure 2.2) of both the starting GO material and AGO show that after the azidation reaction, a new azide peak (2123 cm^{-1}) appeared in the AGO spectrum. This provides evidence for the successful substitution of azide groups onto the GO structure. The absence of a peak at 2065 cm^{-1} (the sodium azide peak) showed that the purification was effective in removing essentially all the unreacted impurities.

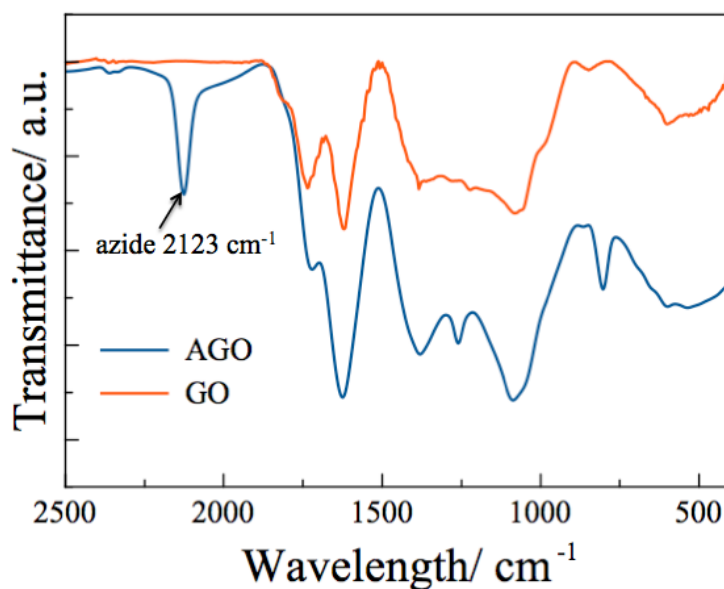


Figure 2.2 FT-IR spectra of GO and AGO.

The final product was then freeze-dried and redispersed in water to make a 10 mg/L AGO dispersion. AFM analysis (Figure 2.3) showed that the as-synthesized

AGO nanosheets have sizes ranging from several hundred nanometers to several micrometers with an average thickness of 1.15 nm. This is comparable to previously reported values for GO²⁹, showing that the azidation process did not have any apparent effect on altering the morphology of the GO sheets.

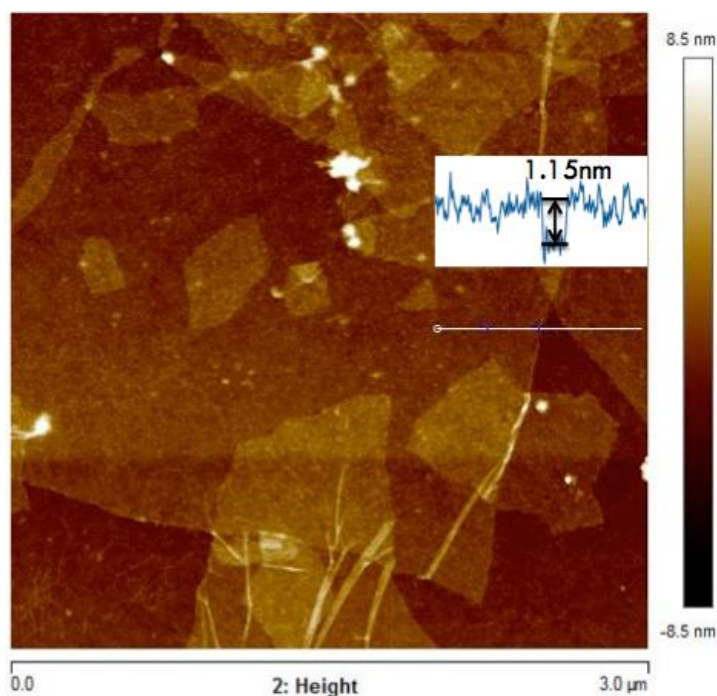


Figure 2.3 AFM height analysis of AGO shows that AGO exhibits a planar morphology with an average thickness of 1.15 nm (inset).

2.3 Membrane Surface Modification

Commercial RO polyamide membranes (i.e. Dow FILMTEC XLE brackish water flat sheet membranes) were dipped into the AGO dispersion and air-dried overnight under ambient conditions. The RO membranes were then placed under UV irradiation (254 nm, 620 $\mu\text{W}/\text{cm}^2$ average intensity) for 1 min before sonication in DI water, which removes any non-bonded AGO. The modification scheme is illustrated in Figure 2.4.

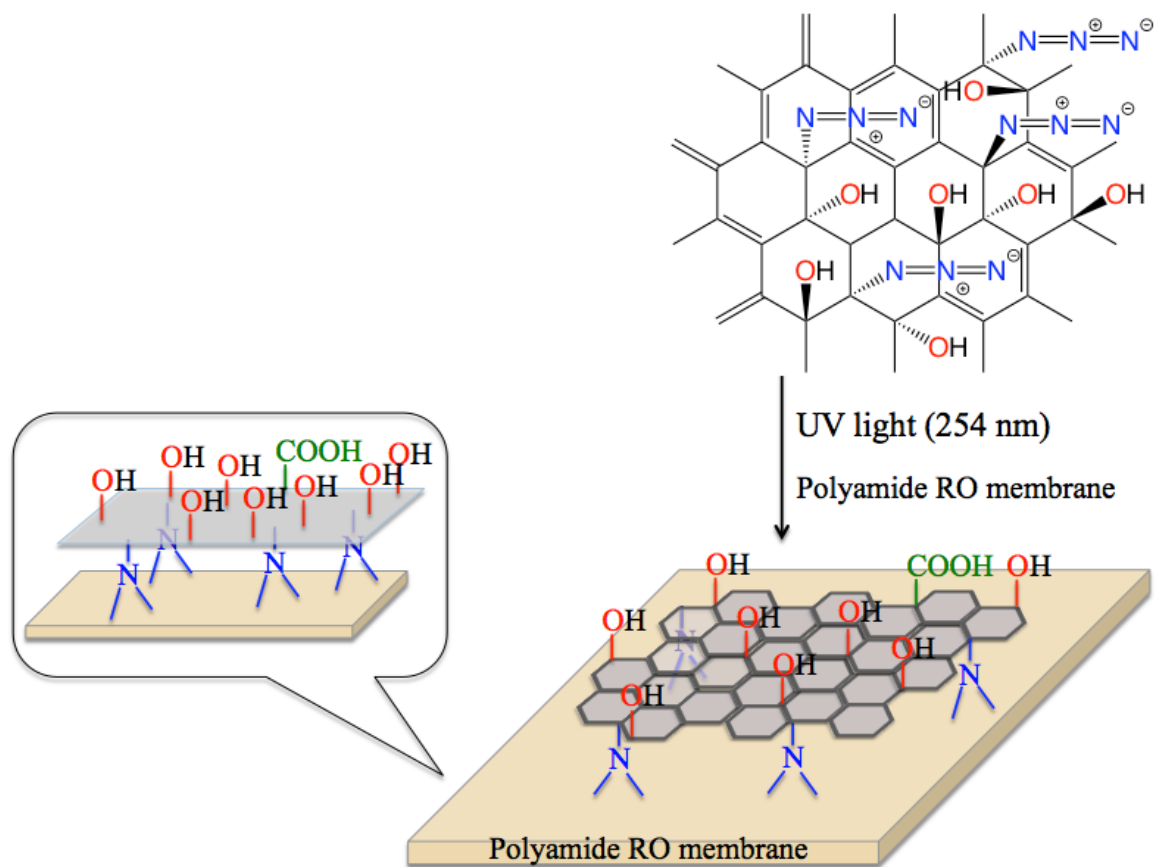


Figure 2.4 Schematic illustration of the modification of a commercial polyamide RO membrane using UV activated AGO.

2.4 Results

Contact angle measurements were conducted to confirm the completion of the modification. Once commercial RO membranes were modified, the apparent pure water contact angle decreased from $85^{\circ} \pm 4^{\circ}$ (comparable to previously reported values for polyamide RO membranes^{11,17}) to $45^{\circ} \pm 2^{\circ}$ (Figure 2.5), indicating a much higher affinity between water and the membrane surface due to the hydrophilic oxygen-containing functional groups within the AGO structure. The enhanced hydrophilicity induces a thin hydration layer on the membrane surfaces which repel foulant adsorption.^{5,7} Commercial RO membranes were also dried and exposed to UV light without the dip-coating step.

Their contact angles did not change compared to a bare RO membrane, indicating that UV light exposure plays little role in the contact angle of the polyamide layer, as previously demonstrated²³. As another control experiment, an AGO-coated RO membrane was dried and sonicated in DI water without UV exposure. Its contact angle showed no apparent change compared to a bare RO membrane. This proves that the sonication/rinsing step was effective in removing essentially all the unbonded AGO.

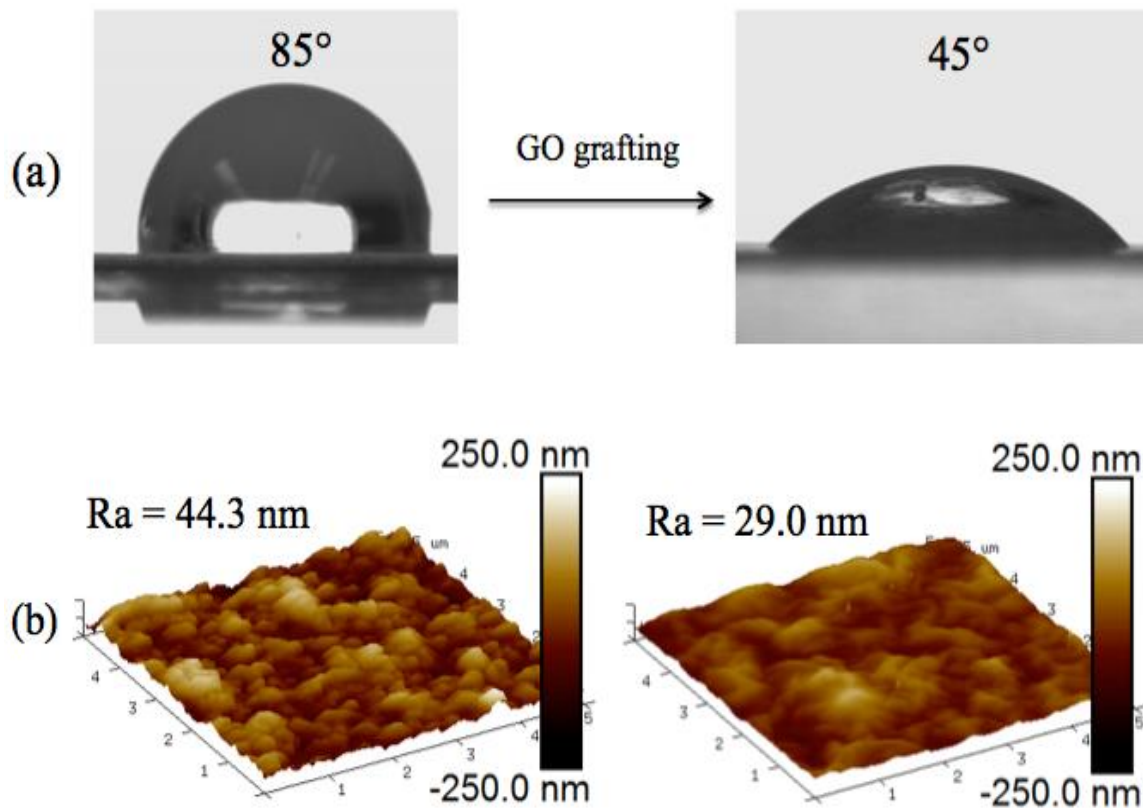


Figure 2.5. After GO grafting on the polyamide RO membrane surface, (a) the water contact angle decreased from 85° to 45° and (b) the average surface roughness decreased from 44.3 nm to 29.0 nm based on a 5 μm \times 5 μm analyzed area.

To investigate changes to the surface topography, atomic force microscopy (AFM) was conducted on the modified and unmodified membranes. The microscopy

demonstrates that the GO-RO membrane had a much smoother surface compared to the unmodified RO membrane. Polyamide RO membranes are manufactured using interfacial polymerization that typically gives a rough ridge-and-valley^{11,23} surface morphology, as shown in Fig. 2b left. After modifying the RO membrane surface with GO, the membrane surface became smoother with an arithmetic average (R_a) roughness of 29.0 nm compared to a R_a of 44.3 nm for the unmodified RO membrane. This can be attributed to the planar GO sheets covering the valley regions of the membrane surfaces. A rough surface, like the pristine RO membrane, tends to trap foulants due to the preferential accumulation of foulants in the valleys of the membrane surfaces.⁷ Therefore, a smooth, hydrophilic membrane surface is expected to have higher resistance to fouling compared to an unmodified RO membrane.

X-ray photoelectron spectroscopy (XPS) analysis of the membrane surface further confirmed successful modification. Following the modification, the chemical composition of the modified membrane surface contained high carbon and oxygen content, similar to the precursor AGO powder (Table 1), suggesting that the modified surface was predominantly covered in GO sheets. The oxygen content of the modified membrane approximately doubled (from 14.5% to 28.6%) after the grafting of GO compared to the pristine membrane, a result of the various oxygen-containing functional groups in AGO. Additionally, the nitrogen content from the polyamide active layer was reduced from 10.9% to 3.0%, as GO sheets on the surface of the membrane material dominate the spectrum.

Table 2.1 XPS Surface Composition Analysis for AGO Powder and RO membranes

	<i>% C 1s</i>	<i>% O 1s</i>	<i>% N 1s</i>
AGO powder	67.8	30.0	2.2
Control RO membrane	74.6	14.5	10.9
AGO-RO membrane	68.4	28.5	3.0

Membrane permeability and rejection were tested with a 2 g/L NaCl aqueous solution under 15.5 bar operating pressure using a cross-flow system with an effective membrane area of 19 cm². After 2 hours of compaction, the commercial RO membrane exhibited a stable flux of 37.8 Lmh with a NaCl rejection of 94.1%. The AGO-RO membrane maintained a comparable flux of 36.3 Lmh and NaCl rejection of 95.3%. Prior attempts to increase the hydrophilicity and fouling resistance of polyamide RO membranes via surface tethering of hydrophilic materials often resulted in significant drops in permeability.^{12,13,15,21} With the AGO modification, only negligible changes to the membrane performance properties occurred.

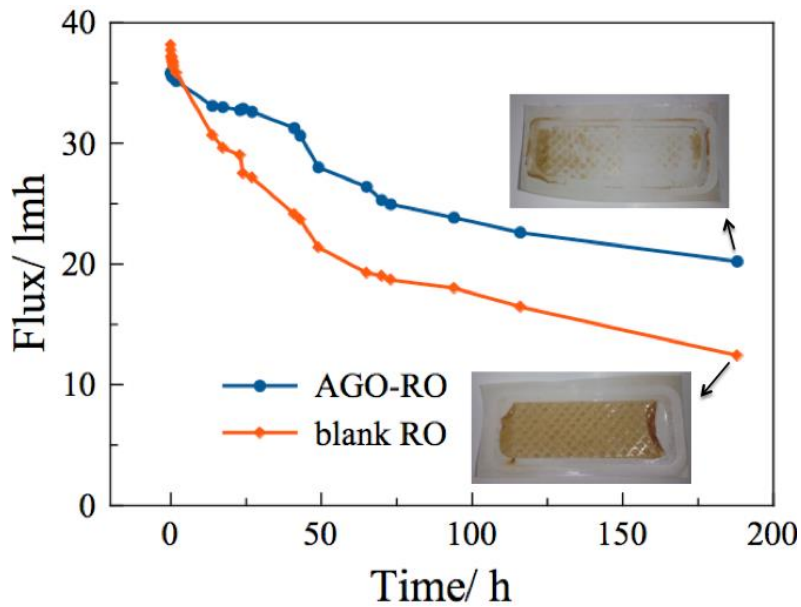


Figure 2.6 A long-term BSA fouling test on the control and modified membranes showing the differences in flux decline. Inset pictures show the membranes with a BSA fouling layer covering the surface at the end of the fouling test.

Once the pure water permeability and rejection was established in the cross-flow system, the fouling propensity of the membranes were evaluated by adding foulants to the feed solution. A feed solution consisting of 0.2 g/L BSA (protein, bovine serum albumin) and 2 g/L NaCl was used and flux was monitored for seven days. The operating pressure was maintained at 15.5 bar over the course of the test. According to Figure 2.6, the flux of the unmodified RO membrane decreased rapidly, with a total of 70% flux reduction after seven days. In contrast, the flux of the modified membrane was consistently higher than the blank RO membrane after 5 hours and demonstrated only a 40% flux reduction after seven days. The cross-flow test was then stopped and the unmodified and modified membranes were taken out for visual comparison. After one week of fouling, a thick layer of yellow BSA covered the entire surface of the pristine RO membrane (Figure 2.6

inset), increasing the thickness of the membrane and lowering its flux. For the modified membrane, the yellow BSA on the surface was greatly reduced and only covered the side edges of the modified membrane. The much improved hydrophilicity significantly increased the membrane's affinity for water and leads to a thin layer water barrier that is effective in resisting the irreversible fouling caused by the attachment of proteins onto the membrane surfaces. The smoother surfaces of the modified membranes further contribute to their low-fouling properties because it becomes more difficult for protein particles to anchor onto the membrane surfaces without the valleys and ridges of a rough surface that protect the protein particles from being flushed away. It is evident that after the grafting of GO, the modified polyamide membrane is able to mitigate the long-term gel layer formation from the accumulation of foulants. Due to its enhanced hydrophilicity and smoothness, the GO-RO membrane can effectively resist the attachment of foulant molecules and provide less accessible sites for foulant deposition.

The antifouling properties of GO-RO was investigated further by a static bacterial adhesion experiment using *E. coli* as a model microorganism. Modified and unmodified membrane cut-outs ($1 \times 1 \text{ cm}^2$) were soaked in an *E. coli* suspension for 24 hours at room temperature before being rinsed with a 0.9% saline solution and stained in a SYTO 9 or propidium iodide (PI) solution for fluorescence imaging. SYTO 9 labels both live and dead bacteria cells by binding to their cell membranes, while PI labels only the dead cells because it can only penetrate damaged cell membranes. Using Image J software, the surface coverage of total attached cells and all attached cells that are dead can be quantified by dividing the amount of colored pixels by the total amount of pixels in the image. Afterwards, the surface coverage of live attached cells can be calculated by

subtracting the percentage of dead attached cells from that of all the attached cells. Fig. 3c illustrates the surface coverage of live (blue) and dead (red) *E. coli* on both unmodified and modified membranes.

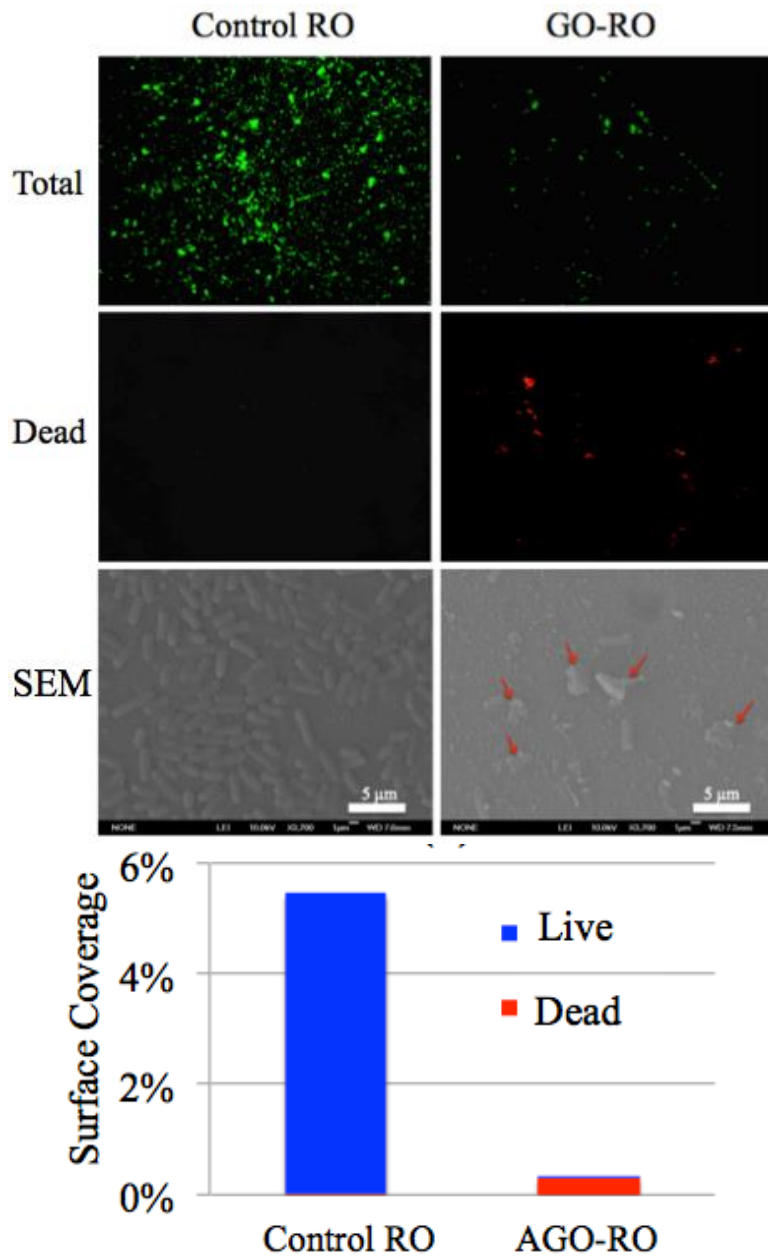


Figure 2.7 (top) Fluorescence and SEM images showing the percentages and condition of *E. coli* cells on membrane surfaces after contact for 24 hours; (bottom) quantitative analysis of live (blue) and dead (red) cell percentages on both membrane surfaces.

As shown in Figure 2.7 above, 5.46% of the surface of the control RO membrane was covered by *E. coli* cells with no deactivation. In comparison, only 0.32% of the GO-RO membrane surface was fouled by *E. coli* (both live and dead species), representing a seventeen fold reduction in cell adhesion compared to the unmodified RO membrane. This shows that the GO-RO membrane can effectively inhibit the initial attachment of bacteria, which is crucial in preventing the growth and spreading of bacteria. Furthermore, among the attached *E. coli* cells, nearly 90% were deactivated owing to the antibacterial properties of GO molecules^{8,22}. The bacteria-fouled membranes were also observed under a scanning electron microscope (SEM) to further confirm the condition of the *E. coli* cells on the membrane surface. In the SEM images, the pristine RO membrane surface was largely covered by intact *E. coli* cells, while that of the AGO-RO membrane had a much lower surface coverage of *E. coli* cells. Many of the *E. coli* cells on the AGO-RO membrane surface appeared to be lysed, indicating the cell damage induced by the GO molecules, as GO is known to inactivate bacteria through physical disruption²⁷, formation of reactive oxygen species²⁷, and extraction of lipids from cell membranes²⁸.

2.5 Conclusions

By anchoring GO molecules onto the polyamide RO membrane surfaces, the surface properties of a commercial polyamide RO membrane were successfully altered, becoming more hydrophilic, smooth, and antibacterial with considerable resistance to protein fouling and biofouling. The UV modification method using azide chemistry was

facile and scalable. It can be easily incorporated into the last step of a commercial roll-to-roll membrane manufacturing process.

2.6 References

- (1) Crittenden, J. C.; Trussell, R. R.; Hand, D. W.; Howe, K. J.; Tchobanoglous, G. *Water Treatment: Principles and Design*, John Wiley & Sons, Inc., Hoboken, New Jersey, 2nd edn, 2005.
- (2) Elimelech, M.; Phillip, W. A. The Future of Seawater Desalination: Energy, Technology, and the Environment. *Science* 2011, 333, 712-717.
- (3) Service, R. F. Desalination Freshens Up. *Science* 2006, 313, 1088-1090.
- (4) Gao, K.; Kearney, L. T.; Wang, R.; Howarter, J. A. Enhanced Wettability and Transport Control of Ultrafiltration and Reverse Osmosis Membranes with Grafted Polyelectrolytes. *ACS Appl. Mater. Interfaces* 2015, 7, 24839-24847.
- (5) Mansouri, J.; Harrisson, S.; Chen, V. Strategies for Controlling Biofouling in Membrane Filtration Systems: Challenges and Opportunities. *J. Mater. Chem.* 2010, 20, 4567-4586.
- (6) Huang, X.; McVerry, B. T.; Marambio-Jones, C.; Wong, M. C. Y.; Hoek, E. M. V.; Kaner, R. B. Novel Chlorine Resistant Low-Fouling Ultrafiltration Membrane Based on a Hydrophilic Polyaniline Derivative. *J. Mater. Chem. A.* 2015, 3, 8725-8733.
- (7) Rana, D.; Matsuura T. Surface Modifications for Antifouling Membranes. *Chem. Rev.* 2010, 110, 2448-2471.
- (8) Perreault, F.; Tousley, M. E.; Elimelech, M. Thin-Film Composite Polyamide Membranes Functionalized with Biocidal Graphene Oxide Nanosheets. *Environ. Sci. Technol. Lett.* 2014, 1, 71-76.
- (9) Khan, M. T.; de O. Manes, C.-L.; Aubry, C.; Gutierrez, L.; Croue, J. P. Kinetic Study of Seawater Reverse Osmosis Membrane Fouling. *Environ. Sci. Technol.* 2013, 47, 10884–10894.
- (10) Glater, J.; Hong, N.; Elimelech, M. The Search for a Chlorine-Resistant Reverse Osmosis Membrane. *Desalination* 1994, 95, 325-345.
- (11) Choi, W.; Choi, J.; Bang, J.; Jee, J. Layer-by-Layer Assembly of Graphene Oxide Nanosheets on Polyamide Membranes for Durable Reverse-Osmosis Applications. *ACS Appl. Mater. Interfaces* 2013, 5, 12510-12519.
- (12) McVerry, B. T.; Wong, M. C. Y.; Marsh, K. L.; Temple, J. A. T.; Marambio-Jones, C.; Hoek, E. M. V.; Kaner, R. B. Scalable Antifouling Reverse Osmosis Membranes Utilizing Perfluorophenyl Azide Photochemistry. *Macromol. Rapid Commun.* 2014, 35, 1528-1533.

- (13) Nikkola, J.; Sievänen, J.; Raulio, M.; Wei, J.; Vuorinen, J.; Tang, C. Y. Surface Modification of Thin Film Composite Polyamide Membrane Using Atomic Layer Deposition Method. *J. Membr. Sci.* 2014, 450, 174-180.
- (14) Lin, N. H.; Kim, M.; Lewis, G. T.; Cohen, Y. Polymer Surface Nano-Structuring of Reverse Osmosis Membranes for Fouling Resistance and Improved Flux Performance. *J. Mater. Chem.* 2010, 20, 4642-4652.
- (15) Belfer, S.; Purinson, Y.; Fainshtein, R.; Radchenko, Y.; Kedem, O. Surface Modification of Commercial Composite Polyamide Reverse Osmosis Membranes. *J. Membr. Sci.* 1998, 139, 175-181.
- (16) Hegab, H. M.; ElMekawy, A.; Barclay, T. G.; Michelmore, A.; Zou, L.; Saint, C. P.; Ginic-Markovic, M. Fine-Tuning the Surface of Forward Osmosis Membranes via Grafting Graphene Oxide: Performance Patterns and Biofouling Propensity. *ACS Appl. Mater. Interfaces*, 2015, 7, 18004-18016.
- (17) He, L.; Dumée, L. F.; Feng, C.; Velleman, L.; Reis, R.; She, F.; Gao, W.; Kong, L. Promoted water transport across graphene oxide-poly(amide) thin film composite membranes and their antibacterial activity, *Desalination* 2015, 365, 126-135
- (18) Xia, S.; Yao, L.; Zhao, Y.; Li, N.; Zheng, Y. Preparation of graphene oxide modified polyamide thin film composite membranes with improved hydrophilicity for natural organic matter removal, *Chem. Eng. J.* 2015, 280, 720-727.
- (19) Banerjee, I.; Pangule, R. C.; Kane, R. S. Antifouling Coatings: Recent Developments in the Design of Surfaces That Prevent Fouling by Proteins, Bacteria, and Marine Organisms. *Adv. Mater.* 2011, 23, 690-718.
- (20) Ren, P.; Yang, H.; Liang, H.; Xu, X.; Wan, L.; Xu, Z. Highly Stable, Protein-Resistant Surfaces via the Layer-by-Layer Assembly of Poly(sulfobetaine methacrylate) and Tannic Acid. *Langmuir* 2015, 31, 5851-5858.
- (21) Faibish, R. S.; Yoshida, W.; Cohen, Y. Contact Angle Study on Polymer-Grafted Silicon Wafers. *J. Colloid Interface Sci.* 2002, 256, 341-350.
- (22) Ray, J. R.; Tadepalli, S.; Nergiz, S. Z.; Liu, K.; You, L.; Tang, Y.; Singamaneni, S.; Jun, Y. Hydrophilic, Bactericidal Nanoheater-Enabled Reverse Osmosis Membranes to Improve Fouling Resistance. *ACS Appl. Mater. Interfaces* 2015, 7, 11117-11126.
- (23) Ghosh, A. K.; Jeong, B.; Huang, X.; Hoek, E. M. V. Impacts of Reaction and Curing Conditions on Polyamide Composite Reverse Osmosis Membrane Properties. *J. Membr. Sci.* 2008, 311, 34-45.
- (24) Eigler S.; Hu, Y.; Ishii, Y.; Hirsch, A. Controlled Functionalization of Graphene Oxide with Sodium Azide. *Nanoscale* 2013. 5, 12136-12139.

- (25) Bräse, S.; Gil, C.; Knepper, K.; Zimmermann, V. Organic Azides: An Exploding Diversity of a Unique Class of Compounds. *Angew. Chem. Int. Ed.* 2005, 44, 5188-5240.
- (26) Liu, L.; Yan, M. Perfluorophenyl Azides: New Applications in Surface Functionalization and Nanomaterial Synthesis. *Acc. Chem. Res.* 2010, 43, 1434-1443.
- (27) Liu, S.; Zeng, T. H.; Hofmann, M.; Burcombe, E.; Wei, J.; Jiang, R.; Kong, J.; Chen, Y. Antibacterial Activity of Graphite, Graphite Oxide, Graphene Oxide, and Reduced Graphene Oxide: Membrane and Oxidative Stress. *ACS Nano* 2011, 5, 6971-6880.
- (28) Tu, Y.; Lv, M.; Xiu, P.; Huynh, T.; Zhang, M.; Castelli, M.; Liu, Z.; Huang, Q.; Fan, C.; Fang, H.; Zhou, R. Destructive Extraction of Phospholipids from Escherichia Coli Membranes by Graphene Nanosheets. *Nat. Nanotechnol.* 2013, 8, 594-601.
- (29) Yin, J.; Zhu, G.; Deng, B. Graphene oxide (GO) enhanced polyamide (PA) thin-film nanocomposite (TFN) membrane for waterpurification. *Desalination* 2016, 379, 93-101

Chapter 3. pH-Responsive Polyethersulfone Ultrafiltration Membrane with Low Bio-Fouling and Low Protein-Fouling

3.1 Introduction

Ultrafiltration (UF) is an important separation technique that is widely used in industries, such as water treatment, pharmaceuticals, blood dialysis, food and beverage manufacturing and so on. The key component of the UF process is the separation membrane. UF membranes typically have an average pore size of 10 nm and are effective in rejecting proteins, viruses and small colloids. Commercial UF membranes are commonly made of polymer materials such as polyethersulfone (PES), polyvinylidene fluoride (PVDF), and polypropylene (PP) due to their low-cost, good processability and flexibility. However, due to their intrinsic hydrophobicity, these polymer membranes are susceptible to fouling, which is one of the biggest issues in the membrane industry that increases production costs and lowers productivity. Fouling occurs when substances in the feed source such as proteins, polysaccharides and microorganisms deposit and anchor onto the membrane surfaces during filtration operation via hydrophobic interactions, resulting in increasing impedance to water permeation, thus lowering flux. The fouling from microorganisms, also known as biofouling, causes the most serious problem because once bacteria attach to the membrane surface, they can proliferate rapidly in the presence of nutrients from other foulants and form biofilms which are difficult to remove by cleaning procedures. Therefore, a good antifouling membrane should not only resist the deposition of bacteria and proteins, but also inhibit the propagation of bacteria.

The commonly used approaches to address the fouling issue are by increasing the membrane hydrophilicity and antibacterial properties. A hydrophilic membrane tends to

have a thin layer of water molecules spontaneously bind to its surfaces that acts as a physical barrier to prevent the attachment of foulants. Antibacterial membrane surfaces have been proven to be effective in deactivating bacteria and limiting their growth. Most membrane modification studies have been carried out on PES membranes although polyethersulfone is relatively less chemically inert compared to polyvinylidene fluoride and polypropylene. PES membrane modifications carried out so far include surface physical coatings^{1,2}, blending³⁻⁶ and covalent grafting of hydrophilic/antibacterial materials⁷⁻⁹.

Besides increasing the hydrophilicity and bacteriacidal ability of the membrane, a new mechanism for creating antifouling membranes known as fouling-release has been recently developed^{10,11}. These fouling-release membranes possess dynamic membrane surfaces that are responsive to external environmental changes such as electricity¹², ionic strength^{13,14}, pH^{15,16} and temperature¹⁷. These stimuli-responsive materials make the membrane surfaces dynamic with the change of hydrophilicity/hydrophobicity and/or surface conformation in response to environmental changes. Such properties will contribute to weakening of the interfacial bonds between the membrane surfaces and the deposited foulants, making the foulants easy to wash away by the shear forces from hydrodynamic mixing during the washing step. Chuo *et al.*¹² prepared poly(tetrafluoroethylene) membranes possessing ferrocene pendant groups cross-linked with β -cyclodextrin and showed that the protein on the fouled membrane surface can be detached via an electrically induced de-cross-linking reaction of the ferrocene- β -cyclodextrin linkages. Meng *et al.*¹⁴ reported that polyamide reverse osmosis membranes tethered by zwitterionic polymers exhibit a response to salts and the fouled membranes

can restore most of their flux after a brine wash due to the swelling of the zwitterion chains which drives the foulants away. Ye *et al.*¹⁷ fabricated thermo-responsive polymers on polypropylene surfaces and showed that the contraction of the polymer chains when exposed to higher temperature will facilitate foulant desorption. These fouling-release membranes have proven to be highly effective in self-cleaning with an adjustment of the feed water parameters. Perhaps surprisingly, to the extent of our knowledge, there have not been any studies done on using pH-responsive materials to modify filtration membranes in order to achieve fouling-release effects.

In this work, tetraaniline (TANi) is used as a pH-sensitive molecule to be grafted onto commercial PES UF membranes in order to create hydrophilic antimicrobial PES membranes with self-cleaning properties. TANi is an oligomer form of polyaniline with similar acid doping/base dedoping properties.¹⁸ As an oligomer, TANi is more processable due to enhanced solubility in common organic solvents.¹⁹ Furthermore, the hydrophilic²⁰ and antimicrobial²¹ nature of TANi make it an even more interesting candidate for filtration membrane modification. By attaching TANi onto PES membranes, the foulant layer deposited onto the membrane surfaces can be disrupted and loosened during an acid wash since TANi chains will become protonated with positive charges inducing conformational changes.

3.2 Synthesis of Azide Functionalized Tetra-aniline and Its Characterization

TANi was first synthesized following the procedure described by Zhang *et al.*²² N-phenyl-1,4-phenylenediamine (dimer, 0.1 mol) was suspended in 500 mL 0.1 M HCl before reacting with 0.1 mol of FeCl₃ dissolved in 100 mL 0.1 M HCl at room

temperature for 2 hours. The as-synthesized product suspension was then dedoped by ammonia hydroxide and purified using centrifugation and dialysis before drying in a vacuum oven overnight.

TANi was grafted onto PES membranes via a bifunctional perfluorophenyl azide (PFPA) linkage. PFPA molecules have two reactive functional groups on both ends of the benzene ring. The azide group is UV-sensitive and will decompose into nitrogen gas, leaving a nitrene radical group that's highly reactive and can form stable covalent bonds with functional groups such as alkyl, amine, unsaturated carbon bonds and benzene rings (abundant in the PES structure).²³ The other end of the functional group is usually an acyl halide or a sulfonyl halide that can be readily modified with other functional materials. In this way, functional materials can be grafted onto inert surfaces using PFPA molecules as the bridge.²⁴ In this study, pentafluorobenzenesulfonyl chloride was used to react with TANi followed by an azidation reaction with sodium azide. The reaction scheme is shown in Figure 3.1. The final product PFPA-TANi was purified by liquid-liquid extraction before drying in a vacuum oven overnight and stored in an aluminum foil wrapped vial, due to the light sensitive nature of the azide group.

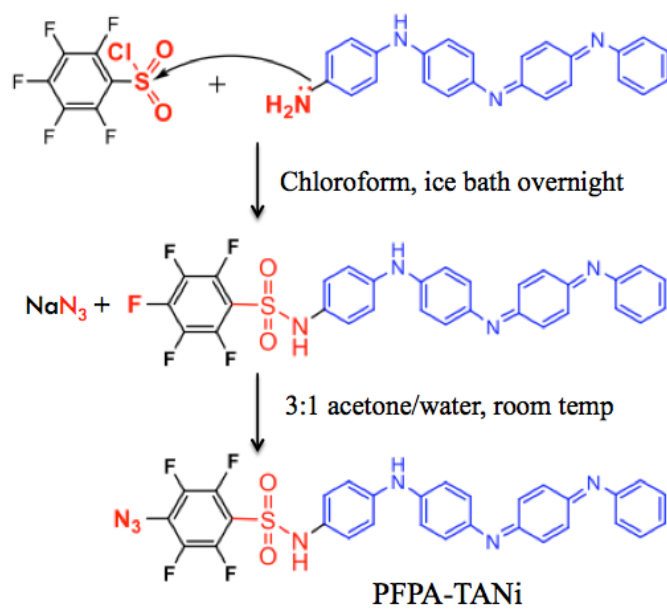


Figure 3.1 Synthesis route for the PFPA-TANi molecule.

^{19}F -NMR spectroscopy was conducted on a Bruker AV 300 NMR instrument for the starting pentafluorobenzenesulfonyl chloride material, the product from the first reaction and the final product. Spectra were recorded in a solution of deuterated acetone at room temperature. Figure 3.2 shows that the starting material pentafluorobenzenesulfonyl chloride has 3 distinctive fluorine peaks with a ratio of 2:1:2, which matches with its chemical structure. The first product also showed 3 distinctive fluorine peaks with a ratio of 2:1:2 with apparent chemical shifts comparable to those of the starting material. Such chemical shifts are due to the addition of tetra-aniline that changes the chemical environment of the nearby fluorine groups. The final PFPA-TANi product only had 2 fluorine peaks due to the substitution of fluorine on the para-position. The 2 peaks had a ratio of 1:1 demonstrating that the azidation reaction was specific and only occurred at the para-position.

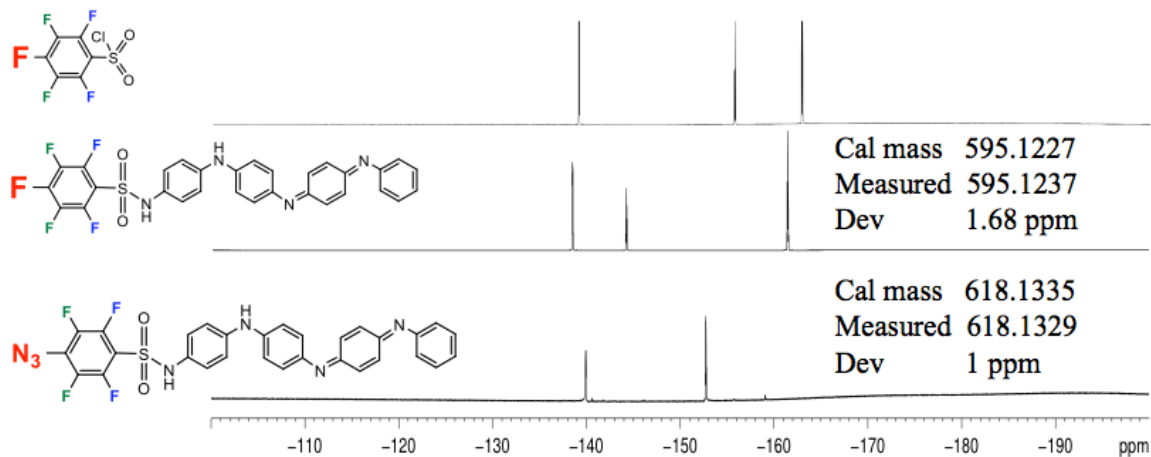


Figure 3.2 ^{19}F -NMR spectra for the starting material, the first step reaction product and the final product as well as the molecular weight of the two products measured by ESI mass spectroscopy.

Molecular weight of the two products were measured using electrospray ionization mass spectroscopy (ESI). The calculated mass of product I is 595.1227 and its measured mass is 595.1237 with only 1.68 ppm deviation. Likewise, the calculated mass of final product is 618.1335 and its measured mass is 618.1329 with barely 1 ppm deviation. These two measurements both gave convincing results within the maximum allowed deviation of 5 ppm. Together with NMR results, it is safe to conclude that our synthesis and purification were successful and gave pure PFPA-TANi product that's ready for use.

3.3 Membrane Surface Modifications

Dried PFPA-TANi powder was dissolved in 200 proof ethanol to make PFPA-TANi solutions with different concentrations. In order to modify the commercial PES UF membrane, a blank PES membrane was dipped in the PFPA-TANi solution before being taken out and placed under a hand-held UV lamp (wavelength 254 nm) for 1 min at room

temperature followed by thorough rinsing with ethanol. The modification scheme is illustrated in Figure 3.3.

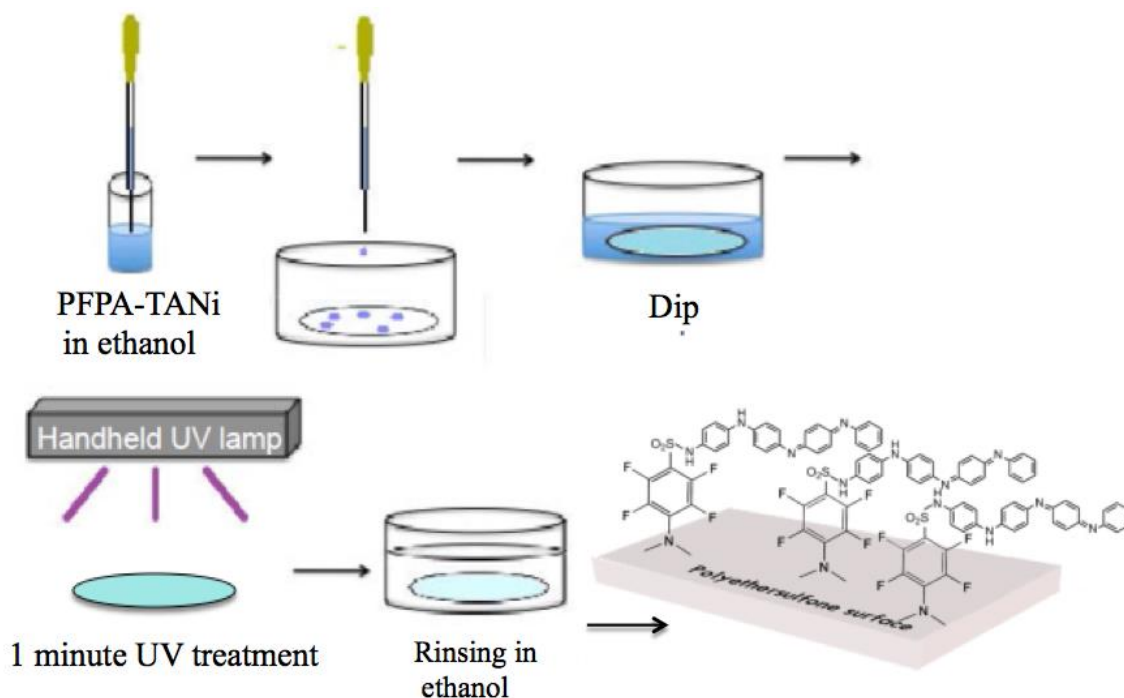


Figure 3.3 Modification scheme for the commercial PES UF membrane using a PFPA-TANi ethanol solution.

The modified PES membrane took on the color of TANi and appeared blue as shown in Figure 3.4a middle compared to the white color of the blank PES membrane. When exposed to acid, the modified PES membrane turned green due to the acid doping of tetra-aniline, shown in Figure 3.4b. As a control experiment, a blank PES membrane was coated with a PFPA-TANi solution for 1 min without exposure to UV light before fully rinsing with ethanol. This control PES membrane showed no color change which demonstrated the effectiveness of the rinsing step and that the azide group must be activated under UV light.

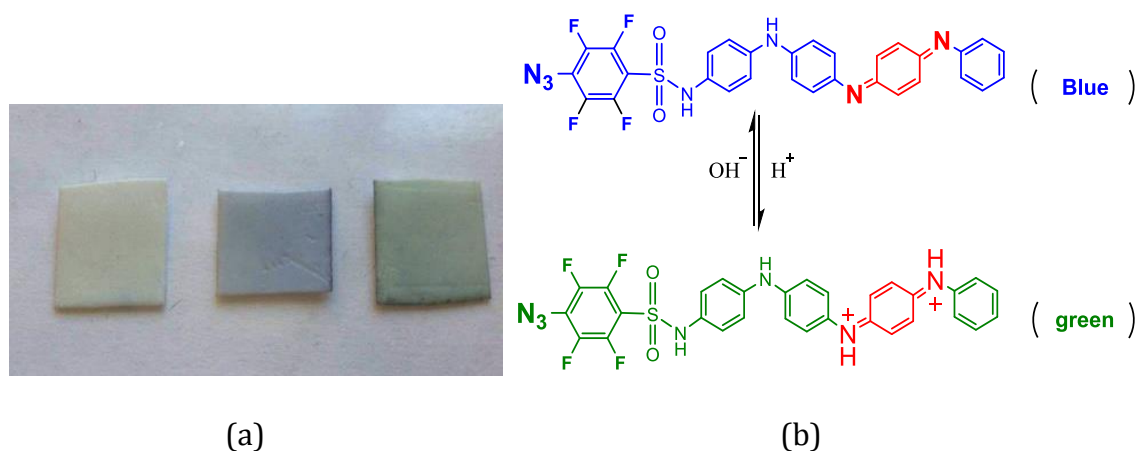
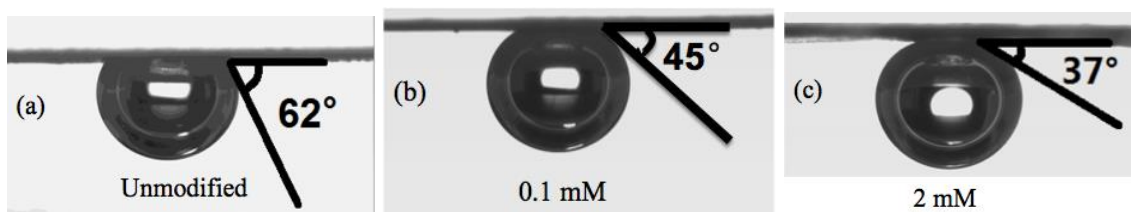


Figure 3.4 (a) Pictures of an unmodified PES membrane (left), a PES membrane modified with a 2 mM PFPA-TANi solution (middle) and a modified PES membrane doped with HCl; (b) an illustration of PFPA-TANi doping/dedoping chemistry.

3.4 Results

A KRÜSS DSA 10 goniometer was employed to measure the contact angle values in order to determine the membrane hydrophilicity. The captive bubble method was chosen over the Sessile drop method so that the membranes remain wet during the measurement without the change of morphology associated with drying. From Figure 3.5, one can see that the modification of PES membrane surfaces with PFPA-TANi was effective in lowering the contact angle of the membrane surfaces. Membranes modified using 0.1 mM concentration of PFPA-TANi showed a contact angle of 45° compared to that of unmodified PES membrane at 62°. A higher concentration (2 mM) of PFPA-TANi solution was able to lower the contact angle even more to 37°, manifesting enhanced hydrophilicity.



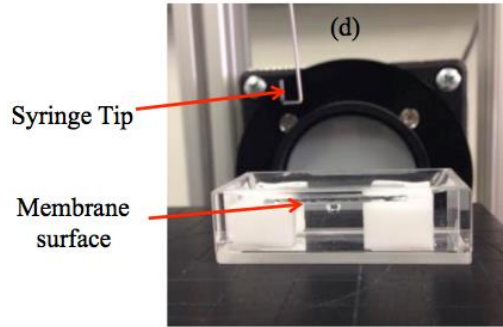


Figure 3.5 Contact angle images of (a) an unmodified PES membrane, (b) a PES membrane modified with a 0.1 mM PFPA-TANi ethanol solution and (c) a PES membrane modified with a 2 mM PFPA-TANi ethanol solution using the captive bubble technique setup as shown in (d).

In order to test the effects of increased hydrophilicity on membrane anti-biofouling properties, *E. coli* was used as a model microorganism and allowed to be in contact with different membranes before quantification of the deposited bacteria cells. *E. coli* cell cultures were first suspended in LB broth and incubated at 35 °C while shaken at 150 rpm for 24 hours in a New Brunswick Scientific I 24 Incubator Shaker. Cells were then harvested and diluted with fresh LB broth to a concentration of 4×10^7 cells/ml. Membrane cutouts of approximately 1 cm² were incubated in an *E. coli* suspension for 24 hours at room temperature followed by rinsing with a 0.9% saline solution. Membrane coupons were then immersed and stained in SYTO 9 or propidium iodide (PI) dye solution (live/dead BacLight Bacterial Viability Kit L13152, Molecular Probes) for 15 min. SYTO 9 (green) labels both live and dead bacteria cells by binding to their cell membranes, while PI (red) labels only the dead cells because it can only penetrate damaged cell membranes. Images with bacteria deposition were taken using a fluorescence microscope (Olympus BX5) and a 4 × CCD camera (FVIEW-II, Soft Imaging System, USA). Using Image J software, the surface coverage of the total attached cells and dead attached

cells can be quantified by dividing the amount of colored pixels by the total amount of pixels in the image. Afterwards, the surface coverage of live attached cells can be calculated by subtracting the percentage of dead attached cells from that of total attached cells.

Table 3.1 Fluorescence images and percentages of *E. coli* cells on the unmodified PES membranes and membranes modified using 0.1 mM and 2 mM PFPA-TANi solutions.

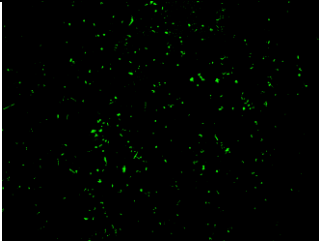
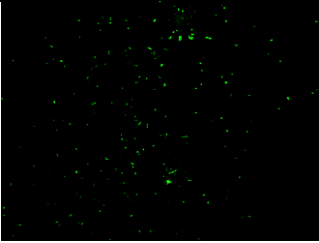
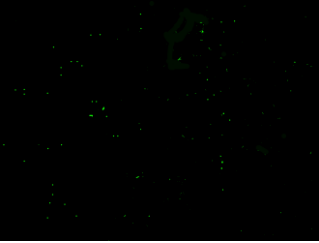

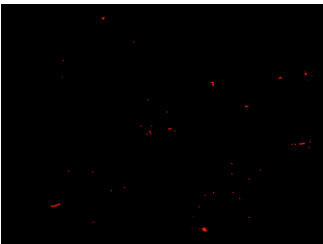

	<i>unmodified</i>	<i>0.1 mM modified</i>	<i>2 mM modified</i>
Total			
	0.93%	0.45%	0.14%
Dead			
	0.06% (7% of total)	0.13% (29% of total)	0.13% (94% of total)

Table 3.1 shows that the modified PES membrane had less biofouling compared to the unmodified. The amount of total biofouling on the 2 mM modified PES membrane (0.14%) was 6 times less compared to that of an unmodified membrane (0.93%). The

enhanced hydrophilicity of the modified membrane surface led to the suppression of hydrophobic interactions between the bacteria foulants and the membrane surfaces, which inhibits the deposition of *E. coli* cells. Furthermore, among all the bacteria cells that were deposited on the membrane modified by 2 mM PFPA-TANi, almost all (94%) of them were deactivated. In contrast, only 7% of the bacteria on the unmodified PES membrane were dead. This proves that the antibacterial ability of TANi. IT may not be surprising that TANI exhibits antibacterial properties because its polymer form, polyaniline, has been shown to be antibacterial due to the electrostatic adherence between slight positively charged polyaniline and negatively charged bacterial cell membranes. Therefore, the enhanced hydrophilicity and antibacterial property of PFPA-TANi grafted PES membranes contribute to their anti-biofouling ability.

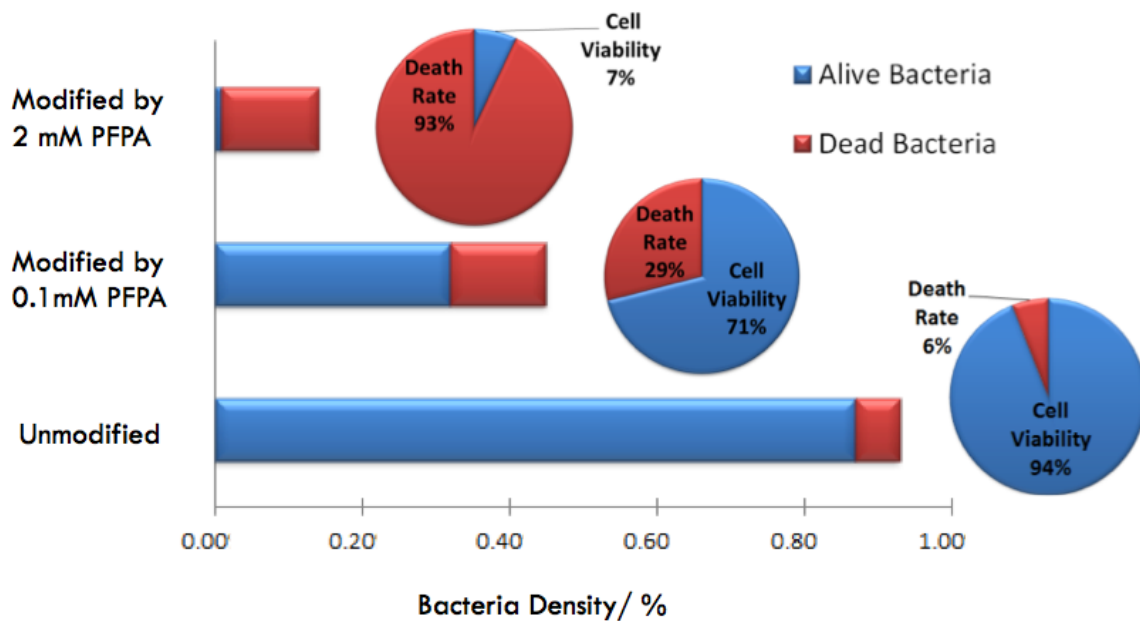


Figure 3.6 Bar and pie chart showing the live/dead bacteria density difference on the modified PES membranes and those modified using 0.1 mM and 2 mM PFPA-TANi solutions.

Fouling-release ability was evaluated using an in-house cross-flow system as illustrated in Figure 3.7. A membrane is placed in the cross-flow cell (6). Once pump (2) is turned on, a feed source from the feed tank (1) is pumped into the cross-flow cell, contacting the membrane active side and creating certain pressure that can be adjusted using the pump (2) setting and flow meter (4) gauge. Water will permeate through the membrane and be collected in the container placed on the electronic balance (7). The balance is connected to a computer that monitors the dynamic change of flux by converting the mass change into flux. Three pressure gauges are placed on the feed, retentate and permeate side of the membrane. During the test, pure DI water (pH = 7.0) was first used to compact the membranes at 16 psi for 3 hours until a stable flux was reached. Then the feed source was changed to 100 ppm Bovine Serum Albumin (BSA) solution while maintaining a constant pressure and solution pH. Membranes were fouled for 90 min with the trans-membrane pressure (TMP) change recorded throughout the test. TMP is calculated using the equation below:

$$\text{TMP} = (\text{P}_{\text{feed}} + \text{P}_{\text{retentate}})/2 - \text{P}_{\text{permeate}}$$

When the membrane gets fouled, the resistance to water permeation increases. At constant pressure, there will be less water going into the permeate side. This will reduce the $\text{P}_{\text{permeate}}$ and increase the TMP. Therefore, by monitoring the TMP change, one can see the differences between fouling rates among the unmodified and modified PES membranes. An HCl (pH = 2) wash was conducted after the first fouling stage for 5 min before changing the feed back to 100 ppm BSA (pH = 7.0) while monitoring the TMP change again for 90 min. During the second wash step, DI water (pH = 7.0) was used for 5 min before switching the feed back to BSA solution again for 90 min.

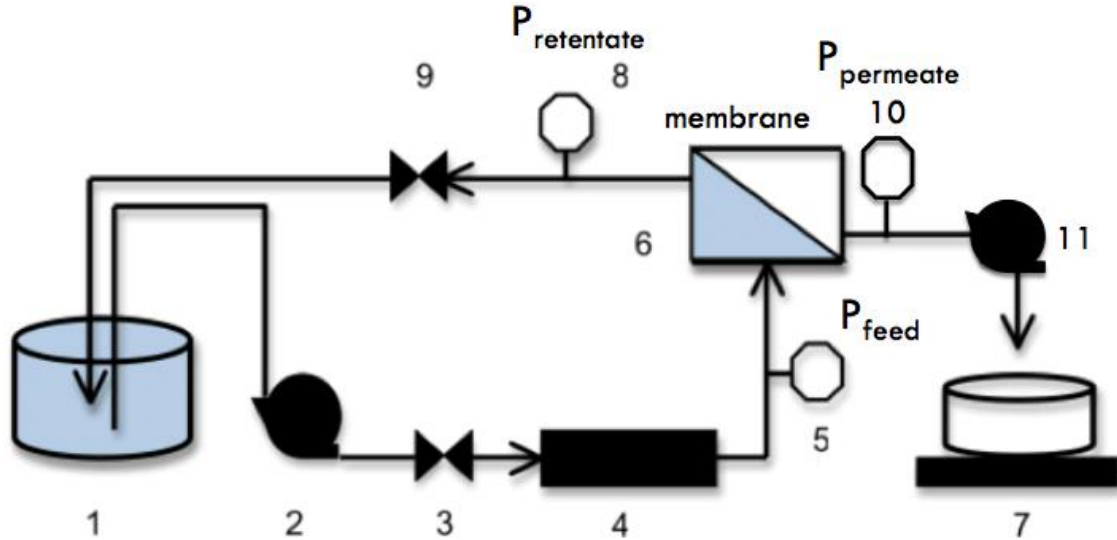


Figure 3.7 Cross-flow system illustration of 1. Feed tank; 2,11. Pump; 3,9. Valve; 4. Flow meter; 5,8,10. Pressure gauge; 6. Cross-flow cell; and 7. Electronic balance.

From Figure 3.8, it can be seen that as soon as BSA is introduced, the TMP starts to increase rapidly for both the unmodified and modified PES membranes due to the deposition of BSA particles on the membrane surfaces. After the first acid wash, the TMP of the modified PES decreased immediately and the starting TMP of the second fouling stage was only 1 psi higher than the starting TMP of the first fouling stage (Table 3.2). In contrast, after the acid wash, the starting TMP of the second fouling stage for the unmodified PES was 2.6 psi higher than that of the first fouling stage. This means that the acid wash for the TANi grafted PES membrane was very effective in restoring the TMP, i.e., the loss of flux as lower TMP equals higher flux. After the second wash using only DI water for 5 min, the starting TMP for the third fouling stage was 2 psi higher than that of the previous fouling stage for modified PES. In comparison, after the DI water wash, the starting TMP for the third fouling stage was 2.8 psi higher than that of the previous fouling stage for unmodified PES. This shows that a water wash was not as effective as

an acid wash for TANI modified PES membranes. Moreover, the overall TMP increase after four and a half hours of operation was 3.5 psi for the modified PES and 7.5 psi for the unmodified PES, proving the fouling resistance of the TANI grafted PES membranes.

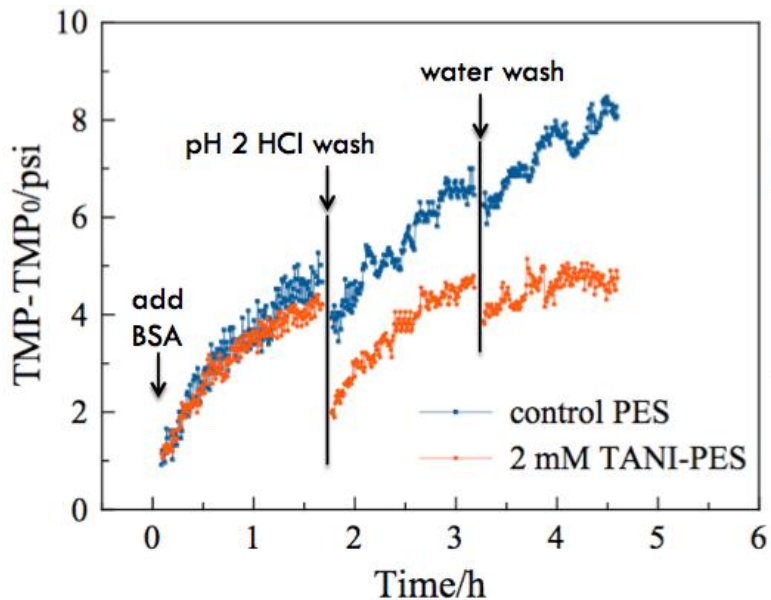


Figure 3.8 Normalized TMP change for an unmodified PES membrane and a 2 mM PFPA-TANI modified PES membrane during three BSA fouling stages.

Table 3.2 Starting TMP difference after each cleaning step compared to the previous fouling stage.

	unmodified	2 mM modified
Acid wash $\Delta_{\text{Starting TMP}}$	2.6 psi	1.0 psi
Water wash $\Delta_{\text{Starting TMP}}$	2.8 psi	2 psi

The fouling-release mechanism for the TANi grafted PES membrane can be understood as follows. When the pH is neutral, as is the case with most water treatment processes, the TANi chains on the PES membrane surface are uncharged (Figure 3.10). All the TANi chains will be collapsed with shorter chain length overlapping each other on the membrane surfaces. Once acid is introduced to the membrane surface, the TANi chains will be doped and become positively charged. Electrostatic repulsion will alter the morphology and configuration of the TANi layer, making them extend and more upright positioned. It's worth noting that the TANi layer grafted onto the membrane surfaces will not be just a single molecule long as the azide reaction is highly nonspecific so that PFPA-TANi molecules can easily bond to the benzene rings of the other PFPA-TANi chains that are already linked to the PES membrane. Further evidence is provided by the intense blue/green color of the modified dedoped/doped TANi-PES membranes because the color of a single-layer of TANi should not be visible. The long chains consisting of multiple TANi molecules can actually contribute to the fouling-release properties of the modified membranes because longer chains can cause more dramatic changes in chain length and configuration during acid washing. Similar to the thermo-responsive fouling-release mechanism, this conformation change will disrupt and loosen the fouling layer, weakening the interfacial bonds between the foulants and membrane surface, thus making the foulants more easily washed away by the cross-flow shear forces.

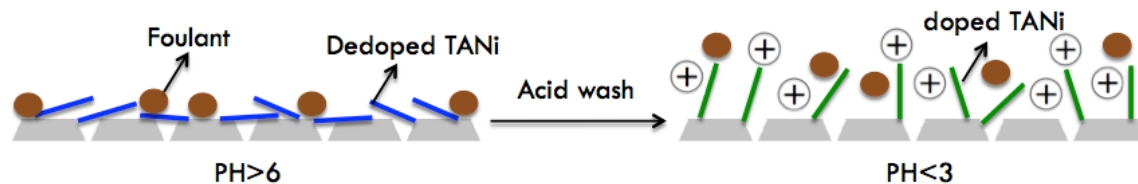


Figure 3.9 Proposed mechanism for the fouling-release ability of TANi grafted PES membrane.

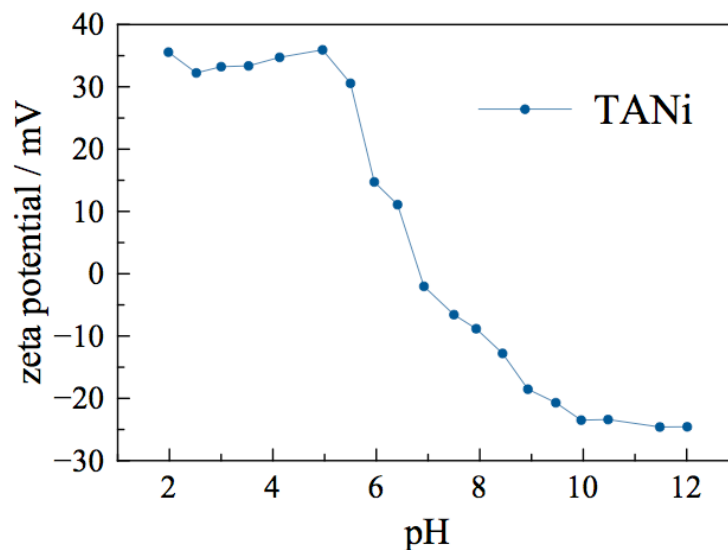


Figure 3.10 Zeta potential plot of TANi material at various pH's.

3.5 Conclusions

Tetraaniline has, for the first time, been used for PES UF membrane surface modifications. It can be covalently grafted onto PES material by functionalizing TANi with azide end groups followed by UV treatment. The modified PES membranes display enhanced hydrophilicity and antibacterial properties that prevent bacteria cell adhesion and limit the proliferation of attached bacteria cells. The TANi layer is also pH-responsive and will undergo dynamic conformation change when exposed to different pH's. Such conformation changes have been shown to be effective in fouling-release,

which contributes to the overall anti-fouling ability of the TANI modified PES membranes.

3.6 References

- (1) L. Liu, D. Y. W. Di, H. Park, M. Son, H. Hur and H. Choi, *RSC Adv.*, 2015, 5, 7340-7348.
- (2) L. Bai, H. Liang, J. Crittenden, F. Qu, A. Ding, J. Ma, X. Du, S. Guo and G. Li, *J. Membr. Sci.*, 2015, 492, 400-411.
- (3) L. Zhu, L. Zhu, Y. Zhao, Bao, Zhu and Y. Xu, *J. Mater. Chem. A*, 2014, 2, 15566-15574.
- (4) S. Zhu, M. Shi, S. Zhao, Z. Wang, J. Wang and S. Wang, *RSC Adv.*, 2015, 5, 27211-27223.
- (5) Q. Zhao, J. Hou, J. Shen, J. Liu and Y. Zhang, *J. Mater. Chem. A*, 2015, 3, 18696-18705.
- (6) X. Zhan, G. Zhang, X. Chen, R. He, Q. Zhang and F. Chen, *Ind. Eng. Chem. Res.*, 2015, 54, 11312-11318.
- (7) Y. Zhao, P. Zhang, J. Sun, C. Liu, Z. Yi, L. Zhu and Y. Xu, *J. Colloid Interface Sci.*, 2015, 448, 380-388.
- (8) M. D. Angione, T. Duff, A. P. Bell, S. N. Stamatina, C. Fay, D. Diamond, E. M. Scanlan and P. E. Colavita, *ACS Appl. Mater. Interfaces*, 2015, 7, 17238-17246.
- (9) J. Wang, X. Gao, Q. Wang, H. Sun, X. Wang and C. Gao, *Appl. Surf. Sci.*, 2015, 356, 467-474.
- (10) M. Elimelech and W. A. Philip, *Science*, 2011, 333, 712-717.
- (11) J. A. Callow and M. E. Callow, *Nat. Commun.*, 2011, 2, 244
- (12) T. Chuo, T. Wei, Y. Chang and Y. Liu, *ACS Appl. Mater. Interfaces*, 2013, 5, 9918-9925
- (13) Y. Zhao, P. Zhang, J. Sun, C. Liu, L. Zhu and Y. Xu, *J. Membr. Sci.*, 2016, 510, 306-313.
- (14) J. Meng, Z. Cao, L. Ni, Y. Zhang, X. Wang, X. Zhang and E. Liu, *J. Membr. Sci.*, 2014, 461, 123-129.
- (15) K. Gao, L. T. Kearney, R. Wang and J. A. Howarter, *ACS Appl. Mater. Interfaces*, 2015, 7, 24839-24847.
- (16) Z. Han, C. Cheng, L. Zhang, C. Luo, C. Nie, J. Deng, T. Xiang and C. Zhao,

Desalination, 2014, 349, 80-93.

(17) Y. Ye, J. Huang and X. Wang, ACS Appl. Mater. Interfaces, 2015, 7, 22128-22136.

(18) Y. Wang, H. D. Tran, L. Liao, X. Duan and R. B. Kaner, J. Am. Chem. Soc., 2010, 132, 10365-10373.

(19) Z. Wei and C. F. J. Faul, Macromol. Rapid Commun., 2008, 29, 280-292.

(20) B. Guo, A. Finne-Wistrand and A. Albertsson, Macromolecules, 2012, 45, 652-659.

(21) N. Shi, X. Guo, H. Jing, J. Gong, C. Sun and K. Yang, J. Mater. Sci. Technol., 2006, 22, 289-290.

(22) W. J. Zhang, J. Feng, A. G. Macdiarmid, A. J. Epstein, Synth. Met., 1997, 84, 119-120.

(23) L. Liu and M. Yan, Acc. Chem. Res., 2010, 43, 1434-1443.

(24) B. T. McVerry, M. C. Y. Wong, K. L. Marsh, J. A. T. Temple, C. Marambio-Jones, E. M. V. Hoek and R. B. Kaner, Macromol. Rapid Commun., 2014, 35, 1528-1533.

Chapter 4. Novel Chlorine Resistant Low-fouling Ultrafiltration Membrane Based on a Hydrophilic Polyaniline Derivative

4.1 Introduction

An abundant supply of fresh water is a fundamental requirement for municipal, industrial and agricultural use. However, rising populations and source contamination have exerted increasing stress on fresh water supplies. Along with pressure from stricter regulations for clean water, improvements in water treatment technology are critical to sustain future generations.^{1,2}

Membrane-based filtration is the most important and widely used method for water purification due to its ability to effectively remove impurities in feed sources on a large scale. Generally, membranes can be categorized into four types: microfiltration (MF), ultrafiltration (UF), nanofiltration (NF) and reverse osmosis (RO) based on their pore size and ability to reject a variety of materials for different applications.¹

Typical UF membranes have an average pore size of ~ 10 nm³. In waste water treatment, ultrafiltration is used to reject pathogenic microorganisms such as viruses, bacteria, protozoa and other colloids³ and can serve as a pre-treatment step for desalination.^{1,4} UF membranes are commonly used for separations in the chemical, pharmaceutical, food, and beverage industries, and are an integral component in blood dialysis.³

When a membrane is used for separation, the flux gradually decreases during operation as the membrane is fouled by inorganic particulates, organic matter and/or biological microorganisms.¹ The susceptibility to fouling by organic

elements varies among different membrane materials due to hydrophobic interactions between the foulant and the surface of the polymeric membrane. Thus, membrane hydrophilicity has been linked to a membrane's propensity to foul, i.e. hydrophilic membranes generally foul less than hydrophobic membranes.^{5,6} A more hydrophobic membrane allows foulants to adhere strongly via van der Waals interactions to the membrane surface that leads to irreversible membrane fouling.⁷ Chemical cleaning is typically used to remove biofilms and adsorbed organic material from the membrane surfaces. Cleaning treatments restore membrane performance to regain flux loss during operation due to membrane fouling. Common chemicals used for cleaning membranes include caustics, oxidants/disinfectants, acids, chelating agents and surfactants.⁸ Chlorine bleach (sodium hypochlorite), is popular in industry for its commercial availability, low cost and ability to effectively reduce fouling when added to the feed solution. Strong oxidants such as hypochlorite not only kill microorganisms, but also oxidize functional groups in natural organic matter into more water-soluble moieties, allowing the new species to be readily washed away during operation. However, strong oxidants simultaneously attack chemical bonds found within the polymeric membrane material, negatively affecting the membrane properties.⁹⁻²¹

Prior studies have suggested that chlorine cleaning of UF membranes often causes more harm than good.¹⁵⁻¹⁹ Multiple cleaning treatments facilitate chain scission of the membrane polymer and deteriorates the mechanical strength of the membrane, leading to failure. Furthermore, these treatments can increase fouling due to changes in surface charge that increase interactive forces between the

foulant and the membrane surface.¹⁵ Similarly with polymeric reverse osmosis membranes, chemical attack by chlorine on polyamide RO membranes results in membrane failure with enhanced passage of salt and water.²⁰⁻²⁴ In response, attempts have been made to modify membrane materials in order to impart resistance to chlorine degradation. Prior research has demonstrated that small molecules and polymers containing secondary arylamines (Figure 4.1) undergo Orton rearrangements²³ when exposed to sodium hypochlorite, leading to chain scission. When n-substituted (tertiary) arylamine derivatives are used, Orton rearrangement is hindered and the small molecules and polymers exhibit higher chlorine tolerance than their di-substituted counterpart.²⁰⁻²⁴

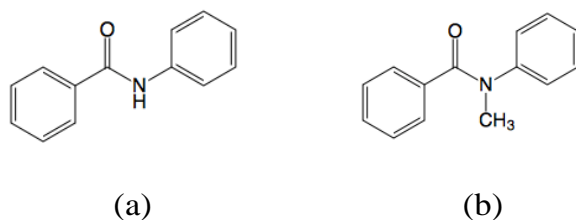


Figure 4.1 A polyamide unit with a secondary amine (a) is more susceptible to chlorine attack than that consisting of a tertiary amine (b).

Recently, conducting polymers and their derivatives have been extensively examined for their potential use in water treatment membranes due to their hydrophilic properties, thermal and chemical stability, low-cost, facile synthesis and straightforward modification via doping.^{5,6,25-34} Polyaniline (PANi), one of the most widely studied conducting polymers, has been blended with the commercial UF membrane material polysulfone (PSf) to form composite UF membranes with enhanced hydrophilicity and permeability.³⁰⁻³³ Pure PANi has also been used to form UF membranes; however, pure PANi membranes do not demonstrate

sufficient protein selectivity for typical UF operation.³³ By adding a secondary amine such as 4-methylpiperidine (4-MP) into the PANi casting solution, the processability of PANi is improved, and casting solutions of higher concentration can be achieved to produce membranes with higher selectivity.³⁴ Unfortunately, the advantageous hydrophilicity of PANi is lost due to the remaining 4-MP in the resulting membrane, as indicated by NMR experiments. In another study, sulfonated PANi (SPANi) was blended with PSf at low loadings to form UF membranes that have shown excellent hydrophilicity and high flux restoration after cleaning only with water.⁵

Despite the improvements in hydrophilicity and performance, the redox properties of PANi cause the polymer to be highly susceptible to chlorine degradation. In its emeraldine base form, approximately half of the aryl rings in the backbone are benzenoid containing secondary amine groups that are vulnerable to attack by sodium hypochlorite.²⁰⁻²⁴ In contrast, n-substituted PANi does not contain secondary amine groups. The reaction rate between hypochlorite and a primary/secondary amine is 5 orders of magnitude higher than the reaction between hypochlorite and a tertiary amine.³⁵ Thus, n-substituted PANi is a suitable candidate for the fabrication of chlorine resistant UF membranes. Thus, our goal is to synthesize an n-substituted PANi-derived membrane material that possesses hydrophilic properties and chlorine resistance to both reduce the rate of fouling and tolerate chemical cleaning conditions.

4.2 N-substituted Polyaniline

Several types of n-substituted PANi derivatives have been reported in the literature.^{36,40-43} Among these, n-alkyl PANi is the most common form. Because the addition of alkyl chains to the backbone increases hydrophobicity, we utilize a hydrophilic poly(n-2-hydroxyethyl aniline) (n-PANi) as a polyaniline derivative to fabricate UF membranes.

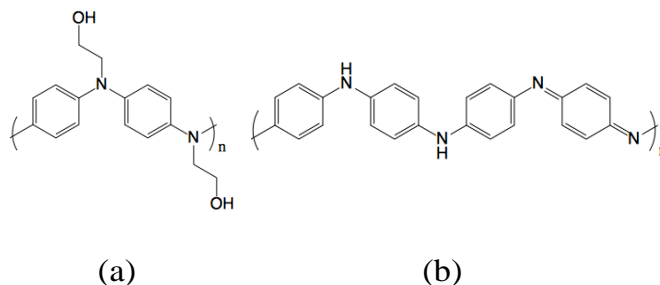


Figure 4.2 The polymer structures of (a) n-PANi and (b) PANi.

n-PANi was prepared from n-(2-hydroxyethyl) aniline via chemical oxidative polymerization. The monomer and APS were dissolved separately in 1.0 M HCl aqueous solutions. The solution of APS was added drop-wise at room temperature into the monomer solution under vigorous stirring. The reaction was allowed to proceed for 24 hours. n-PANi was purified from the crude mixture via centrifugation at 3000 rpm for 5 minutes followed by dialysis using dialysis tubing with 12,000-14,000 MWCO (Fisherbrand) in a deionized (DI) water bath. The water bath was replaced with fresh DI water every two hours until the pH of the water bath remained neutral. The dark green polymer powder was isolated by removing the polymer dispersion from the dialysis bag and dried in vacuo at 60 °C overnight (yield = 65%).

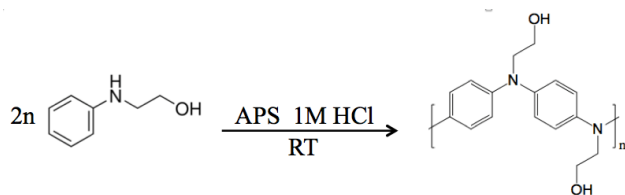


Figure 4.3 Polymerization scheme for n-PANi.

PANi was prepared following the procedure described by Guillen *et al.*³³ It was synthesized via chemical oxidative polymerization from a 0.5 M solution of H₂SO₄ using APS as an oxidant with a 4:1 monomer to oxidant ratio. PANi was recovered with a microfiltration (0.45 μm membrane, Millipore) and washed with NaOH and DI water. The violet PANi dispersion was dried *in vacuo* at 60 °C overnight (yield = 25%).

The molecular weight of as-synthesized n-PANi was measured using a Brookhaven NanoBrook 90Plus Molecular Weight Analyzer equipped with a 660 nm diode laser for light scattering experiments. A series of n-PANi/NMP solutions with different concentrations were made for the analysis. Scattered light intensities were measured at several angles for each of the solutions and the pure solvent. Molecular weight can thus be calculated based on the relationship between scattered light intensities and solution concentrations.^{49,50}

To determine molecular weight, dynamic light scattering was used (DLS), giving a molecular weight for the synthesized n-PANi of 17.2 kDA, which is lower than the reported value for PANi⁵². In this case, molecular weight of the synthesized PANi could not be measured with DLS due to PANi's strong absorption at 660 nm, which is the wavelength of the DLS laser (see the later

discussion of UV-Vis, Fig. 8). However, PANi synthesized by chemical oxidative polymerization typically produces polymers in the (20-40) kDa range.³³

4.3 Membrane Fabrication

An n-PANi casting solution was prepared by dissolving 30 wt% of n-PANi powder in 70 wt% NMP. The pure PANi casting solution was prepared following the procedure by Guillen *et al.*³⁴ by dissolving 21 wt% of PANi in 11.67 wt% of 4-MP and 67.33 wt% of NMP as a co-solvent. The weight percent of PANi and 4-MP were chosen to maintain 2 moles of 4-MP: 1 mole PANi base tetramer (0.547 g 4-MP: 1 g PANi tetramer). Membranes were hand-cast with a doctor blade (Gardco Adjustable Micrometer Film Applicator) from polymer solutions onto a non-woven polyester fabric (Hirose, Japan) using a blade height of 152 μm . As-cast solution films were immediately immersed in a DI water coagulation bath to induce polymer precipitation via non-solvent induced phase inversion.⁴⁴ The membrane films were left in the coagulation bath overnight before being transferred to a DI water bath and stored in a refrigerator at 4 °C.

PANi is known to gel rapidly at relatively low solution concentrations, even as low as 5 wt%.³⁷ In order to achieve a high concentration for casting highly selective membranes, secondary amines such as 4-MP have been used to prevent PANi solutions from gelling.^{38,39} Unfortunately, the addition of 4-MP results in a loss of hydrophilicity.³⁴ Due to the aliphatic side chains in the polymer structure,^{36,43} n-PANi derivatives are generally very soluble in common organic solvents such as NMP and DMSO. With regard to membrane casting, n-PANi can be readily dissolved in NMP at high concentration without gelation.

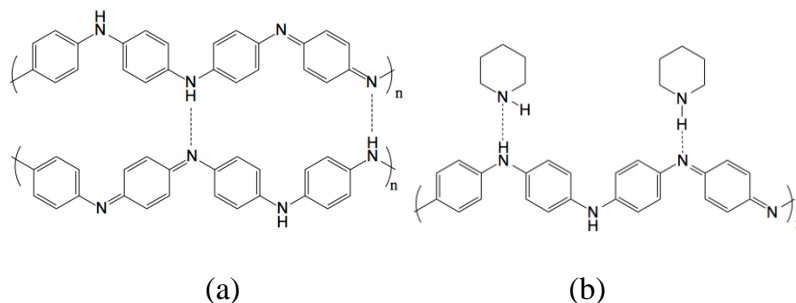


Figure 4.4 (a) Gelling of PANi is caused by intermolecular hydrogen bonding. (b) 4-MP inhibits PANi from gelling by taking up some of the hydrogen bonding sites.

We found that n-PANi solution concentrations as high as 30 wt% can be achieved without gelation. n-PANi is comprised mostly of aniline rings in its benzenoid form with a flexible aliphatic side chain which increases the flexibility of the polymer backbone, compared to PANi. This flexibility prevents two adjacent polymer chains from forming a critical number of intermolecular hydrogen bonds that causes gelation. Additionally, steric hindrance from the long flexible side chains increases the distance between two adjacent polymer chains, which further suppresses intermolecular polymer interactions.

The n-PANi membrane was cast with a 30 wt% polymer solution (higher than that of PANi membrane at 21%) to increase the casting solution viscosity to make the solution suitable for casting. The lower viscosity is likely due to the lower molecular weight of the n-PANi. N-substituted aniline derivatives typically produce lower molecular weight polymers compared to PANi, due to increased steric hindrance⁵¹.

4.4 Chlorine Tolerance comparison

The membranes' performance was tested before and after exposure to a sodium hypochlorite solution to evaluate the chlorine tolerance of the membranes. Membrane permeability and rejection tests were carried out using a dead-end stirred cell (Sterlitech) with a membrane area of 14.6 cm². Permeate flow rates were measured using a digital flow meter. Pristine membranes were compacted first using DI water at 1.38 bar (20 psi) until the flux decline was <5% over a 30 min time period. Membrane flux was measured under pressures of 1.38, 1.04, 0.69, 0.34 bar (20, 15, 10 and 5 psi). Pure water permeability data were determined by plotting the flux as a function of pressure. BSA (6 nm in diameter³³) was used to evaluate the membrane rejection properties. Concentrations were determined using an Agilent 8453 UV-Visible Spectrophotometer. BSA rejection was calculated from

$$R = 1 - c_p/c_f,$$

where c_p is the BSA concentration in the permeate and c_f is that in the feed solution.

To evaluate chlorine tolerance, 250 ppm sodium hypochlorite solutions (pH = 8.5) were prepared by diluting a concentrated sodium hypochlorite solution with DI water. The concentration of free chlorine was measured using an HACH Pocket Colorimeter™ II chlorine test kit. N-PANi and PANi membranes were compacted as described above before being soaked in 250 ppm hypochlorite solution for different periods of time. Pure water permeability and BSA rejection were measured as described above for pristine membranes.

Cross-sectional morphologies and surface images were taken using a JEOL JSM-6701F scanning electron microscope. Unsupported membrane samples were used for cross-sectional imaging. The membranes were prepared from polymer

solutions cast unsupported on a glass plate followed by precipitation via non-solvent induced phase inversion in a DI water bath. The resulting unsupported membrane films were peeled off and dried in vacuo overnight at 60 °C. Membrane surface images were observed at 3,000× and 100,000× to visualize the pore size and porosity. In order to determine the chlorine damage on membrane morphology, n-PANi and PANi membranes were soaked in 250 ppm free chlorine for 2 days before drying. Cross-sectional and surface images of the pristine and chlorine exposed membranes were viewed at 600× magnification.

Table 4.1 Permeability and BSA Rejection of Membranes Before and After Soaking in 250 ppm Free Chlorine

	Pristine	Chlorine 1 d	Chlorine 2 d	Chlorine 30 d
N-PANi	86.9	103.3	100.6	108.7
Permeability (lmh/bar)				
N-PANi	65.8	62.9	75.7	70.2
rejection (%)				
PANi	280.4	642.1	1328	N/A
Permeability (lmh/bar)				
PANi	12.9	1.8	0	N/A
rejection (%)				

To determine the flux and selectivity of the n-PANi membranes, pure water permeability and BSA rejection tests were performed (Table 4.1). The % rejection was determined using the equation below:

$$R = 1 - A_p/A_f$$

where A_p and A_f are the UV-Vis absorbance of the permeate and feed solution at 280 nm, respectively. For comparison, a pristine PANi membrane was also tested. The n-PANi membrane exhibited a permeability of 86.8 lmh/bar (3.53 gfd/psi), while rejecting 65.8% BSA. The pure PANi membrane possesses a higher permeability (280.4 lmh/bar), but lower BSA rejection (12.9%).

Membrane surface SEM images (Figure 4.5a) show large pores on the PANi membrane surface. The pores are several hundred nanometers in diameter, comparable to PANi membranes previously reported³³. The large pores contribute to the relatively high permeability but low BSA rejection of the PANi membrane. At the same magnification, the n-PANi membrane surface appears to be defect-free and continuous. At 100,000 \times , slit-pores are observed on the n-PANi membrane surface (Figure 4.5c). The image was converted to black and white (Figure 4.5d) using NIH Image J software³³ in order to estimate the pore size. From these converted images, the slit-pores appear to be approximately 50 nm in length and 10 nm in width, manifesting the n-PANi membrane's higher BSA rejection.

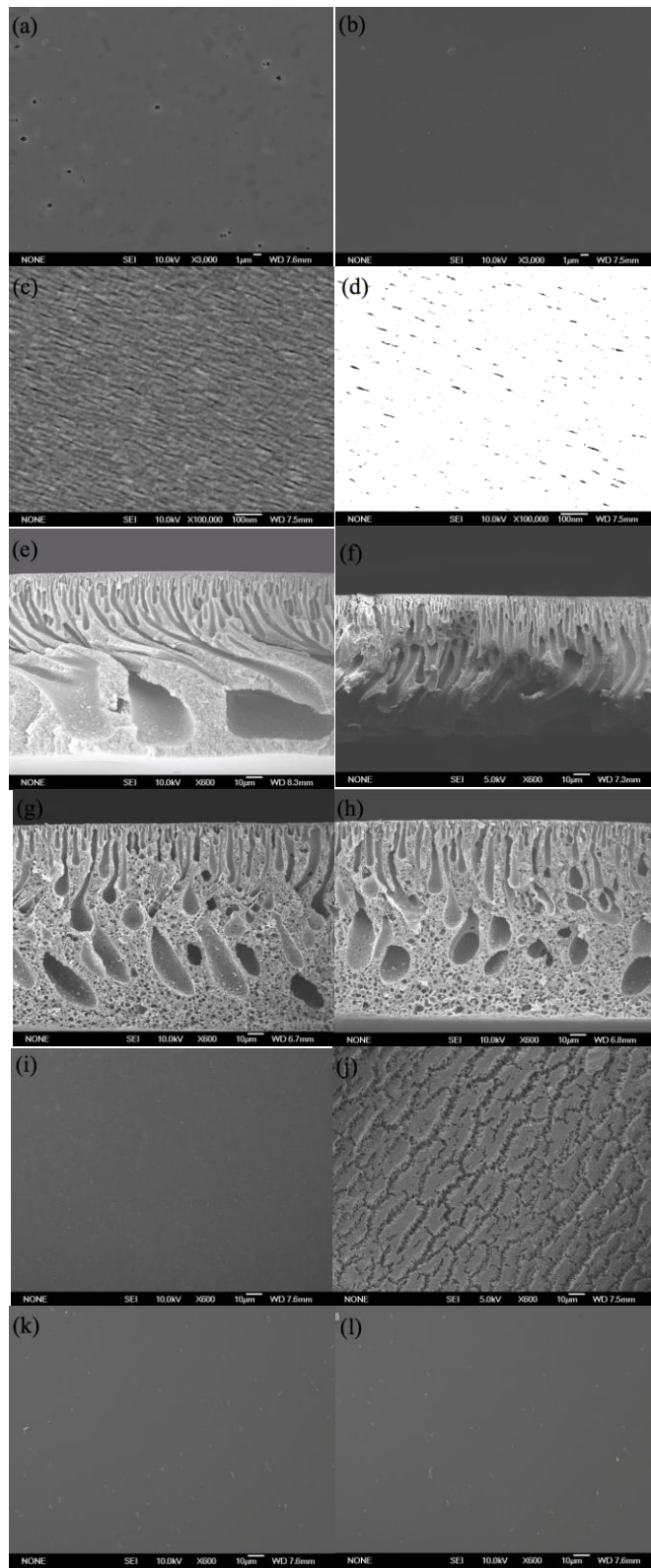


Figure 4.5 SEM images of (a) a PANi membrane and (b) an n-PANi membrane surface at 3,000 \times magnification, (c) an n-PANi membrane surface at 100,000 \times magnification and (d) its black-white picture after conversion using Image J

software. Cross-sectional images of (e) a pristine PANi membrane, (f) a PANi membrane after chlorine exposure, (g) a pristine n-PANi membrane and (h) an n-PANi membrane after chlorine exposure at 600× magnification. Surface images of (i) a pristine PANi membrane, (j) a PANi membrane after chlorine exposure, (k) a pristine n-PANi membrane and (l) an n-PANi membrane after chlorine exposure at 600× magnification.

Generally, increased polymer concentration in a casting solution leads to higher polymer density at the nonsolvent interface⁴⁶ during the phase inversion process. Therefore the volume fraction of the polymer increases while the porosity decreases⁴⁴, resulting in lower permeability and higher rejection. To investigate changes in performance, surface and cross-sectional SEM images of membrane samples were taken. As can be seen in Figure 4.5e and g, the morphology of the PANi membrane shows finger-like voids that extend across the entire span of the membrane. In contrast, the n-PANi membrane's finger-like voids extend only through the upper half of the membrane, indicating a denser morphology, consistent with its lower permeability compared to the PANi membrane.

To evaluate changes in chlorine tolerance based on chemical structure, PANi and n-PANi membrane coupons were exposed to sodium hypochlorite solutions for 2 days and the performance and rejection were examined. After soaking in the 250 ppm sodium hypochlorite solution, the permeability of the pure PANi membrane increased drastically from 280.4 lmh/bar to 1328.4 lmh/bar (Table 4.1). The BSA rejection of the pure PANi membrane also decreased significantly from 12.9% to 0 indicating that exposure to chlorine damaged the PANi membrane. The surface SEM image in Figure 4.5j clearly shows the damage that the chlorine exposure causes to the membrane. The exposed PANi membrane

possesses large defects in the surface. Chlorine also damages the interior structure of the PANi membrane, which appears to lose mass and thickness (Figure 4.5f). On the other hand, the permeability of the n-PANi membrane changes only slightly from 86.9 lmh/bar to 100.6 lmh/bar upon chlorine exposure, with little change in BSA rejection. Figure 4.5h and i indicate that the n-PANi membrane surface and interior structure are unaffected by chlorine exposure. It is also worth noting that there was visible bleaching of the PANi membrane sample upon exposure to the chlorine treatment (Figure 4.6). Chlorine oxidizes the benzenoid groups (as discussed in the following section) and decreases the extent of conjugation across the polymer backbone. This phenomena reduces the absorption of photons giving rise to π - π^* transitions, resulting in chemical bleaching.

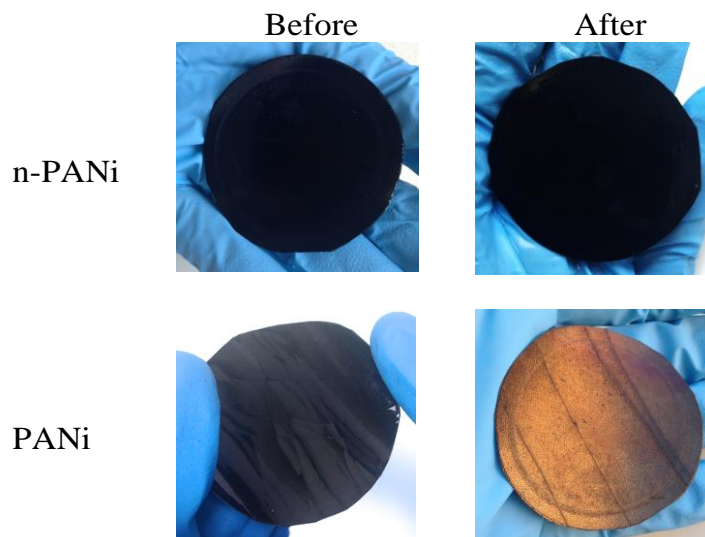


Figure 4.6 Photos of PANi and n-PANi membranes before and after being soaked in a 250 ppm free chlorine solution for 2 days.

During industrial operation, chlorine cleaning is performed either by back-flushing with 2-8 ppm hypochlorite solution for 1 min or soaking in 20-400 ppm

free chlorine for 1 h periodically. The combined effect of chlorine oxidation can be expressed in a concentration \times time manner.¹⁵ Long-term chlorine resistance of n-PANi membrane was tested by extending the soaking time in 250 ppm free chlorine solution to 30 days. Fresh hypochlorite solutions were prepared and exchanged every 2 days. At the end of the 30-day period, the membrane performance was evaluated. After 30 days, the n-PANi membrane maintained its pure water permeability of 108.7 lmh/bar and a BSA rejection of 70.2%, indicating outstanding long-term chlorine resistance. n-PANi is able to withstand at least 180,000 mg h/L of free chlorine exposure. Therefore, we believe n-PANi is a viable candidate for long-term use in water treatment plants without failure due to chlorine degradation.

4.5 Degradation Mechanism

The polymeric materials were characterized with FT-IR, UV-vis and NMR to probe the mechanism associated with membrane degradation from chlorine exposure. Fourier Transform Infrared Spectrometry (FT-IR) was conducted using a JASCO FT/IR-5300. Membrane samples were cut into 1 cm x 2 cm small rectangular pieces and dried in vacuo overnight before making measurements. An Agilent 8453 UV-Visible Spectrophotometer was utilized for UV-Vis characterization with polymer powders using DMSO as a blank solvent. Polymer powders were chlorinated by being submerged in 250 ppm chlorine solution for 2 days before drying and dissolving in DMSO. ¹H-Nuclear Magnetic Resonance (¹H-NMR) experiments were carried out in a Bruker Avance AV300 (300.1 MHz) instrument at room temperature. The unsupported membrane was grinded into powder with a

mortar and pestle and dissolved in deuterated DMSO. The $^1\text{H-NMR}$ chemical shifts are reported relative to the deuterated DMSO solvent signal.

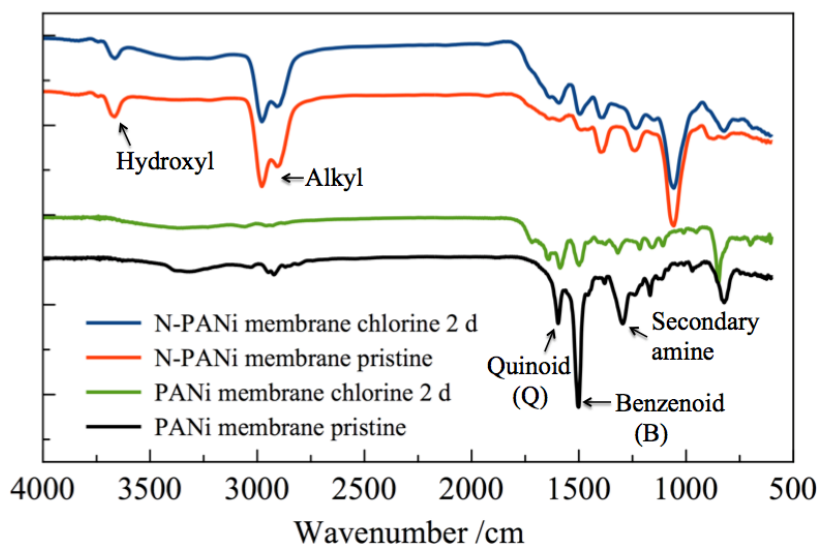


Figure 4.7 FT-IR spectra of membranes before and after being soaked in bleach containing 250 ppm of free chlorine. The small peak at 875 cm^{-1} for the pristine n-PANi membrane is due to the chloride counter-ion attached to the doped n-PANi membrane. After the n-PANi membrane is soaked in a basic sodium hypochlorite solution, n-PANi becomes dedoped, as indicated by the disappearance of the chloride counter-ion peak.

To probe redox chemistry induced by chlorine treatment, ATR-IR was employed. Upon examination of the benzenoid and quinoid moieties within the PANi and n-PANi backbones after chlorination, the differences in chemical structure are discernible (Figure 4.7). In the PANi IR spectrum, the quinoid peak shifts from 1597 cm^{-1} to 1587 cm^{-1} and the benzenoid peak shifts from 1501 cm^{-1} to 1498 cm^{-1} upon chlorine exposure. However, the quinoid and benzenoid peaks of the n-PANi remain at 1591 and 1495 cm^{-1} , respectively, after being soaked in 250 ppm free chlorine for 2 days. Additionally, the intensity ratio of the quinoid group to the benzenoid group in the PANi membrane increases from 0.5 to 1 (Table 4.2). A decrease in the intensity of secondary amines, corresponding to a

decrease in benzenoid rings, in the PANi membrane is also observed at 1270 cm^{-1} . The alkyl peak around 2900 cm^{-1} in the as-cast PANi membrane is indicative of remaining NMP and 4-MP within the film (also observed in the NMR spectrum in Figure 4.9). After being exposed to 250 ppm free chlorine for two days, the alkyl peaks almost disappear due to the fewer available benzenoid units for NMP to bond to. These changes suggest that the benzenoid groups are oxidized by chlorine. In contrast, the n-PANi membrane remains unchanged upon chlorine exposure. The benzenoid:quinoid ratio is only slightly altered from 1.2 to 1.3, while the peak positions do not shift, indicating the polymer's tolerance to oxidation.

Table 4.2 The FT-IR Benzenoid (B) and Quinoid (Q) Peak Positions and Intensity Ratios for N-PANi Membranes

	Pristine	Chlorine 2 d
N-PANi B/cm⁻¹	1495	1495
N-PANi Q/cm⁻¹	1591	1591
N-PANi Q/B	1.2	1.3
PANi B/cm⁻¹	1501	1498
PANi Q/cm⁻¹	1597	1587
PANi Q/B	0.5	1.0

To further investigate benzenoid to quinoid oxidation from chlorine exposure, UV-Vis spectroscopy was utilized. In the UV-vis spectra (Figure 4.8), n-PANi absorbs in one region with a λ_{max} at 331 nm, corresponding to the benzenoid

π - π^* transition. For PANi, a separate peak appears at 601 nm, corresponding to the quinoid π - π^* .⁵³ With chlorine exposure, n-PANi displays no apparent change in its UV-Vis spectrum. In contrast, the spectrum of PANi varies markedly upon chlorine exposure. A blue shift is observed for the benzenoid peak (338 nm \rightarrow 329 nm) and a red shift is observed for the quinoid peak (601 nm \rightarrow 624 nm) due to chain cleavage and chloride substitution on the quinoid rings (Table 4.3). The intensity ratio of the quinoid to benzenoid peak also increases, which is consistent with the IR spectra, further indicating benzenoid ring oxidation reactions.

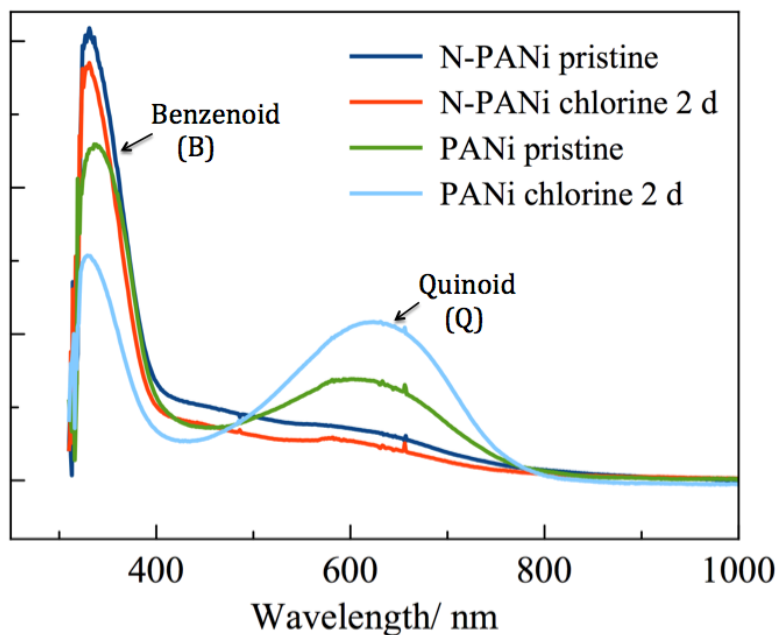


Figure 4.8 UV-Vis spectra of membranes before and after being soaked in bleach containing 250 ppm of free chlorine.

Table 4.3 The Benzenoid (B) and Quinoid (Q) Peak Positions and Ratios for N-PANi and Pure PANi Membranes

	N-PANi B/nm	PANi B/nm	PANi Q/nm	Q/B
Pristine	331	338	601	0.33

Chlorine 2d	331	329	624	0.71
--------------------	-----	-----	-----	------

To determine chemical changes to the polymers, ¹H-NMR spectroscopy experiments were conducted on representative samples of the PANi and n-PANi polymers, before and after chlorine exposure (Figure 4.9). The NMR spectra of the PANi membrane indicates that both NMP and 4-MP remain in the membrane after the phase inversion process with thorough rinsing. After exposure to chlorine, NMP is partially removed from the membrane. NMP interacts with the PANi backbone via hydrogen bonding³⁴ as depicted in Figure 4.9b. As mentioned above, the decreased number of benzenoid rings in the backbone (after oxidation) removes hydrogen bond sites for the NMP to interact with. In the spectrum for n-PANi, NMP is not present. Due to the presence of long n-alkyl side chains, the NMP solvent cannot interact strongly with the n-PANi backbone, and is removed during rinsing after the phase inversion process. Additionally, there is no visible change upon chlorination, manifesting the chlorine stability of the n-PANi membranes.

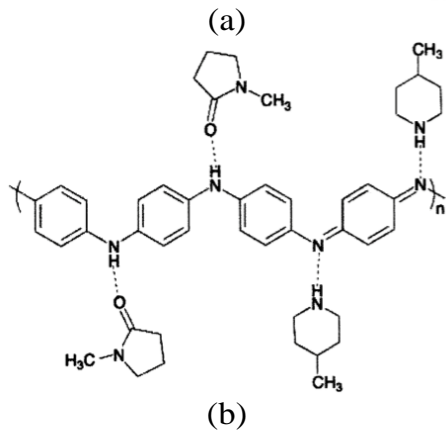
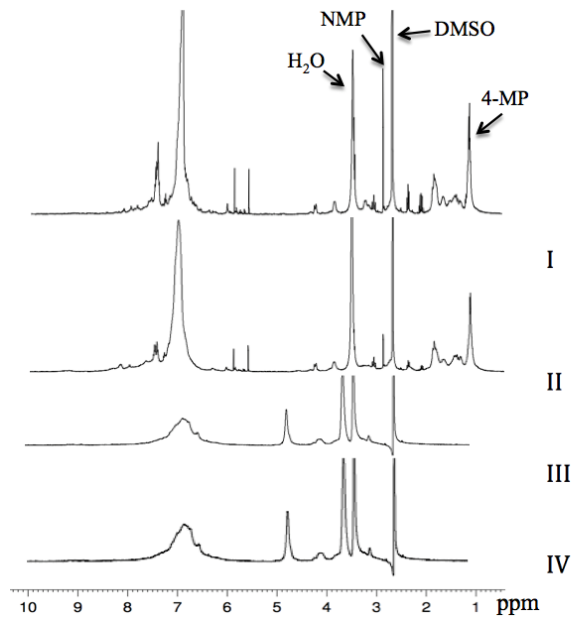


Figure 4.9 (a) NMR spectra of I. a pristine PANi membrane; II. A PANi membrane soaked in 250 ppm of free chlorine for 2 days; III. A pristine n-PANi membrane; IV. An n-PANi soaked in 250 ppm of free chlorine for 2 days and (b) a schematic representation of the PANi/4-MP/NMP complex formed by hydrogen bonding³⁴.

4.6 Antifouling Properties

Captive bubble contact angle measurements were employed to determine membrane hydrophilicity with a KRÜSS DSA 10 goniometer. The captive bubble method was chosen instead over sessile drop method so that the membranes remain wet during the measurement without the change of morphology associated with drying.⁴⁵

Bacterial attachment tests were performed on n-PANi and PANi membranes using *E. coli* as a model microorganism to evaluate bacteria deposition resistance. *E. coli* cell cultures were suspended in LB broth and incubated at 35 °C while shaken at 150 rpm for 24 hours in a New Brunswick Scientific I 24 Incubator Shaker. Cells were then harvested by centrifugation at $3800 \times g$ for 8 min. After, the cells were diluted with fresh LB broth to a concentration of 4×10^7 cells/ml. Membrane coupons of approximately 1 cm² were incubated in *E. coli* suspension for 24 hours at 35 °C while shaken at 25 rpm followed by rinsing with fresh LB broth. Membrane coupons were then immersed and stained in SYTO 9 dye solution (live/dead BacLight Bacterial Viability Kit L13152, Molecular Probes) for 15 min. Images with bacteria deposition were taken using a fluorescence microscope (Olympus BX5) and a $4 \times$ CCD camera (FVIEW-II, Soft Imaging System, USA).

A cross-flow system was used to determine the fouling behavior of the membranes using the same method described by McVerry *et al.*⁵ A 19 cm² cutout of each supported membrane was placed in the cross-flow cell. A computer connected to a balance recorded the mass change of the permeate with time, enabling the flux to be monitored in real-time. The membranes were compacted using DI water at 16 psi until the flux stabilized. The flux was then normalized to 68 lmh (40 gfd) by manually reducing the operational pressure. Once stable, DI water in the feed tank was replaced by 1.5 g/L BSA solution to observe flux decline due to BSA fouling. The fouling test was continued for 25 min followed by flushing with DI water for 25 min.

The n-PANi membrane exhibits an observed contact angle of $36.0 \pm 0.8^\circ$ indicating its increased hydrophilicity compared to a PANi membrane (CA =

52.8±2.3°) as shown in Figure 4.10. Bacterial attachment test results are also shown in Figure 4.10 with green fluorescence representing *E. coli* colonies adhered to the membrane surface. It is evident that n-PANi membranes are less prone to fouling compared to PANi membranes. This is in agreement with n-PANi's lower water contact angle values, i.e. higher hydrophilicity, which suppresses the undesirable hydrophobic interactions between microorganisms and the membrane surface. A hydrophilic surface is able to form a hydration layer which prevents foulants from absorbing onto the surface.^{47,48}

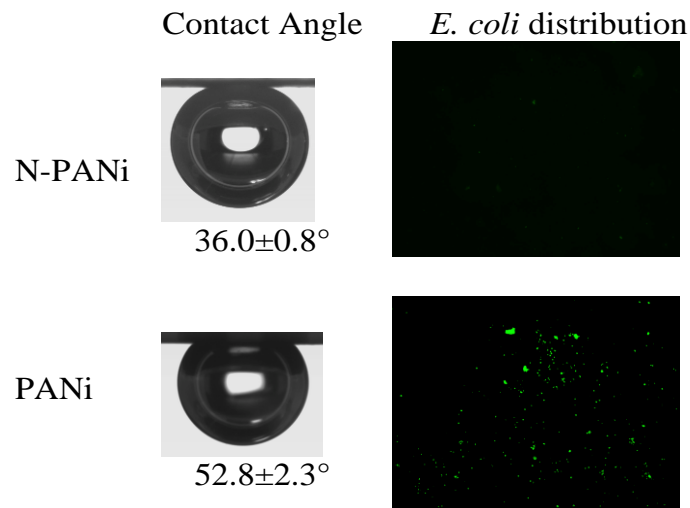


Figure 4.10 Contact angles of n-PANi and PANi membranes and their *E. coli* adhesion test microscopic images.

The antifouling properties of n-PANi membranes were further investigated using a cross-flow fouling test (Figure 4.11). After 10 min of stable flux, the feed was switched to a 1.5 g/L BSA solution. As soon as the BSA solution was introduced, there was a sudden decrease in flux caused by membrane fouling. The PANi membrane lost 63% of its initial flux due to fouling and only regained 44% of its initial flux when the feed was switched back to DI water after 35 min. The n-PANi membrane exhibits greater fouling resistance than the PANi membrane, only

losing 11% of its initial flux from exposure to the BSA solution, while regaining 91% of its initial flux when rinsed with DI water. It's also worth noting that McVerry *et al.*⁵ performed similar testing on a polysulfone membrane in which the same fouling technique was applied, and a commercial polysulfone membrane exhibited a greater amount of fouling with 50% flux decline after 10 min of fouling and 62% flux recovery after flushing with DI water. Therefore, n-PANi has proven to be a promising new membrane material due to its outstanding ability to effectively mitigate fouling.

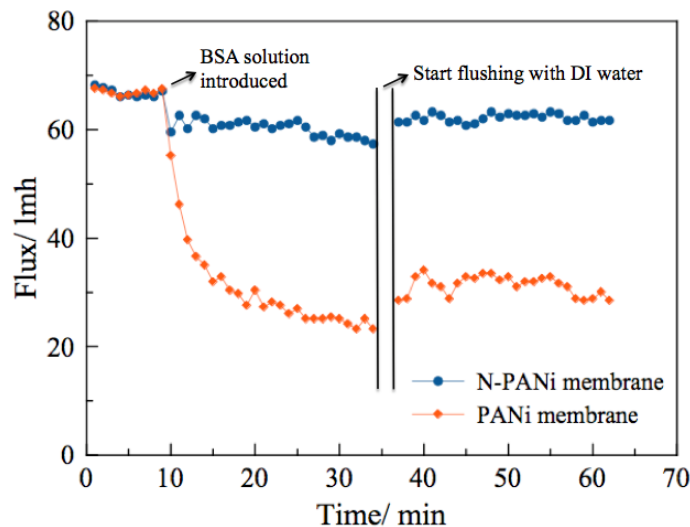


Figure 4.11 Flux decline and recovery results for membranes fouled by 1.5 g/L BSA solution before being washed with DI water.

4.7 Conclusions

We have successfully fabricated n-PANi chlorine resistant UF membranes with enhanced hydrophilicity. Due to the n-substitution on the PANi backbone, the n-PANi polymer membranes can withstand exposure to 250 ppm free chlorine for as long as 30 days without showing any significant degradation in permeability or BSA rejection. In comparison, native PANi membranes completely lose its

membrane integrity and ability to reject BSA after being soaked in 250 ppm free chlorine for just 2 days. Additionally, n-PANi membrane shows less bacterial adhesion and much lower BSA fouling during cross-flow operation compared with a PANi membrane. We believe n-PANi membrane is an exceptional candidate for UF applications with better fouling resistance, improved membrane longevity and reduced operational costs.

4.8 References

- 1 J. C. Crittenden, R. R. Trussell, D. W. Hand, K. J. Howe and G. Tchobanoglous, *Water Treatment: Principles and Design*, John Wiley & Sons, Inc., Hoboken, New Jersey, 2nd edn, 2005.
- 2 R. F. Service, *Science*, 2006, 313, 1088-1090.
- 3 M. Cheryan, *Ultrafiltration and Microfiltration Handbook*, Technomic Publishing Co., Lancaster, PA, 1998.
- 4 R. Rosberg, *Desalination*, 1997, 110, 107-114.
- 5 B. T. McVerry, J. A. T. Temple, X. Huang, K. L. Marsh, E. M. V. Hoek, R. B. Kaner, *Chem. Mater.*, 2013, 25, 3597-3602.
- 6 Y. Liao, T. P. Farrell, G. R. Guillen, M. Li, J. A. T. Temple, X. Li, E. M. V. Hoek, R. B. Kaner, *Mater. Horiz.*, 2013, 1, 58-64.
- 7 N. Hilal, O. O. Ogunbiyi, N. J. Miles, R. Nigmatullin, *Sep. Sci. Technol.*, 2005, 40, 1957-2005.
- 8 C. Liu, S. Caothien, J. Hayes, T. Caothuy, T. Otoyoy, T. Ogawa, *Membrane Chemical Cleaning: From Art to Science*, in: *Proceedings of the AWWA Water Quality Technology Conference*, Mar 4-7, 2001, San Antonio, Texas, USA.
- 9 W. Eykamp, *Microfiltration and Ultrafiltration*. In *Membrane Separation Technology: Principles and Applications*, R. D. Noble, S. A. Stern, Eds; Elsevier Science: Amsterdam, 1995.
- 10 V. Gitis, R. C. Haught, R. M. Clark, J. Gun, O. Lev, *J. Membr. Sci.*, 2006, 276, 185-192.
- 11 I. M. Wienk, E. E. B. Meuleman, Z. Borneman, T. Van Den Boomgaard, C. A. Smolders, *J. Polym. Sci., Part A: Polym. Chem.*, 1995, 33, 49-54.
- 12 M. Nyström, H. Zhu, *J. Membr. Sci.*, 1997, 131, 195-205.
- 13 S. H. Wolff, A. L. Zydny, *J. Membr. Sci.*, 2004, 243, 389-399.
- 14 H. Zhu, M. Nyström, *Colloid Surf. A: Physicochem. Eng. Aspects*, 1998, 138, 309-321.
- 15 E. Arkhangelsky, D. Kuzmenko, V. Gitis, *J. Membr. Sci.*, 2007, 305, 176-184.
- 16 S. Rouaix, C. Causserand, P. Aimar, *J. Membr. Sci.*, 2006, 277, 137-147.

- 17 E. Gaudichet-Maurin, F. ThomINETTE, J. Membr. Sci., 2006, 282, 198-204.
- 18 F. ThomINETTE, O. Farnault, E. Gaudichet -Maurin, C. Machinal, J. Schrotter, Desalination, 2006, 200, 7-8.
- 19 D. Kuzmenko, E. Arkhangelsky, S. Belfer, V. Freger, V. Gitis, Desalination, 2005, 179, 323-333.
- 20 J. Glater, S. Hong and M. Elimelech, Desalination, 1994, 95, 325-345.
- 21 D. H. Shin, N. Kim, Y. T. Lee, J. Membr. Sci., 2011, 376, 302-311.
- 22 T. Kawaguchi and H. Tamura, J. Appl. Polym. Sci., 1984, 29, 3359-3367.
- 23 V. T. Do, C. Y. Tang, M. Reinhard, J. O. Leckie, Environ. Sci. Technol., 2012, 46, 852-859.
- 24 T. Shintani, H. Matsuyama, N. Kurata, Desalination, 2007, 207, 340-348.
- 25 Y. Liao, X. Wang, W. Qian, Y. Li, X. Li, D. Yu, J. Colloid and Interface Sci., 2012, 386, 148-157.
- 26 V. Bocchi, G. P. Gardini, M. Golinelli, E. Bellelli, G. Sansebastiano, J. Mater. Sci., 1991, 26, 3354-3355.
- 27 W. E. Price, C. O. Too, G. G. Wallace and D. Zhou, Synth. Met., 1999, 102, 1338-1341.
- 28 R. G. Alargova, J. T. Petkov, N. D. Denkov, D. N. Petsev, I. B. Ivanov, Colloid Surf. A: Physicochem. Eng. Aspects, 1998, 134, 331-342.
- 29 X. Li, P. Vandezande, I. F. J. Vankelecom, J. Membr. Sci., 2008, 320, 143-150.
- 30 Z. Fan, Z. Wang, M. Duan, J. Wang, S. Wang, J. Membr. Sci., 2008, 310, 402-408.
- 31 Z. Fan, Z. Wang, N. Sun, J. Wang, S. Wang, J. Membr. Sci., 2008, 320, 363-371.
- 32 S. Zhao, Z. Wang, X. Wei, B. Zhao, J. Wang, S. Yang, S. Wang, J. Membr. Sci., 2011, 385-386, 251-262.
- 33 G. R. Guillen, T. P. Farrell, R. B. Kaner and E. M. V. Hoek, J. Mater. Chem., 2010, 20, 4621-4628.

- 34 G. R. Guillen, B. T. Mcverry, T. P. Farrell, R. B. Kaner, E. M. V. Hoek, Tuning the properties of polyaniline-based ultrafiltration membranes with chemical post-treatments. Manuscript in process.
- 35 J. M. Antelo, F. Arce, J. L. Armesto, A. Garcia-Verugo, F. J. Penedo and A. Varela, *Int. J. Chem. Kinet.*, 1985, 17, 1231-1245.
- 36 J. W. Chevalier, J. Y. Bergeron, L. H. Dao, *Macromolecules*, 1992, 25, 3325-3331.
- 37 D. Yang, B. R. Mattes, *J. Polym. Sci., Part B: Polym. Phys.*, 2002, 40, 2702-2713.
- 38 D. Yang, B. R. Mattes, *Synth. Met.*, 1999, 101, 746-749.
- 39 D. Yang, G. Zuccarello, B. R. Mattes, *Macromolecules*, 2002, 35, 5304-5313.
- 40 S. K. Manohar and A. G. Macdiarmid, K. R. Cromack, J. M. Ginder, A. J. Epstein, *Synth. Met.*, 1989, 29, 349-356.
- 41 J. J. Langer, *Synth. Met.*, 1990, 35, 295-300.
- 42 J. S. Shin, J. H. Kim, I. W. Cheong, *Synth. Met.*, 2005, 151, 246-255.
- 43 A. Watanabe, K. Mori, Y. Iwabuchi, Y. Iwasaki, Y. Nakamura, O. Ito, *Macromolecules*, 1989, 22, 3521- 3525.
- 44 G. R. Guillen, Y. Pan, M. Li, E. M. V. Hoek, *Ind. Eng. Chem. Res.*, 2011, 50, 3798-3817.
- 45 W. Zhang, M. Wahlgren, B. Sivik, *Desalination*, 1989, 73, 263-273.
- 46 D. B. Mosqueda-Jimenez, R. M. Narbaitz, T. Matsuura, G. Chowdhury, G. Pleizier, J. P. Santerre, *J. Membr. Sci.*, 2004, 231, 209-224.
- 47 I. Banerjee, R. C. Pangule, R. S. Kane, *Adv. Mat.*, 2011, 23, 690-718.
- 48 B. T. McVerry, M. C. Y. Wong, K. L. Marsh, J. A. T. Temple, C. Marambio-Jones, E. M. V. Hoek, R. B. Kaner, *Macromol. Rapid Commun.*, 2014, 35, 1528-1533.
- 49 C. H. Hsu, P. M. Peacock, R. B. Flippen, S. K. Manohar, A. G. MacDiarmid, *Synth. Met.*, 1993, 60, 233-237.
- 50 H. S. Kolla, S. P. Surwade, X. Zhang, A. G. MacDiarmid, S. K. Manohar, *J. Am. Chem. Soc.*, 2005, 127, 16770-16771.

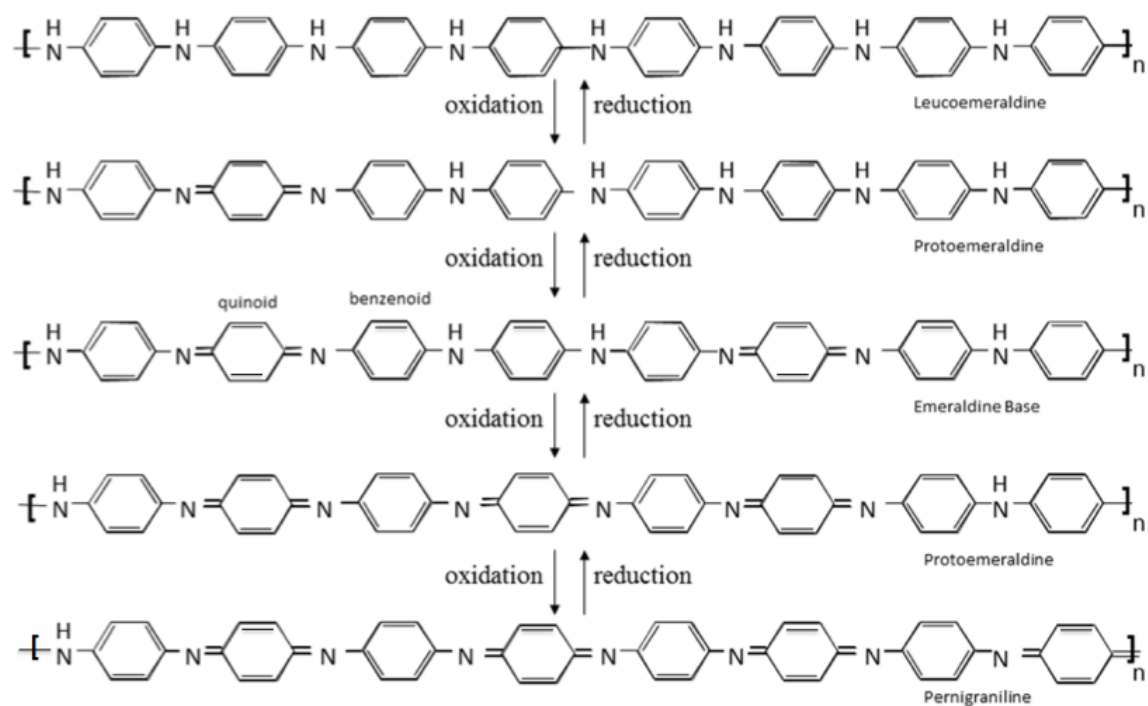
- 51 H. D. Tran, I. Norris, J. M. D'Arcy, H. Tsang, Y. Wang, B. R. Mattes, R. B. Kaner, *Macromolecules*, 2008, 41, 7405-7410.
- 52 P. N. Adams, P. J. Laughlin, A. P. Monkman, A. M. Kenwright, *Polymer*, 1996, 37, 3411-3417.
- 53 M. G. Han, S. K. Cho, S. G. Oh, S. S. Im, *Synth. Met.*, 2002, 126, 53-60.

Chapter 5. Polyaniline Nanofibers: Broadening Applications for Conducting Polymers

5.1 Introduction

Inherently conducting polymers (ICPs), including polyanilines, polythiophenes and polypyrroles are organic materials that have electrical properties similar to inorganic materials such as semiconductors and metals. ICPs have the potential to replace many of these materials due to lower manufacturing costs, lower density, better processability, higher mechanical flexibility and broader chemical functionalization capabilities. The light weight of conducting polymers makes them attractive alternatives to dense metals and oxides for anti-static coatings and electromagnetic shielding. This is especially important in weight sensitive fields including aerospace and auto manufacturing. ICPs are malleable like most polymers and can be used as flexible, transparent electrodes for electrochromic devices and solar cells. Conducting polymers also have similar thermal expansion coefficients and mechanical properties to structural polymers making the development of stable conductive plastic composite components a real possibility. Despite the many potential advantages of using an organic material over a metal, oxide or other inorganic compound, limitations in processing, stability and conductivity have prevented broad utilization of most conducting polymers. New methods for manufacturing nanoscale conducting polymers offer promise for broader commercial interest in conducting polymers, suggesting that academically driven developments could eventually have an impact in the marketplace.

Aniline is an inexpensive starting material that is readily manufactured from benzene, or extracted as a by-product from oil and coal tar refining. The primary oxidation product of aniline, polyaniline (originally called aniline black), has been around in various forms for over a century.¹ Its high environmental stability, interesting redox chemistry and unique doping/dedoping properties have resulted in extensive academic studies of this material in recent decades.² Unfortunately, due to poor solution and melt processability, polyaniline has not yet been widely adopted in commercial products. The starting materials to make polyaniline are the least expensive of all the inherently conducting polymers and polyaniline is the most thermally stable of the ICPs. Polyaniline also has relatively good processability and conductivity leading to the supposition that it may be the best of the inherently conducting polymers.³ Despite this, additional improvements are needed before polyaniline can find wide use in commercial products.



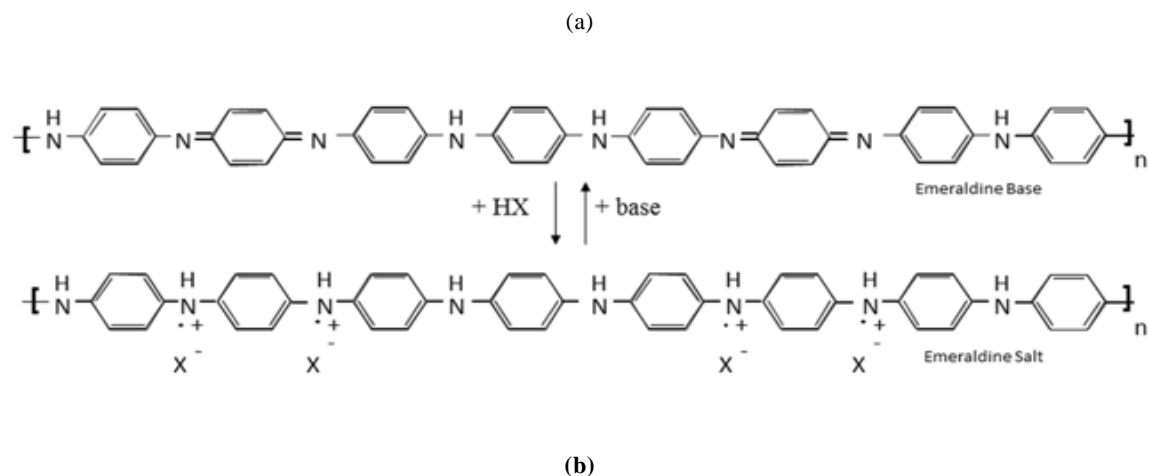


Figure 5.1 (a) Each of the five polyaniline oxidation states shown on top can be interconverted by either oxidation (removal of electrons) or reduction (addition of electrons) as indicated. (b) The undoped emeraldine base, can be doped with an acid to yield the conductive emeraldine salt structure as shown on the bottom.

Much of the initial and continued academic interest in polyaniline lies in its unique redox states and doping mechanisms when compared to other conducting materials, especially other conjugated polymers. This concept is often stated, but seldom explained in any detail. Consider polythiophene, which possesses only 2 distinct oxidation states. “Doping” of polythiophene typically refers to the removal of some electrons from polythiophene (p-doping). “Dopants” or counter-anions are required to stabilize the positive charges generated by partial oxidation. Polypyrrole is analogous, having just two major oxidation states which correspond to doped (partially oxidized) or undoped (reduced) forms. In comparison, polyaniline has three major oxidation states known as leucoemeraldine (fully reduced), emeraldine (half-oxidized) and pernigraniline (fully oxidized) as shown in Figure 5.1. In reality, the oxidation states are not really distinct, as essentially any degree of oxidation along

the polyaniline chain can occur. Under controlled conditions this can give rise to the intermediate half oxidation states, protoemeraldine, which lies between leucoemeraldine and emeraldine and nigraniline which lies between emeraldine and pernigraniline. Structurally, the differences between the oxidation states is determined by the number of quinoid and benzenoid units in the polyaniline as labeled in Figure 5.1. If polyaniline has only benzenoid rings in the undoped form, then the oxidation state is leucoemeraldine; if the polyaniline has one quinoid ring for every 8 total monomer units, the rest being benzenoid, then the structure is known as protoemeraldine; if there are two quinoids for every 8 monomer units, then the polyaniline is in its most stable oxidation state known as emeraldine; if there are three quinoid rings for every 8 monomer units, then the polymer is in the nigraniline oxidation state; and if the polyaniline is fully oxidized with every alternating ring being a quinoid (4 total), then the oxidation state is called pernigraniline. The names of the different oxidation states are related to the different colors. Leucoemeraldine, is nearly transparent in solution and white in solid form, emeraldine is green when doped, but changes to blue when it is undoped, and pernigraniline appears deep violet in solution, that approaches black as a solid. These color changes help to explain interest in using polyaniline in electrochromic devices and displays.^{4,5,6}

The two most general methods used for synthesizing polyaniline are electrochemical and chemical oxidative polymerizations.⁸ Both conventional methods for producing conducting polymers result in materials that are difficult to process and generate large amounts of organic waste. New methods to manufacture conducting polymer nanostructures, particularly polyaniline nanofibers, provide a

means to exploit the many advantageous properties of conducting polymers at a lower cost than conventional polymerization methods. These new polymerization techniques have led to higher surface area, solvent processability and morphological control.

Early synthetic methods to produce nanostructured polyaniline required templating agents or special processing techniques.⁹ The first report of a template-free method was made in 2003 with the introduction of the interfacial synthesis of polyaniline nanofibers.¹⁰ This method allows for the spontaneous reaction between aniline monomer and an oxidant such as ammonium peroxydisulfate at the interface between two immiscible liquids. This procedure requires much less energy input than the conventional polyaniline oxidative polymerization, which has increasingly focused on low temperatures, slow addition of reactants and thorough mixing to improve yields and molecular weights. These methods have actually moved the reaction away from the intrinsic nanofibrillar morphology of polyaniline and resulted in inconsistent products from researcher to researcher.^{2,11} In order to use the conventional polyaniline product, it is filtered and dried, ground into a powder and then dispersed in one of the few solvents that can dissolve polyaniline: N-methylpyrrolidinone (NMP), dimethylformamide (DMF), meta-cresol or hexafluoroisopropanol (HFIP). In comparison, many of the oxidative polymerization methods for producing polyaniline nanofibers allow room temperature synthesis of nearly uniform nanofibrillar morphologies (Figure 5.2, left). There have been several reviews on the synthesis of polyaniline nanofibers that describe this topic in some detail.^{2,9,12} There has also been continued improvements in the morphological control

of conducting polymers, leading to the synthesis of nanofibers of polypyrroles, polythiophenes and polyaniline derivatives with similar opportunities to pure polyaniline, as discussed in greater detail elsewhere.^{7,8}

Polyaniline nanofibers readily disperse in water directly from the aqueous synthesis (Figure 5.2, right) and can be redispersed in alcohols, ketones and many other organic solvents with appropriate processing. The large surface area (>50 m²/g)¹³ improves reactivity in applications such as sensors and supercapacitors and has led to the uniform deposition of metal nanoparticles (e.g. gold silver and platinum) with <2 nm diameters, leading to applications in non-volatile memory and aqueous catalysis.^{14,15} Some of the additional commercially relevant properties of polyaniline and polyaniline nanofibers, as well as their applications, are described in subsequent sections.

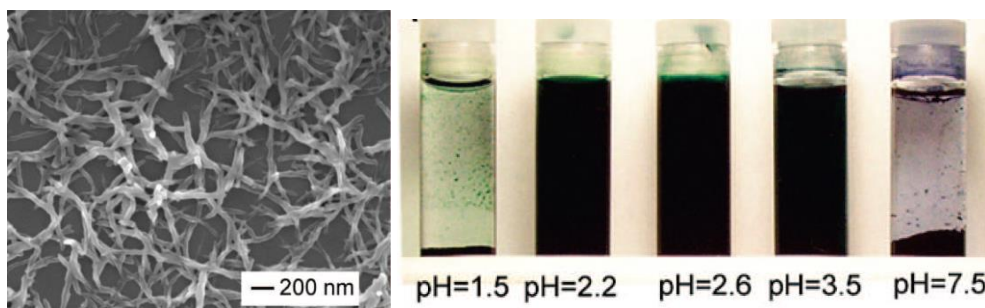


Figure 5.2 The as-synthesized polyaniline with uniform nanofiber morphology (left) can be readily dispersed in water at an appropriate pH (right). Reproduced with permission from ref. 3. Copyright 2005 Royal Society of Chemistry.

5.2 Sensors

5.2.1 Gas Vapor Sensors

One of the most noticeable advantages of using nanostructured materials in sensors is a very fast response time, due to the high surface area and short diffusion lengths inherent in this morphology. These qualities can also lead to ultra-low detection limits. Polyaniline nanofiber gas sensors are easy to develop and test, and they can be used to detect a vast range of chemical vapor analytes. The native oxidation state of polyaniline, emeraldine, can be doped to the conductive emeraldine salt with protonic acids, or dedoped by base to the insulating emeraldine form. This reversible behavior has been the driving force behind many of the acidic (e.g. HCl²²) and basic (e.g. NH₃²²) vapor sensors that have been developed because there are >10 orders of magnitude change in conductivity (σ) between polyaniline in the emeraldine salt form ($\sigma \geq 1$ S/cm) to the emeraldine base form ($\sigma \leq 10^{-10}$ S/cm). These conductivity changes are monitored through a gap electrode (Figure 5.3, upper left) or an interdigitated electrode (Figure 5.3, upper right) for more precise readings. These are simple devices to set-up and have been used in highschool, undergraduate and graduate courses.¹⁶ Recent versions have also been used in high accuracy polyaniline nanofiber CMOS sensors.^{16,17} Additives can also be used to detect a specific reactant that causes the formation of an acid or base that in turn dopes or dedopes the polyaniline, respectively.¹⁸ For example, the addition of CuCl₂ has been used to detect the weak acid H₂S since this reaction produces CuS and the by-product HCl. Analogous strategies have led to the detection of the lethal gases hydrazine,¹⁹

phosgene,²⁰ and arsine²¹. The change in conductivity resulting from chloroform swelling and methanol-induced polymer chain conformational changes has also led to the successful detection of those chemical vapors.²²

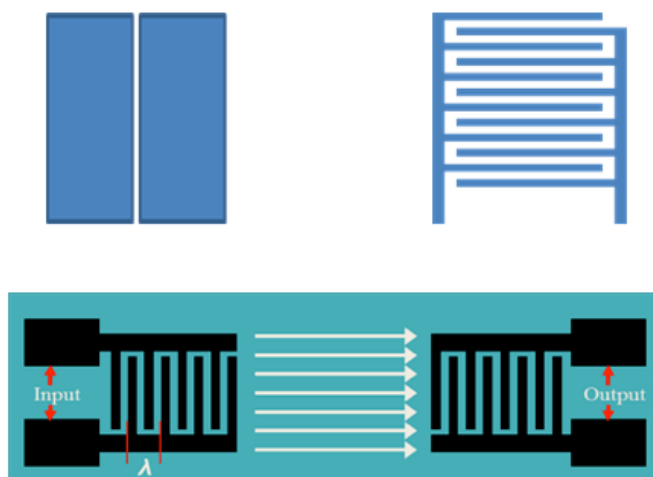


Figure 5.3 A gap electrode configuration (top left) and an interdigitated electrode configuration (top right) are used to measure resistance changes. The lower image shows the configuration of a surface acoustic wave device.

Hydrogen sensing has been a hot topic for polyaniline sensors during the past few years as it has been found that polyaniline nanofibers can detect hydrogen well below the dangerous explosion threshold of ~3% hydrogen at room temperature. This detection occurs in the presence of oxygen, where many metal-based hydrogen sensors cannot function. Polyaniline nanofiber hydrogen sensors have been demonstrated both with resistive,^{23,24} and surface acoustic wave (SAW)^{25,26} transduction mechanisms. A surface acoustic wave device such as that depicted in the lower image in Figure 5.3 uses two interdigitated transducers above a piezoelectric material. The input transducer on the left has an input electronic

signal that creates a piezoelectric wave that propagates across the surface and is converted back to an electronic signal at the output interdigitated transducer. A SAW device detects changes in the electrical conductivity and/or mass changes in the active material, which has been deposited on top of the interdigitated transducers. The change in the velocity of the acoustic waves is measured as a frequency change from the output transducer. In SAW sensor papers on the detection of hydrogen, the signal change has generally been attributed to an increase in conductivity of the polyaniline. This is interesting because it is not obvious that hydrogen actually dopes polyaniline. However, a mechanism in which protons are produced to account for the conductivity change have been suggested.^{23,25,27,28}

Additional work has also shown that polyaniline nanofibers can be used to detect humidity²⁹, NO₂^{30,31}, CO³², aromatic organics³³, trinitrotoluene (TNT)³⁴ and for many biological applications that will be discussed further in the next section.

5.2.2 Biological Sensors

A wide range of polyaniline nanostructures and nanocomposites have been used in biological sensors for the detection of small molecules, proteins and DNA utilizing the well understood redox chemistry of polyaniline for signal amplification.³⁵⁻³⁸ The higher surface area and easier incorporation of biological materials are major advantages for the nanofiber form of polyaniline over conventional dense films.^{37,39-42} In the cases of dense films, reactions are limited to the top surface of the film and interactions between the conducting polymer or

reactant and the analyte happen furthest from the underlying electrode. Additionally, the low surface area-to-volume ratio of dense films, relative to nanofibers, greatly limits the active surface area and thus limits sensitivity. Polyaniline nanofibers and nanocomposites are prime candidates for this application because they can be electroactive at neutral pH and covalently attached to various organic and inorganic materials in order to achieve synergistic effects.

Polyaniline has been used in sensitive DNA sensors because redox activity of the polymer coincides with oligonucleotide binding events and thus provides signal amplification.⁴³ While polyaniline is known for being more chemically and mechanically stable than most other conducting polymers, its implementation has been limited in pH sensitive biological sensing applications which typically require $\text{pH} \approx 7$ because the acidic ($\text{pH} < 4$) environments often required for polymerization and electroactivity can be unsuitable for biomolecules. However, doping can be maintained at neutral pH levels by modifying the polyaniline molecule (e.g. by using self-doped polyaniline)⁴⁴⁻⁴⁶ or incorporating a dopant into the polymer matrix, (e.g., polymerization or blending with a polyacid such as poly(styrenesulfonate)).⁴⁷⁻⁵⁰ As an example of the former technique, Wang *et al.* reported a sulfonic acid-doped polyaniline nanofiber/graphene oxide composite to successfully detect DNA hybridization.⁵¹ In this work, graphene oxide was used in order to improve the self-redox reaction signal of polyaniline. Hybridization events were recorded by electrochemical methods (cyclic voltammetry and electrical impedance sensing). The reported device achieved rapid, direct and label-free detection of DNA with high sensitivity and an ultralow detection limit (0.0656

fM). Chang *et al.* used templated electropolymerization to fabricate a regular polyaniline nanotube array onto a graphite electrode that had a very low detection limit of 1.0 fM and demonstrated the ability to differentiate single base-pair mismatches at 37.59 fM.⁵² The authors assert that ultra-sensitivity was achieved by using oriented nanotubes (instead of a thin film or a layer of randomly oriented nanotubes), which exhibited high conductivity and fast hybridization kinetics. Hao *et al.* reported the synthesis of uniform polyaniline nanowires using peptide assembled fibers as templates. The resulting polyaniline nanowires were then utilized to construct a highly sensitive and selective sensor for hepatitis B virus gene with low detection limit of 1 fM.³⁷ Spain *et al.* bound single stranded DNA to gold nanoparticles attached to polyaniline nanofibers to detect *Staphylococcus aureus*, the main cause of mastitis, a problematic disease in which cows produce sour milk.³⁸

Other than the applications mentioned above, polyaniline nanofibers have been recently demonstrated to also be effective in stretchable electronic skin temperature sensing⁵³ and pressure sensing⁵⁴.

5.3 Printable Electronics

The high dispersability of nanostructured polyaniline has made possible inks that can be painted or deposited by using a paintbrush, a fountain pen or an airbrush in either the doped (conducting) or dedoped (insulating) state. This can be used to create conducting, semiconducting or insulating regions. The ink can simply be replaced with a polyaniline nanofiber dispersion and applied normally. An airbrush does, however, have

the added requirement that the nozzle must be large enough so that the nanofibers do not clog the spigot.

Polyaniline nanofiber ink can also be printed by an ink-jet printer to create sensors, circuits, conducting films and other structures. Inkjet printing is an ideal method for controlled deposition of a material in a pattern with small features. This technique for deposition has been considerably more difficult to utilize than the previously mentioned methods due to the small openings and problems in replacing the ink in modern inkjet printers. Often the print head will clog in the middle of printing, or if successful, become clogged after the print head dries. This problem has been overcome with the use of a Dimatix materials printer (Figure 5.4, top). Such a printer was used by Small, *et al.* to deposit a polyaniline/multi-walled carbon nanotube (MWCNT) composite (Figure 5.4, bottom).⁵ Other research groups have also demonstrated printing of polyaniline nanofibers and nanoparticles for applications such as sensors^{17,55-58} and electromagnetic interference shielding⁵⁹. The printing capability of polyaniline nanofibers and nanoparticles can also be combined with flash welding to create printed sensors⁶⁰ and mechanical actuators⁹².





Figure 5.4 A Dimatix printer (top) was used to print an image of Jimi Hendrix (bottom) using a carbon nanotube polyaniline composite ink. Reproduced with permission from ref. 5. Copyright 2007 Royal Society of Chemistry.

One-dimensional nanostructures also possess a favorable percolation threshold relative to other shapes. This means that less material is needed for polyaniline nanofibers to form conducting pathways from one end of the material to the other. For example, much higher concentrations (at least 17% by volume) of amorphous or spherical particles (including carbon black, copper spheres or conventional polyaniline particles) are required as a minimum addition to create a conductive pathways (i.e. to reach the percolation threshold) than with one-dimensional fibers (only 2.9% or less).⁶¹ This property of polyaniline nanofibers is beneficial for printed electronics application because lower concentrations of polyaniline nanofibers contribute to better dispersability and less clogging of the print head.

5.4 Electro-Optical Applications

5.4.1 Electrochromics

Conducting polymers are excellent materials for electrochromic applications.^{4,62-64} Conducting polymers typically go through dramatic color changes when their oxidation

state is varied. Applying a potential to a conducting polymer film causes these color changes to occur due to a change in oxidation state of the conducting polymer. Color changing films have several potential applications including windows that let in light and heat in winter, but reflect radiant energy in summer; flexible displays; mirrors; and other devices. Layer-by-layer (LBL) assembly using oppositely charged materials is a straight forward way to generate such devices.⁶⁵⁻⁶⁸ Because polyaniline nanofibers form stable dispersions in water, aqueous dispersions can be used to deposit the polyaniline layers. Doped, dedoped and self-doped (sulfonated) polyaniline nanofibers can be used to create layer-by-layer films. Because of their high solution stability at various pHs, self-doped nanofibers are often preferred. These sulfonated aniline nanofibers have been synthesized using a combination of aniline monomer and aniline-2-sulfonic acid in a known synthesis for the formation of aniline nanofiber derivatives.⁶⁹ When the LBL films are made, each layer consists of a layer of polyaniline nanofibers and an appropriate polymeric counter-ion, such as poly(sodium styrene sulfonate), poly(allyl amine) or poly(acrylic acid). Doped and self-doped polyanilines are cationic with a positive surface charge, while dedoped polyaniline are anionic with a negative surface charge.

Polyaniline nanowires can also be deposited *in situ* onto supporting substrates such as PET via a dilute polymerization process as reported by Wang, *et al.*⁷⁰ In order to observe the electrochromic response of the polyaniline film, different voltages were applied to the film. When the film was discharged to 0 V, it appeared green (the emeraldine oxidation state) (Figure 5.5 top). When the film was charged to 1 V, it appeared blue (the pernigraniline oxidation state). These authors also developed a flexible energy storage smart window that utilizes both polyaniline's electrochromism function

and its supercapacitive property (which will be discussed further in Section 6). This energy storage smart window can be integrated with a solar cell to form a smart device system (Figure 5.5 bottom) that can simultaneously harvest, store and use renewable energy. During the day-time when sunlight is abundant, solar energy is converted to electricity that can be stored electrochemically by charging the polyaniline smart window. Meanwhile, the color of the window darkens, blocking sunshine and heat. The generated power can then be used to provide power to the room. Zhao *et al.* fabricated a $W_{18}O_{49}$ /polyaniline smart supercapacitor electrode with an energy level indication provided by the color change that occurs at different charging states.⁷¹ Erro *et al.* showed that polyaniline nanofibers display ultrafast electrochromic effects with response times as short as 20 ms.⁷²

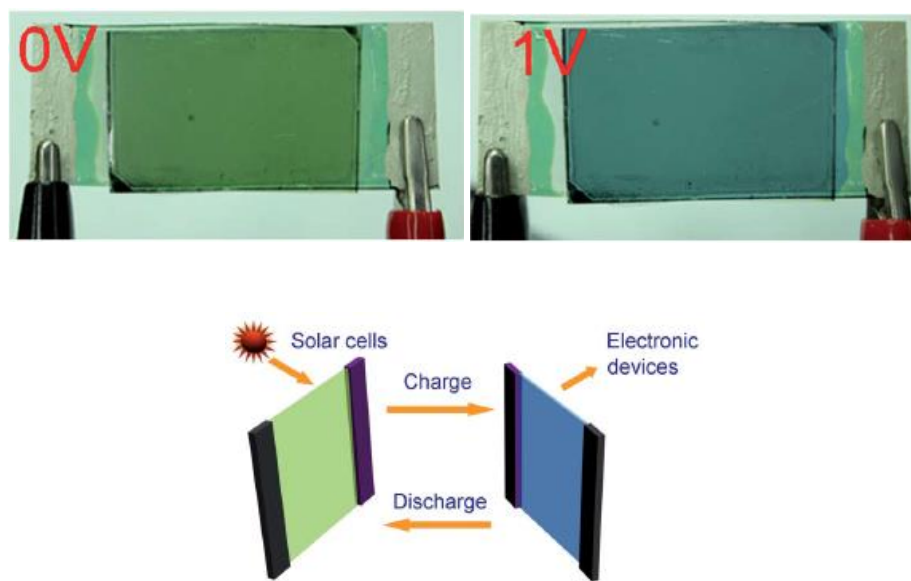


Figure 5.5 Image of a polyaniline nanowire film at different potentials (top) and a schematic showing an integrated energy storage smart window device system. Reproduced with permission from ref. 70. Copyright 2012 Royal Society of Chemistry.

5.4.2 Photovoltaics

Nanostructured polyaniline has been explored for use in organic solar cells.⁷³⁻⁸³ The polyaniline is typically used as a hole-conducting material that is either blended with or coated onto an electron donor material. Nanofibrous polyaniline can form an interpenetrating network in a solar cell device that enhances the diffusion of electrolyte and available donor/acceptor interfacial area for photogenerated excitons. The small domain size reduces the distance that the excitons need to travel before reaching an interface, which increases the probability of exciton dissociation across the heterojunction. Additionally, such porous morphology allows for the efficient transport of charge carriers to the respective electrodes before recombination, increasing the device's current and voltage.⁷³ Tang *et al.* fabricated a counter-electrode using double-layered polypyrrole nanoparticles and polyaniline nanofibers which gave significantly increased solar-to-electricity conversion efficiency due to abundant active sites and high specific area for improved electrocatalytic activity and electrolyte loading.⁷⁴ In other work, Tang *et al.* prepared a polyaniline nanofiber/platinum nanoparticle film as a counter-electrode for a dye sensitive solar cell (DSSC) device with high conductivity, high surface area, enhanced catalytic activity and a conversion efficiency of 7.69% which was higher than those made with either material by itself.⁷⁵ Bahramian and Vashae used polyaniline nanofibers as a counter-electrode and TiO₂ as the photoanode to make a transparent DSSC device which exhibited 8.22% conversion efficiency under irradiation from both sides.⁷⁶

In addition to photon absorption, other properties that affect the utility of polyaniline in solar cells are its conductivity, the highest occupied molecular orbital (HOMO) level, the lowest unoccupied molecular orbital (LUMO) level, the bandgap, and stability. One study found that a common conductivity for polyaniline, 3.5 S/cm, is ideal when compared to several different conductivity levels in applications as the hole-conducting layer in a dye sensitized solar cell.⁷⁷ Yet as this study also pointed out, the particle aggregate size and film smoothness also play an important role in performance and repeatability.

The need for material control and uniformity is an indicator of the current lack of synthetic control over conducting polymers. The influence of different synthetic aspects such as temperature, mixing, concentration of reagents and ratio of reagents has become increasingly well understood over the past decade, particularly for nanofiber synthesis. The fundamental properties of the material continue to make it attractive, and even more so with the increased materials property control and dispersability. Polyaniline has been touted one of the most stable conducting polymers in terms of the environment, temperature, UV and visible light.³ For polyaniline, the stability of the conductivity can be affected by dopant mobility or loss, but efforts to use bulky and low volatility dopants, polymeric dopants and covalently linked dopants, e.g. self-doping, can mitigate the risk of conductivity variability.⁷⁸⁻⁸¹

Table 5.1. Reported Properties of Polyaniline*

Property	Energy Reference	Conductivity	Dopant	Solvent	Morphology
----------	------------------	--------------	--------	---------	------------

	(eV)	(S/cm)				
LUMO	-2.8			water	SAM	84
HOMO	-4.8					85
HOMO	-5.2					84
HOMO	-4 to -6				CVD	86
HOMO	-5.1	3 to 4	HCl		nanotube	87
HOMO	-5.4					88
HOMO	-6.2					88
HOMO	-4.75 ₈₉	1.5x10 ⁻²	1:1.2 PSS*	water	spher., 99 nm	
HOMO	-4.81	2.1x10 ⁻³	1:1.7 PSS*	water	spher., 90 nm	⁸⁹
HOMO	-4.96	9x10 ⁻⁵	1:3.0 PSS*	water	spher., 59 nm	⁸⁹
HOMO	-5.06	3.6x10 ⁻⁵	1:3.9 PSS*	water	spher., 79 nm	⁸⁹
HOMO	-5	2.5x10 ⁻⁶	1:6.2 PSS*	water	spher., 48 nm	⁸⁹
HOMO	-4.88 ₈₉	5.3x10 ⁻⁷	1 : 7.4 PSS*	water	spher., 46 nm	
HOMO	-4.88	5x10 ⁻⁵	DNNS	xylene	sphere., NP	⁸⁹
HOMO	-4.56	1	pTS	xylene	sphere., NP	⁸⁹
HOMO	-4.38	5	pTS+additive		xylene	
		sphere., NP	⁸⁹			
HOMO	-4.55	8x10 ⁻²	pTS	ethyl alc.	sphere., NP	⁸⁹
HOMO	-4.59	0.01	pTS	octanol	sphere., NP	⁸⁹
HOMO	-4.61	0.07	pTS	tert-butanol	sphere., NP	⁸⁹
HOMO	-4.74	3	pTS	benzyl alc.	sphere., NP	⁸⁹
HOMO	-4.69	1	pTS	methanol	sphere., NP	⁸⁹
HOMO	-4.67	10	pTS	ethanol	sphere., NP	⁸⁹
HOMO	-4.96	1x10 ⁻³	pTS	water	sphere., NP	⁸⁹
HOMO	-4.61	2	pTS	2-propanol	sphere., NP	⁸⁹
HOMO	-4.78	5x10 ⁻⁴	DBS	2-propanol	sphere., NP	⁸⁹
Bandgap	2.61	5x10 ⁻⁴	n/a	water	large aggr.	90
Bandgap	3.37	71.9	HCl	water	large aggr.	90
Bandgap	2.79	109.04	HNO ₃	water	large aggr.	90
Bandgap	2.45	92.13	HClO ₄	water	large aggr.	90
Bandgap	2.65	0.02	H ₂ SO ₄	water	large aggr.	90
Bandgap	3.02		HI	water	large aggr.	90

*The highest occupied molecular orbital (HOMO) energy level, lowest unoccupied molecular orbital (LUMO) energy level, bandgap energy and conductivity of polyaniline with different morphology and dopants in different solvents are listed. The solvent indicates the solvent used for synthesis or dispersion prior to deposition. SAM – self-assembled monolayer, CVD – chemical vapor deposited films, PSS – polystyrene sulfonic acid, spher. – spherical, alc. – alcohol, NP – nanoparticle, aggr. – aggregates, pTS – p-toluenesulfonic acid, DNNS – dinonylnaphthalenesulfonic acid.

A summary of several of the important polyaniline properties are presented in Table 5.1 shown for both nanostructured and conventional forms of polyaniline. Dopant, additives (particularly meta-cresol), chain length and polymer alignment have known effects on polyaniline's conductivity. Many of the high conductivity levels for polyaniline that have been reported are based on improved chain length and crystallinity. To date, there is limited analysis on the effects that various morphologies and synthetic methods have on these parameters.⁸² Morphology, and the method of synthesis are also likely to have major impacts on conductivity, molecular orbitals and other properties. Further exploration in these areas may lead to more strategic developments in polyaniline and conducting polymer structures with specific and tunable properties. Side chains have also been explored with many other conducting polymers, particularly polythiophene,⁸³ to improve functionality, solubility, conductivity, and other properties. While side chains typically reduce the conductivity of polyanilines, they may still be useful for tuning energy levels for materials needed in photovoltaic applications.

5.5 Actuators

Polyaniline and other conjugated polymers have been explored extensively for use in actuators. These polymers can change their structural conformation by the insertion of charged dopants and their solvating molecules (such as water) or with changes in the oxidation state to induce conformational changes as reported by Baker *et al.*⁹¹ Polyaniline nanofibers can even be used in a single material bimorph actuator by using flash welding to create an asymmetric membrane.⁹²

These bimorph actuators move rapidly and to a greater extent than other known heterogeneous or single material bending actuators. This is attributed to the extensive freedom of expansion of the nanofiber mat. The stimulus in this actuator is chemical doping and dedoping of the films in acid and base, respectively. This device may have applications in a sensor or valve that opens with exposure to acid or in nano- or micro-actuators. Gao *et al.* incorporated polyvinyl alcohol into a polyaniline nanofiber actuator that displayed a tunable degree of actuation and a response rate with better recoverability compared to a pure polyaniline nanofiber actuator.⁹³

Electrophoretic deposition has been used to form microstructures of polyaniline nanofibers as described by Shedd *et al.*⁹⁴ An electrode array charged a substrate to attract the polyaniline nanofibers to precise locations. Adjacent electrodes were given an opposite charge to prevent deposition at undesired sites. These microstructures can then be flash-welded to create a monolithic material. The article proposes its use in sensors, but if the flash-welded micro-films can be dislodged from the substrate they could also be used as micro-actuators.

There are several other actuator structures that have been explored with polyaniline and polyaniline nanostructures. To determine their feasibility in a high-strain all-polymer electro-acoustic actuator, Zhang *et al.*, explored the current density limitations of polyaniline. They found that polyaniline (in the conventional form) doped with camphorsulfonic acid (CSA) can withstand a current density as high as 1200 A/cm².⁹⁵ The polyaniline activated electrostrictive copolymer was as

effective as gold from -50°C to 120°C and from 1 Hz to 1 MHz frequencies. More recent experiments have led to the development of high breakdown field dielectric elastomer actuators using encapsulated conductive polyaniline nanoparticles as the high dielectric constant filler.⁹⁶ A dielectric elastomer is a smart material that shows considerable strain and/or stress in response to an applied electric field. In order to enhance the actuation strain, the dielectric constant of the elastomer should be increased by adding conducting fillers without compromising the elasticity of the polymer matrix.⁹⁷ Because polyaniline is a polymer it has more flexibility and better mechanical properties compared to metal particle fillers when used in conjunction with highly expansive polymer actuator materials. Wang *et al.* introduced polyaniline nanorods into a silicon rubber nanodielectric elastomer actuator to improve its dielectric constant and electromechanical properties and enhance electro-induced strain. Kim *et al.* fabricated an actuator using polyaniline nanorods/Nafion blend with electrical pathways showing improved actuating ability compared to that made with Nafion alone.⁹⁸ Uh *et al.* developed an electrolyte-free polyaniline microfiber actuator that undergoes a flapping wing motion in the presence of a magnetic field. Such an actuator has great potential in biomimetic artificial muscles, robotics and sensors.⁹⁹ Liu *et al.* constructed an air working ionic actuator by sandwiching a H₂SO₄-PVA gel electrolyte between two pieces of a reduced graphene oxide/polyaniline nanocomposite electrode. Actuating takes place when an electric field causes ion migration that induces volume differences between the cathode and anode. Such nanocomposite electrodes display excellent electrochemical stability over thousands of cycles due to the synergistic

effects of polyaniline nanowires and graphene oxide sheets.¹⁰⁰ Future work should lead to more structural bimorph and high-strain actuators, as well as concepts to be developed for future use such as nanoactuators with controllable motions and functions for building nanomachines¹⁰¹.

5.6 Supercapacitors

Supercapacitors are promising energy storage devices that have long cycle life (>100,000 cycles), high power density (>10,000 W/kg) and can be safely charged and discharged within seconds. Supercapacitors typically consist of positive and negative electrodes separated by an insulating separator with an ionic electrolyte. Two types of capacitance, double-layer capacitance and pseudo-capacitance are typically utilized. Double-layer capacitance results from the electrostatic charge stored at the interface between the electrode and electrolyte. Pseudo-capacitance is associated with a reversible redox or Faradaic charge transfer.¹⁰² Polyaniline has demonstrated high capacitance values due to its multiple redox states, which create a large total surface charge potential when sweeping from one oxidation state to another. Polyaniline nanofibers have demonstrated higher capacitance values than their bulk counterparts¹⁰³ due to the high surface area available for charging. Because of their high charge storage, low weight and good environmental stability, nanostructured polyaniline have the potential for a very high capacitance per unit of mass that is competitive with some considerably more expensive materials such as ruthenium oxide¹¹⁸.

The theoretical specific capacitance for nanofibrous polyaniline is estimated to be around 1200 F/g with the contribution of both pseudo-capacitance and electrical double-

layer capacitance.^{104,105} Currently, the reported values for the specific capacitance of pure polyaniline nanofiber electrodes in H₂SO₄ aqueous electrolyte are within 400-900 F/g using a three-electrode configuration.¹⁰⁶⁻¹⁰⁸ This gap shows that the part of polyaniline effective in contributing to capacitance is limited. According to Fig. 5.6, the diffusion of dopants (counter-anions) determines the amount of insertion/expulsion of counter-anions that can take place from the polyaniline surface. Since the light gray core part is essentially inaccessible at the timescale used in the charge/discharge process, it provides no contribution to the capacitance.¹⁰⁴ Therefore, it is critical to use nanostructured polyaniline because this provides greater electroactive material with shorter migration pathways for ions and mitigates mechanical deformation.¹⁰⁹

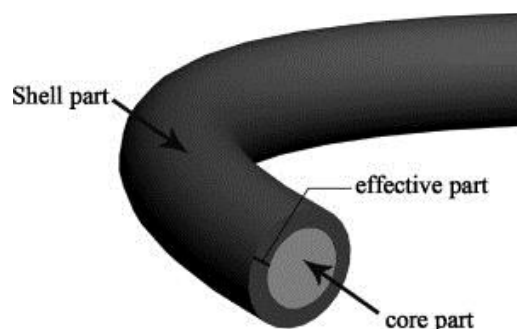


Figure 5.6 Core-shell model of polyaniline for charge storage influenced by the diffusion of dopants. Reproduced with permission from ref. 104. Copyright 2009 Elsevier Ltd.

Carbon materials are often incorporated into the polyaniline nanofibers in order to further improve their conductivity and mechanical stability. Polyaniline suffers from large volumetric shrinking and expansion during the doping/dedoping process due to the repeated insertion/expulsion of electrolyte ions¹¹⁰. Carbon materials such as activated carbon (AC), carbon nanotubes (CNTs) and graphene show high conductivity, good cycle

stability, but relatively low capacitance limited by their microstructures. Therefore, hybrid electrode materials based on nanostructured polyaniline and carbon materials can provide a synergetic combination of outstanding conductivity/stability from the carbon materials and high pseudo-capacitance from the polyaniline. Extensive research has been done on such hybrid supercapacitors. For example, Zhang *et al.* prepared a chemically modified graphene/polyaniline nanofiber composite by *in situ* polymerization of aniline in the presence of graphene oxide followed by hydrazine reduction and the reprotonation of polyaniline. Polyaniline fibers adsorbed onto the graphene sheets formed a uniform nanocomposite with a specific capacitance of 480 F/g at a current density of 0.1 A/g.¹¹¹ Cong *et al.* fabricated a freestanding flexible polyaniline nanorod/graphene paper via electropolymerization of polyaniline nanorods on the graphene paper. Such a nanocomposite possesses excellent conductivity with an equivalent series resistance of only 4.1 Ω . It also exhibits great performance as a supercapacitor with a specific capacitance of 763 F/g at 1 A/g discharge current and 82% capacity retention after 1000 cycles.¹¹² Kulkarni *et al.* used a 3D porous graphene framework on which polyaniline nanofibers were grown chemically. The 3D graphene framework was prepared via CVD growth of graphene on Ni foam followed by Ni etching. This electrode achieved a specific capacitance as high as 1024 F/g in 1.0 M H₂SO₄ at 10 mV/s scan rate. The conductive porous graphene framework offered a high surface area for the effective utilization of polyaniline and improved the charge transport and storage. Such an electrode had only 10 Ω resistance and demonstrated good cycle stability with 86.5% capacitance retention after 5000 cycles.¹¹³ A similar concept has been applied by Wang *et al.* to produce a 3D graphene/polyaniline nanofiber composite electrode using a

hydrothermal method, achieving 356 F/g even at a current density of 20 A/g.¹¹⁴ Pedrós *et al.* reported a 3D hierarchical porous composite supercapacitor electrode made of a polyaniline nanofiber sponge filled graphene foam (Figure 5.7). The graphene foam ensures efficient electronic transport within the scaffold with electrolyte rapidly diffusing into the high-surface-area polyaniline nanofibers. Such synergy led to rather high gravimetric capacitance (1474 F/g) and volumetric capacitance (86 F/cm³) at a current density of 0.47 A/g. The capacitance retention was 83% after 15,000 cycles.¹¹⁵ Hyder *et al.* used a LBL assembly of positively charged polyaniline nanofibers and carboxylic acid functionalized CNTs to obtain a thin film electrode with an interpenetrating network structure, creating well-developed nanopores that led to a very high volumetric capacitance (238 F/cm³).¹¹⁶

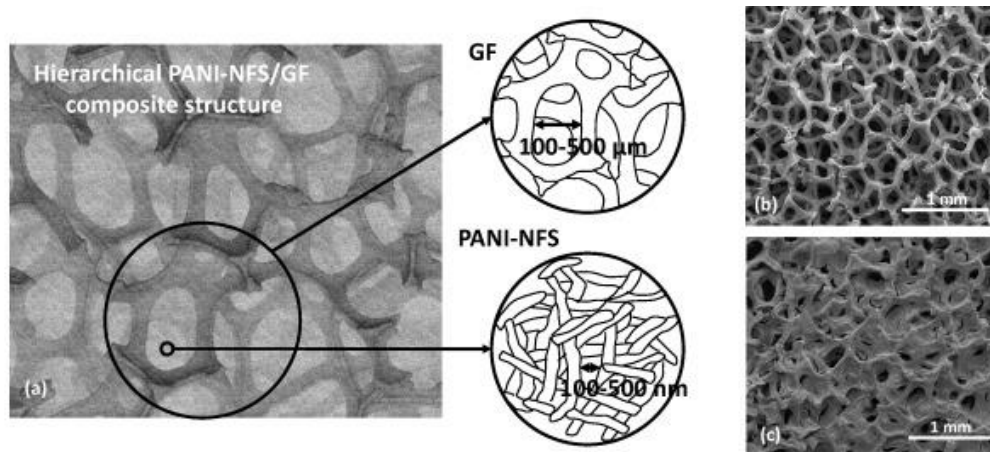


Figure 5.7 Schematic 3D hierarchical porous polyaniline nanofiber sponge/graphene foam composite electrode (a) showing the pore size ranges for each structure, as analyzed from SEM images of (b) a graphene foam and (c) a polyaniline sponge. Reproduced with permission from ref. 115. Copyright 2016 Elsevier Ltd.

Other materials, such as metal oxides, have also been combined with polyaniline nanofibers in order to obtain high-performance supercapacitors. Jiang *et al.* coated the

surface of polyaniline nanofibers with ultrafine loosened MnO₂ floccules. The high surface area of the MnO₂ floccules provided enhanced electroactive sites and the polyaniline nanofiber backbone served as the conductive pathways. The combination of the two pseudocapacitive materials gave a specific capacitance of 383 F/g at 0.5 A/g with an enhanced rate capability and cycling stability.¹¹⁷ Xia *et al.* grew a thin layer of RuO₂ on polyaniline nanofibers using atomic layer deposition (ALD) in order to stabilize the polyaniline and improve its energy density. A good specific capacitance of 710 F/g at 5 mV/s was achieved with an impressive power density of 42.2 kW/kg and an energy density of 10 Wh/kg. This electrode was able to maintain 88% of its capacitance after 10,000 cycles at a high current density of 20 A/g. This again demonstrated the excellent buffering effects of metal oxides on polyaniline nanofibers.¹¹⁸

An ionic liquid electrolyte was employed to further increase the energy storage capability of polyaniline pseudocapacitors by Chen *et al.*¹¹⁹ Full-cell pseudo-capacitors using polyaniline nanotubes as the electrode material and EMIMBF₄ (1-ethyl-3-methylimidazolium tetrafluoroborate) ionic liquid as the electrolyte demonstrated a remarkable energy density of 84 Wh/kg_(cell) and a power density of 182 kW/kg_(cell), about a 5 times improvement compared to cells using acidic aqueous electrolyte. This ionic liquid has very high voltage window (up to 6 V) with low vapor pressure and non-flammability. It is promising in producing supercapacitors with high energy density as the energy stored in a supercapacitor is proportional to the voltage squared ($E = 0.5 CV^2$). The hollow nanotube morphology of polyaniline was also advantageous as the electrolytes can access some inner portions of the nanotubes as well, further increasing the capacitance.

5.7 Protective Applications

5.7.1 Electrostatic dissipation

Antistatic and electrostatic dissipative (ESD) materials are used to prevent electrostatic discharge, which can be dangerous and/or costly in data storage devices, computer internals as well as moving machine arms and airplanes. Electrostatic build-up is typically caused by triboelectric charging. This occurs when an insulating material is brought into contact with another material and then separated. The resulting charge can dissipate when electrons are brought in contact with a conducting material. An antistatic material allows slow discharge of electrons that can build up on an insulating surface, preventing their rapid discharge to a more conducting surface as it can damage electronic components and even lead to sparking or even explosion. A specific range of conductivity is required so that the electrical charge does not move so quickly as to create a discharge event. The Electronic Industries Association (EIA) standard 541 points out that the optimal surface conductivity for ESD should be in the range of 10^{-6} - 10^{-10} S/cm.¹²⁰

Polyaniline has been demonstrated to be useful in several antistatic applications due to its suitable conductivity, low cost, good transparency and minimal mechanical change in a matrix. The conductivity for polyaniline is typically between 1 S/cm and 10^{-10} S/cm and can be easily tuned by dedoping, addition of metals/metal oxide nanoparticles/insulating polymeric fillers, or applying thinner films to reach values that are ideal for antistatic applications. Dhawan *et al.*¹²¹ and Lv *et al.*¹²² coated polyester fabric and polyimide fiber, respectively with polyaniline as a lightweight conductive materials for antistatic textiles. Anand *et al.*¹²⁰ developed a polyaniline/ZnO nanoparticle impregnated cotton fabric with a conductivity range of 10^{-3} - 10^{-9} S/cm depending on the

loading concentration. Static decay meter measurements showed that the static decay time of the fabric film was in the range of 0.5-3.4 s from 5000 V to 500 V, exhibiting great potential as an effective antistatic material.

Flexibility is another key benefit of a polyaniline nanofiber network for this type of application as polyaniline maintains its conductivity after bending and/or creasing. Pramanik *et al.*¹²³ reported a hyperbranched poly(ester amide)/polyaniline nanofiber nanocomposite as an antistatic material with good rheological behavior, mechanical strength and thermal stability. Nanofibrous polyaniline is promising in such applications because its high aspect ratio requires less material to generate a conductive pathway throughout the entire coating to reach the percolation threshold. A low percolation threshold of 2.2% was reported by Wang *et al.* for polyaniline nanofibers in a polymethylmethacrylate composite.¹²⁴

5.7.2 Electromagnetic Interference (EMI) shielding

The advantageous conducting properties of polyaniline nanofibers that make them useful in antistatics are also beneficial in electromagnetic interference (EMI) shielding applications. Electrical devices, radio and television signals, magnetic devices (e.g. NMRs and MRIs) and even nuclear blasts can generate electromagnetic interference that can disrupt telecommunication signals, and electronic device performance. Shielding from EMI interference is generally accomplished by wrapping a device, wire, etc. with a conductive material, such as the braided shielding used in electrical cables. Typical EMI shields have conductivities in the range of 1 to 1,000 S/cm.¹²⁵ The demand for lighter weight and lower cost materials that are effective for EMI shielding is rapidly increasing as electronics in handheld devices, vehicles, homes and workplaces are becoming more

advanced and more compact. There are also important security concerns as communication via cellphones are more heavily relied upon, which can be impacted by electromagnetic and radiofrequency pollution. Inherently conducting polymers offer distinct advantages over the more commonly used metal/carbon imbedded polymers due to their corrosion resistance, light-weight, low-cost and variable frequency absorption ranges.¹²⁶ With metallic fillers, the loading levels necessary to achieve conductivities sufficient for effective shielding can compromise the mechanical stability, add weight, and make the materials susceptible to corrosion. Additionally, it is difficult to achieve a uniform dispersion of metal particles.¹²⁶ Carbon fillers such as carbon black are chemically stable, but loadings must be very high, leading to mechanical issues and sloughing, which can cause contamination and shorting of electrical components. High-aspect-ratio carbon nanostructures such as carbon nanotubes (CNTs) can provide high conductivity at relatively low loading levels.¹²⁷ However, they are far more expensive to produce than polyaniline nanofibers, which can be solution synthesized from inexpensive aniline monomer with a low environmental impact.

Shielding effectiveness (SE) is measured as the ratio of the electrical field strength before and after attenuation by a given material. The shielding mechanism is highly dependent on filler properties, loading level, and frequency.¹²⁸ In general, 40 dB and 80 dB SEs are required for commercial and military applications, respectively. Polyaniline has been tested for EMI shielding in numerous research studies and its EMI shielding performance was found to be comparable to CNT composites.¹³¹ Polyaniline absorbs electromagnetic radiation through the effective interaction of polarons with incident electromagnetic radiation. Niu *et al.* reported polyaniline nanofiber-polyacrylate

composite coatings with an SE of 38 to 63 dB over a frequency range from 100 kHz to 10 GHz.¹²⁹ Liu *et al.* dispersed polyaniline nanoparticles in an epoxy matrix to form a coating with an SE of 30 to 60 dB in the range of 100 to 1000 MHz.¹³⁰ Joseph *et al.* formulated a 1 mm polyaniline nanofiber/graphite composite absorbing ink with an SE of 87 dB in the frequency range of 8.2-18 GHz. It's worth noting that ink made with polyaniline nanofibers alone with the same thickness had an SE of 74 dB in the same range. The 2.3% graphite composite resulted in improvement in conductivity and acts as a stable underlying conductive network. The optimized nanofibrillar morphology of polyaniline contributes to its good conductivity and shielding capability. The nanosized fibers can cause multiple reflections of electromagnetic waves within the matrix that eventually leads to more dissipation of electromagnetic energy due to longer propagation pathways.¹³² Polyaniline nanofibers have also been combined with gold nanoparticles¹³³ and NiZn-ferrite nanoparticles¹³⁴ for such applications. For medical and military applications, it is desirable to protect the human body from EMI by incorporating conductive fillers into clothing. Fabric made with a polyaniline coating showed a lower shielding efficiency, 35 dB, but these materials were not made with a variable loading rate of polyaniline^{121,126,129}. Also of note is the finding that EMI shielding using ICP fillers block a significant portion of the incident field by an absorptive mechanism, making them especially attractive for stealth applications.¹²⁶

5.8 Inorganic Nanocomposite Applications

Various combinations of metal compounds and polyaniline nanofibers have been used for many applications including supercapacitors¹³⁵, sensors¹⁸, catalysts¹⁵ and non-volatile memory¹³⁶. Many of these composites take advantage of the

inherent redox properties of polyaniline to spontaneously reduce some metal cations, especially noble metals, to form uniform metal nanoparticles. The morphology of the polyaniline nanofibers were demonstrated to be capable of template growth of uniform (<2 nm) nanoparticles of gold that adhere to the nanofibers following exposure to chloroauric acid (HAuCl₄).¹⁴ This was accomplished through the use of low reaction temperatures and reagent concentrations. These nanostructures were surprising because previous studies¹³⁶ showed that conventional forms of polyaniline and chloroauric acid, which when dissolved and cast as a dense sheet, resulted in irregular micron scale gold particles.

These metal nanoparticles demonstrated the ability to store charge with relatively low turn on voltages in a cross-bar memory device.¹⁴ In these devices after a minimum voltage is applied between the two electrodes, charge is stored in the metal nanoparticles. This charge is stabilized by a counter-ion in the conducting polymer backbone. Prior and subsequent work has used other organic molecules for charge stabilization. The advantage of the polyaniline nanofiber metal nanoparticle system is that the metal nanoparticles do not have to be produced in a separate step. The polyaniline nanofibers also appear to facilitate uniform growth and prevent Ostwald ripening of the particles. The small and uniform deposition of gold nanoparticles and the charge stabilization provided by the nitrogens on the conducting polymer backbone allowed for stable turn on (i.e. “1”, high conductivity) and turn off (i.e. “0”, low conductivity) with only a small applied voltage. The simple process for making these composite materials

combined with the stability and the large number of fast read-write-erase cycles made the system interesting for non-volatile applications. Once the composite in a memory device is dried and thermoset in a cross-linked poly (vinyl alcohol) matrix, the device is quite stable and can be turned on/off months later. However, if the gold polyaniline nanofiber composite is left in solution for a period of months, agglomeration of the metal nanoparticles is observed. This may occur to some degree with the metal nanoparticles in the device, particularly under a continuous applied voltage. Alkane thiol coating of the metal nanoparticles after formation on the polyaniline nanofibers may increase the materials stability, and the long-term device stability and cyclability.

The reaction between polyaniline nanofibers and metal cations can be controlled by altering the temperature, reaction time and stabilizers used in the reaction, in order to yield gold nanoparticles of different sizes and morphologies on the polyaniline nanofibers.^{137,138} Figure 5.8 shows the various sizes of gold particles grown on polyaniline nanofibers through *in situ* autoreduction of chloroauric acid. Gold nanoparticles with sizes of <1, 2 and 6 nm were achieved by cooling reactants to different temperatures prior to reaction, during reaction and during dialysis purification. Larger particle sizes were generated using higher chloroauric acid concentrations. Gold sheets were obtained by carrying out the reaction under reflux and purifying at room temperature. Memory devices fabricated using a 2 nm gold nanoparticle/polyaniline nanofiber composite demonstrated the best performance with a low turn-on voltage which required less

power consumption and large on/off ratios which provided good stability with hundreds of write-read-erase cycles.

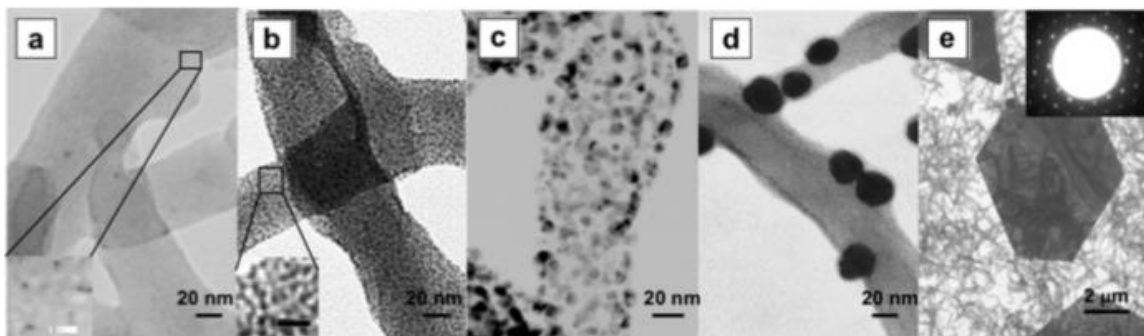


Figure 5.8 TEM images of autoreduced gold nanoparticles with (a) <1, (b) 2, (c) 6, (d) >20 nm and (e) gold sheets grown on polyaniline nanofibers. Reproduced with permission from ref. 137. Copyright 2011 American Chemical Society.

In addition to gold, as discussed above, platinum¹³⁹, silver¹⁴⁰ and palladium nanoparticles¹⁴¹ have also been deposited on polyaniline nanofibers with exposure to the appropriate metal salt. Palladium nanoparticles grown on polyaniline nanofibers have been shown to be effective in catalysis, for example, high yield aqueous Suzuki coupling reactions between aryl halides and boronic acids have been demonstrated.¹⁵ Evidence has been found for a semi-heterogeneous catalytic mechanism¹⁴².

5.9 Other Applications

5.9.1 Corrosion Protection

Aniline, polyaniline and derivatives including aniline black have all been considered for use in corrosion protection.¹⁴³⁻¹⁴⁶ Several polyaniline suppliers have

sold the material as an undercoating for corrosion protection to be applied directly to the surface of the metal under a top-coat. Polyaniline, along with other conducting polymers, is redox active allowing it to reduce metal cations as mentioned in the previous section. Unlike alternative anti-corrosion materials such as chromates, phosphates and molybdates, polyaniline is more environmentally friendly and exhibits reversible electrochemical properties by controlled charge transfer in air.

Previous research using the conventional organic cast film form of polyaniline has suggested anodic protection of metal surfaces.¹⁴³ Testing is usually conducted by placing a scratch in the surface of the coating film in a heated, humid and/or salty environment and observing the extent of corrosion over time. These tests have shown conventional polyaniline (coated electrochemically or via an organic solvent) and nanofibrillar polyaniline¹⁴⁴ are effective additives to protect metals from corrosion. The high surface area of polyaniline nanofibers are especially beneficial in large-scale coating applications for corrosion protection due to the outstanding processability of polyaniline nanofibers which allows direct incorporation with other coating materials for a single step corrosion protection layer.^{145,146}

5.9.2 Biocomposites

Starting in the early 2000's conductive and particularly nanostructured conductive materials were identified as excellent materials for tissue engineering.¹⁴⁷⁻¹⁵⁰ Tissue engineering is a rapidly growing field, and one of the most critical portions of this work is the development of conducting materials to interface

with biological tissue for the stimulation of neurons and muscles. Conducting polymers are especially attractive as they allow variable conductivity via simple chemical and structural modification. Polyaniline is essentially inert in *in vivo* studies using mice without causing inflammation, indicating potential for use in bioengineering applications like muscle scaffolding or neuron stimulation. Nanostructured polyaniline is also an excellent candidate for tissue growth as reported by Bidez, *et al.*¹⁴⁷ Another study showed that polyaniline nanofibers can be blended with collagen and used for culturing porcine skeletal muscle cells.¹⁴⁸ Wang *et al.* designed core-shell scaffolds using aligned polyaniline and silk fibroin nanofibers for mimicking the structure of native skeletal muscle.¹⁴⁹ Zhang *et al.* reported on the synergistic effects of electrical stimulation and nerve growth factor on neuron growth using a polyaniline nanofiber composite mesh incorporated with nerve growth factor.¹⁵⁰

5.9.3 Filtration Membranes

Polyaniline and its derivatives have been used to fabricate water filtration membranes with enhanced hydrophilicity, permeability, chlorine resistance and anti-fouling properties.^{151,152} Polyaniline nanofibers have also been blended into existing membrane materials as pore forming agent and hydrophilic modifiers.¹⁵³ Polyaniline nanofibers and CNTs were incorporated into a polysulfone membrane matrix by Liao *et al.*¹⁵⁴ By adjusting the nanofiber content and applying flash welding, the structure, morphology, hydrophilicity, conductivity and permeability of the membrane can be controlled. Membranes fabricated using an N-substituted derivative of polyaniline were found by Huang *et al.*¹⁵² to be chlorine tolerant and

anti-fouling. These materials are now being developed by the membrane company Water Planet, Inc.

As the best-studied and potentially most useful conducting polymer, polyaniline has had a wide portfolio of applications owing to its facile synthesis, intrinsic conductivity and unique doping/dedoping chemistry. The development of one-dimensional nanostructured polyaniline with enhanced processability and exceptional functionality offers great promise in fields such as sensors, electrochromics, supercapacitors and antistatic materials, which have all been described in this review along with many other applications. The nanofiber morphology can be easily achieved through electrochemical polymerization, interfacial polymerization or rapid mixing method. The latter method is readily scalable for practical use. Devices fabricated using nanostructured polyanilines generally have better performance compared to the ones made using their conventional counterparts. For example, polyaniline nanofiber sensors show much faster response and higher sensitivity, while supercapacitors made with polyaniline nanofibers exhibit higher specific capacitance and better cycle stability. Polyaniline nanofibers readily disperse in water at an appropriate pH, making them easy to be incorporated into matrices for electrostatic dissipative and electromagnetic interference shielding. No matter how many applications are discussed in a review article such as this, there are always more ideas that can be achieved with the development of new materials, especially when the material can be manufactured cost-effectively at a large scale. The rapid development in the

synthesis, morphology control and novel properties of one-dimensional polyaniline will continue to spur further commercial interest in this promising material.

5.10 References

- (1) H. Endemann, *J. Am. Chem. Soc.*, 1886, **8**, 189-191.
- (2) D. Li, J. Huang and R. B. Kaner, *Acc. Chem. Res.*, 2008, **42**, 135-145.
- (3) D. Li and R. B. Kaner, *Chem. Commun.*, 2005, 3286-3288.
- (4) X. Yu, Y. Li, N. Zhu, Q. Yang and K. Kalantar-zadeh, *Nanotechnology*, 2007, **18**, 015201.
- (5) W. R. Small, F. Masdarolomoor, G. G. Wallace and M. in het Panhuis, *J. Mater. Chem.*, 2007, **17**, 4359-4361.
- (6) L. Hu, G. Gruner, D. Li, R. B. Kaner and J. Cech, *J. Appl. Phys.*, 2007, **101**, 016102.
- (7) C. Li, H. Bai and G. Shi, *Chem. Soc. Rev.*, 2009, **38**, 2397-2409.
- (8) H. D. Tran, D. Li and R. B. Kaner, *Adv. Mater.*, 2009, **21**, 1487-1499.
- (9) J. Huang, *Pure and Appl. Chem.*, 2006, **78**, 15-27.
- (10) J. Huang, S. Virji, B. H. Weiller and R. B. Kaner, *J. Am. Chem. Soc.*, 2003, **125**, 314-315.
- (11) J. Stejskal and R. G. Gilbert, *Pure Appl. Chem.*, 2002, **74**, 857-867.
- (12) J. Wang and D. Zhnag, *Adv. Polym. Tech.*, 2013, **32**, E323-E368
- (13) J. Huang and R. B. Kaner, *J. Am. Chem. Soc.*, 2004, **126**, 851-855.
- (14) R. J. Tseng, C. O. Baker, B. Shedd, J. Huang, R. B. Kaner, J. Ouyang and Y. Yang, *Appl. Phy. Lett.*, 2007, **90**, 053101.
- (15) B. J. Gallon, R. W. Kojima, R. B. Kaner and P. L. Diaconescu, *Angew. Chem. Int. Ed.*, 2007, **46**, 7251-7254.
- (16) S. Virji, B. H. Weiller, J. Huang, R. Blair, H. Shephard, T. Faltens, P. C. Haussmann, R. B. Kaner and S. H. Tolbert, *J. Chem. Educ.*, 2008, **85**, 1102.
- (17) M. Liu, C. Dai, C. Chan and C. Wu, *Sensors*, 2009, **9**, 869-880.
- (18) S. Virji, J. D. Fowler, C. O. Baker, J. Huang, R. B. Kaner and B. H. Weiller, *Small*, 2005, **1**, 624-627.
- (19) S. Virji, R. B. Kaner and B. H. Weiller, *Chem. Mater.*, 2005, **17**, 1256-1260.
- (20) S. Virji, R. Kojima, J. D. Fowler, J. G. Villanueva, R. B. Kaner and B. H. Weiller, *Nano Res.*, 2009, **2**, 135-142.

- (21) S. Virji, R. Kojima, J. D. Fowler, R. B. Kaner and B. H. Weiller, *Chem. Mater.*, 2009, **21**, 3056-3061.
- (22) S. Virji, J. Huang, R. B. Kaner and B. H. Weiller, *Nano Lett.*, 2004, **4**, 491-496.
- (23) J. D. Fowler, S. Virji, R. B. Kaner and B. H. Weiller, *J. Phys. Chem. C*, 2009, **113**, 6444-6449.
- (24) K. Kim and G. Chung, *Synth. Met.*, 2012, **162**, 636-640.
- (25) R. Arsat, X. Yu, Y. Li, W. Wlodarski and K. Kalantar-zadeh, *Sens. Actuators, B*, 2009, **B137**, 529-532.
- (26) X. Yu, Y. Li and K. Kalantar-Zadeh, *Sens. Actuators, B*, 2009, **B136**, 1-7.
- (27) A. Z. Sadek, C. O. Baker, D. A. Powell, W. Wlodarski, R. B. Kaner and K. Kalantar-zadeh, *IEEE Sens. J.*, 2007, **7**, 213-218.
- (28) P. C. Wang, E. C. Venancio, A. Wu, A. Ignatiev, A. G. MacDiarmid and J. A. T. Johnson, *DOE Hydrogen Program Fall 2007 Annual Progress Report*, 2007, 567-569.
- (29) Q. Lin, Y. Li and M. Yang, *Anal. Chim. Acta*, 2012, **748**, 73-80.
- (30) S. P. Surwade, S. R. Agnihotra, V. Dua, N. Manohar, S. Jain, S. Ammu and S. K. Manohar, *J. Am. Chem. Soc.*, 2009, **131**, 12528-12529.
- (31) Y. Zhang, J. Kim, D. Chen, H. Tuller and G. Rutledge, *Adv. Funct. Mater.*, 2014, **24**, 4005-4014.
- (32) J. Zhao, G. Wu, Y. Hu, Y. Liu, X. Tao and W. Chen, *J. Mater. Chem. A*, 2015, **3**, 24333-24337.
- (33) W. Li, N. D. Hoa, Y. Cho, D. Kim and J. Kim, *Sens. Actuators, B*, 2009, **143**, 132-138.
- (34) F. Wang, W. Wang, B. Liu, Z. Wang and Z. Zhang, *Talanta*, 2009, **79**, 376-382.
- (35) X. Wang, H. Wang, T. Ge, T. Yang, S. Luo and K. Jiao, *J. Phys. Chem. C*, 2015, **119**, 9076-9084.
- (36) P. M. Ndongili, T. T. Waryo, M. Muchindu, P. G. L. Baker, C. J. Ngila and E. I. Iwuoha, *Electrochim. Acta*, 2010, **55**, 4267-4273.
- (37) Y. Hao, B. Zhou, F. Wang, J. Li, L. Deng and Y. Liu, *Biosens. Bioelectron.*, 2014, **52**, 422-426.
- (38) E. Spain, R. Kojima, R.B. Kaner, G.G. Wallace, L. Dennany, J. O'Grady, K. Lacey, T. Barry, T.E. Keyes and R.J. Forster, *Biosensors and Bioelectronics*, 2011, **26**, 2613-2618.

- (39) H. Zhou, H. Chen, S. Luo, J. Chen, W. Wei and Y. Kuang, *Biosensors and Bioelectronics*, 2005, **20**, 1305-1311.
- (40) A. Morrin, F. Wilbeer, O. Ngamna, S. E. Moulton, A. J. Killard, G. G. Wallace and M. R. Smyth, *Electrochem. Commun.*, 2005, **7**, 317-322.
- (41) T. Yang, N. Zhou, Y. Zhang, W. Zhang, K. Jiao and G. Li, *Biosens. Bioelectron.*, 2009, **24**, 2165-2170.
- (42) S. Radhakrishnam, S. Prakash, C. R. K. Rao and M. Vijayan, *Electrochem. Solid-State Lett.*, 2009, **12**, A84-A87.
- (43) Z. Hu, J. Xu, Y. Tian, R. Peng, Y. Xian, Q. Ran and L. Jin, *Electrochim. Acta*, 2009, **54**, 4056-4061.
- (44) A. J. Epstein, J. A. O. Smallfield, H. Guan and M. Fahlman, *Synth. Met.*, 1999, **102**, 1374-1376.
- (45) C. Yang, Y. Chih, H. Cheng and C. Chen, *Polymer*, 2005, **46**, 10688-10698.
- (46) F. Masdarolomoor, P. C. Innis, S. Ashraf, R. B. Kaner and G. G. Wallace, *Macromol. Rapid Commun.*, 2006, **27**, 1995-2000.
- (47) I. J. Ball, S. Huang, K. J. Miller, R. A. Wolf, J. Y. Shimano and R. B. Kaner, *Synth. Met.*, 1999, **102**, 1311-1312.
- (48) M. Kulkarni, A. Viswanath and P. Khanna, *J. Macromol. Sci., Pure Appl. Chem.*, 2006, **43**, 759-771.
- (49) C. P. L. Rubinger, R. Faez, L. C. Costa, C. R. Martins and R. M. Rubinger, *Polym. Bull.*, 2008, **60**, 379-386.
- (50) S. K. Shukla, M. A. Quraishi and R. Prakash, *Corros. Sci.*, 2008, **50**, 2867-2872.
- (51) X. Wang, H. Wang, T. Ge, T. Yang, S. Luo and K. Jiao, *J. Phys. Chem. C*, 2015, **119**, 9076-9084.
- (52) H. Chang, Y. Yuan, N. Shi and Y. Guan, *Anal. Chem.*, 2007, **79**, 5111-5115.
- (53) S. Y. Hong, Y. H. Lee, H. Park, S. W. Jin, Y. R. Jeong, J. Yun, I. You, G. Zi and J. S. Ha, *Adv. Mater.*, 2016, **28**, 930-935.
- (54) H. Park, Y. R. Jeong, J. Yun, S. Y. Hong, S. Jin, S. Lee, G. Zi, J. S. Ha, *ACS Nano*, 2015, **9**, 9974-9985.
- (55) J. Jang, J. Ha and J. Cho, *Adv. Mater.*, 2007, **19**, 1772-1775.
- (56) Y. Xia, A. Karwa, F. Sigg, D. M. Clark and B. E. Kahn, *Materials Research Society Symposium Proceedings*, 2005, **828**, A5.28.1 - A5.28.3.
- (57) N. B. Clark and L. J. Maher, *React. Funct. Polym.*, 2009, **69**, 594-600.

- (58) K. Crowley, M. R. Smyth, A. J. Killard and A. Morrin, *Chem. Pap.*, 2013, **67**, 771-780.
- (59) N. Joseph, J. Varghese and M. T. Sebastian, *J. Mater. Chem. C*, 2016, **4**, 999-1008.
- (60) J. Huang and R. B. Kaner, *Nat. Mater.*, 2004, **3**, 783-786.
- (61) C. Wang, J. Song, H. Bao, Q. Shen and C. Yang, *Adv. Funct. Mater.*, 2008, **18**, 1299-1306.
- (62) W. Lu, A. G. Fadeev, B. H. Qi, E. Smela, B. R. Mattes, J. Ding, G. M. Spinks, J. Mazurkiewicz, D. Z. Zhou, G. G. Wallace, D. R. MacFarlane, S. A. Forsyth and M. Forsyth, *Science*, 2002, **297**, 983-987.
- (63) W. Lu, A. G. Fadeev, B. H. Qi and B. R. Mattes, *J. Electrochem. Soc.*, 2004, **151**, H33-H39.
- (64) E. M. Genies, M. Lapkowski, P. Noel, S. Langlois, M. N. Collomb and F. Miquelino, *Synth. Met.*, 1991, **43**, 2847-2852.
- (65) V. Jain, H. M. Yochum, R. Montazami and J. R. Heflin, *Appl. Phys. Lett.*, 2008, **92**, 033304.
- (66) R. Montazami, V. Jain and J. R. Heflin, *Electrochim. Acta*, 2010, **56**, 990-994.
- (67) P. Jia, A. A. Argun, J. Xu, S. Xiong, J. Ma, P. T. Hammond and X. Lu, *Chem. Mater.*, 2010, **22**, 6085-6091.
- (68) C. H. B. Silva, N. A. Galiote, F. Huguenin, É. Teixeira-Neto, V. R. L. Constantino and M. L. A. Temperini, *J. Mater. Chem.*, 2012, **22**, 14052-14060.
- (69) H. D. Tran and R. B. Kaner, *Chem. Commun.*, 2006, 3915-3917.
- (70) K. Wang, H. Wu, Y. Meng, Y. Zhang and Z. Wei, *Energy Environ. Sci.*, 2012, **5**, 8384-8389.
- (71) Y. Tian, S. Cong, W. Su, H. Chen, Q. Li, F. Geng and Z. Zhao, *Nano Lett.*, 2014, **14**, 2150-2156.
- (72) E. M. Erro, A. M. Baruzzi and R. A. Iglesias, *Polymer*, 2014, **55**, 2440-2444.
- (73) C. Hu, S. Chen, S. Peng, X. Liu and J. Liu, *Appl. Surf. Sci.*, 2015, **358**, 443-448.
- (74) Q. Tang, H. Cai, S. Yuan and X. Wang, *J. Mater. Chem. A*, 2013, **1**, 317.
- (75) Z. Tang, J. Wu, M. Zheng, Q. Tang, Q. Liu, J. Lin and J. Wang, *RSC Adv.*, 2012, **10**, 4062-4064.
- (76) A. Bahramian and D. Vashaee, *Sol. Energy Mater. Sol. Cells*, 2015, **143**, 284-295.

- (77) S. Tan, J. Zhai, B. Xue, M. Wan, Q. Meng, Y. Li, L. Jiang and D. Zhu, *Langmuir*, 2004, **20**, 2934-2937.
- (78) C. Han, C. Lu, S. Hong, K. Yang, *Macromolecules*, 2003, **36**, 7908-7915.
- (79) D. Chaudhuri, P. W. Menezes and D. D. Sarma, *Appl. Phys. Lett.*, 2003, **83**, 2348-1253.
- (80) T. Chen, C. Dong, X. Li and J. Gao, *Polym. Degrad. Stab.*, 2009, **94**, 1788-1794.
- (81) S. Bhadra and D. Khastgir, *Polym. Degrad. Stab.*, 2008, **93**, 1094-1099.
- (82) K. Lee, S. Cho, S. H. Park, A. J. Heeger, C. Lee and S. Lee, *Nature*, 2006, **441**, 65-68.
- (83) L. Torsi, A. Tafuri, N. Cioffi, M. C. Gallazzi, A. Sassella, L. Sabbatini and P. G. Zambonin, *Sens. Actuators, B*, 2003, **93**, 257-262.
- (84) G. K. R. Senadeera, T. Kitamura, Y. Wada and S. Yanagida, *J. Photochem. Photobiol., A*, 2004, **164**, 61-66.
- (85) V. A. Zakrevskii, S. V. Kuz'min and N. T. Sudar', *Polym. Sci. Ser. A*, 2008, **50**, 411-416.
- (86) B. Xu, J. Choi, A. N. Caruso and P. A. Dowben, *Appl. Phys. Lett.*, 2002, **80**, 4342-4344.
- (87) Y. Han, Y. Lee and P. Huang, *J. Electrochem. Soc.*, 2009, **156**, K37-K43.
- (88) P. Barta, T. Kugler, W. R. Salaneck, A. P. Monkman, J. Libert, R. Lazzaroni and J. L. Brédas, *Synth. Met.*, 1998, **93**, 83-87.
- (89) J. R. Posdorfer, B. Werner, B. Wessling, S. Heun, H. Becker, 1 ed.; Z. H. Kafafi, P. A. Lane, Eds.; SPIE: San Diego, CA, USA, 2004; Vol. 5214; pp 188-196.
- (90) M. D. Catedral, A. K. G. Tapia, R. V. Sarmago, J. P. Tamayo and E. J. Rosario, *Science Diliman*, 2004, **16**, 41-46.
- (91) J. Xie, C. Zong, X. Han, H. Ji, J. Wang, X. Yang and C. Lu, *Macromol. Rapid Commun.*, 2016, **37**, 637-642.
- (92) C. O. Baker, B. Shedd, P. C. Innis, P. G. Whitten, G. M. Spinks, G. G. Wallace and R. B. Kaner, *Adv Mater.*, 2008, **20**, 155-158.
- (93) H. Gao, J. Zhang, W. Yu, Y. Li, S. Zhu, Y. Li, T. Wang and B. Yang, *Sens. Actuators, B*, 2010, **145**, 839-846.
- (94) B. Shedd, C. O. Baker, M. J. Heller, R. B. Kaner and H. T. Hahn, *Mater. Sci. Eng., B*, 2009, **162**, 111-115.

- (95) H. Xu, V. Bharti, Z. Cheng, Q. M. Zhang, *Materials Research Society Symposium Proceedings*, 2000, **600**, 185-190.
- (96) M. Molberg, D. Crespy, P. Rupper, F. Nüesch, J. E. Månson, C. Löwe, D. M. Opris, *Adv. Func. Mater.*, 2010, **20**, 3280-3291.
- (97) D. Wang L. Zhang, L. Zhang, J. Zha, H. Yu, S. Hu and Z. Dang, *Appl. Phys. Lett.*, 2014, **104**, 242903.
- (98) S. H. Kim, K. W. Oh and J. H. Choi, *J. Appl. Polym. Sci.*, 2010, **116**, 2601-2609.
- (99) K. Uh, B. Yoon, C. W. Lee and J. Kim, *ACS Appl. Mater. Interfaces*, 2016, **8**, 1289-1296.
- (100) Q. Liu, L. Liu, K. Xie, Y. Meng, H. Wu, G. Wang, Z. Dai, Z. Wei and Z. Zhang, *J. Mater. Chem. A*, 2015, **3**, 8380.
- (101) Y. Ke, T. Meyer, W. M. Shih, G. Bellot, *Nat. Commun.*, 2016, **7**, 10935.
- (102) Y. Shao, M. F. El-Kady, L. J. Wang, Q. Zhang, Y. Li, H. Wang, M. F. Mousavi and R. B. Kaner, *Chem. Soc. Rev.*, 2015, **44**, 3639-3665.
- (103) R. Ganesan, S. Shanmugam and A. Gedanken, *Synth. Met.*, 2008, **158**, 848-853.
- (104) H. Li, J. Wang, Q. Chu, Z. Wang, F. Zhang and S. Wang, *J. Power Sources*, 2009, **190**, 578-586.
- (105) C. Peng, D. Hu and G. Z. Chen, *Chem. Commun.*, 2011, **47**, 4105-4107.
- (106) H. Mi, X. Zhang, S. Yang, X. Ye and J. Luo, *Mater. Chem. Phys.*, 2008, **112**, 127-131.
- (107) G. Li, Z. Feng, J. Zhong, Z. Wang and Y. Tong, *Macromolecules*, 2010, **43**, 2178-2183.
- (108) F. Ran, Y. Tan, J. Liu, L. Zhao, L. Kong, Y. Luo and L. Kang, *Polym. Adv. Technol.*, 2012, **23**, 1297-1301.
- (109) H. Xu, X. Li and G. Wang, *J. Power Sources*, 2015, **294**, 16-21.
- (110) C. Xia, W. Chen, X. Wang, M. N. Hedhili, N. Wei and H. N. Alshareef, *Adv. Energy Mater.*, 2015, **5**, 1401805.
- (111) K. Zhang, L. Zhang, X. Zhao and J. Wu, *Chem. Mater.*, 2010, **22**, 1392-1401.
- (112) H. Cong, X. Ren, P. Wang and S. Yu, *Energy Environ. Sci.*, 2013, **6**, 1185-1191.
- (113) S. B. Kulkarni, U. M. Patil, I. Shackery, J. S. Sohn, S. Lee, B. Park and S. Jun, *J. Mater. Chem. A*, 2014, **2**, 4989-4998.

- (114) J. Wang, H. Xian, T. Peng, H. Sun and F. Zheng, *RSC Adv.*, 2015, **5**, 13607-13612.
- (115) J. Pedrós, A. Boscá, J. Martínez, S. Ruiz-Gómez, L. Pérez, V. Barranco and F. Calle, *J. Power Sources*, 2016, **317**, 35-42.
- (116) M. N. Hyder, S. W. Lee, F. Ç. Cebeci, D. J. Schmidt, Y. Shao-Horn and P. T. Hammond, *ACS Nano*, 2011, **5**, 8552-8561.
- (117) H. Jiang, J. Ma and C. Li; *J. Mater. Chem.*, 2012, **22**, 16939-16942.
- (118) C. Xia, W. Chen, X. Wang, M. N. Hedhili, N. Wei and H. N. Alshareef, *Adv. Energy Mater.*, 2015, **5**, 1401805.
- (119) W. Chen, R. B. Rakhi and H. N. Alshareef, *J. Mater. Chem. A*, 2013, **1**, 3315-3324.
- (120) A. Anand, N. Rani, P. Saxena, H. Bhandari and S. K. Dhawan, *Polym. Int.*, 2015, **64**, 1096-1103.
- (121) S. K. Dhawan, N. Singh, and S. Venkatachalam, *Synth. Met.*, 2001, **125**, 389-393.
- (122) P. Lv, Y. Zhao, F. Liu, G. Li, X. Dai, X. Ji, Z. Dong and X. Qiu, *Appl. Surf. Sci.*, 2016, **367**, 335-341.
- (123) S. Pramanik, J. Hazarika, A. kumar, N. Karak, *Ind. Eng. Chem. Res.*, 2013, **52**, 5700-5707.
- (124) Y. Wang and X. Jing, *Mater. Sci. Eng., B*, 2007, **138**, 95-100.
- (125) L. Ruppert, *Conductive Polymers and Plastics in Industrial Applications*; William Andrew publishing/Plastics Design Library, 1999.
- (126) Y. Wang and X. Jing, *Polym. Adv. Technol.*, 2005, **16**, 344-351.
- (127) K. Yoshino, H. Kajii, H. Araki, T. Sonoda, H. Take and S. Lee, *Fullerene Sci. Technol.*, 1999, **7**, 695-711.
- (128) Z. Liu, G. Bai, Y. Huang, Y. Ma, F. Du, F. Li, T. Guo and Y. Chen, *Carbon*, 2007, **45**, 821-827.
- (129) Y. Niu, *Polym. Eng. Sci.*, 2008, **48**, 355-359.
- (130) C. Liu, S. Lee, C. Ho, J. Han and K. Hsieh, *J. Phys. Chem. C*, 2008, **112**, 15956-15960.
- (131) S. Pande, B. P. Singh, R. B. Mathur, T. L. Dhami, P. Saini and S. K. Dhawan, *Nanoscale Res. Lett.*, 2009, **4**, 327-334.
- (132) N. Joseph, J. Varghese and M. T. Sebastian, *J. Mater. Chem. C.*, 2016, **4**, 999-1008.

- (133) J. Tahalyani, K. K. Rahangdale, R. Aepuru, B. Kandasubramanian and S. Datar, *RSC Adv.*, 2016, **6**, 36588-36598.
- (134) C. Wang, Y. Shen, X. Wang, H. Zhang, A. Xie, *Mater. Sci. Semicond. Process.*, 2013, **16**, 77-82.
- (135) K. Machida, K. Furuuchi, M. Min, K. Naoi, *Electrochemistry*, 2004, **72**, 402-404.
- (136) R. J. Tseng, J. Huang, J. Ouyang, R. B. Kaner and Y. Yang, *Nano Lett.*, 2005, **5**, 1077-1080.
- (137) C. O. Baker, B. Shedd, R. J. Tseng, A. A. Martinez-Morales, C. S. Ozkan, M. Ozkan, Y. Yang and R. B. Kaner, *ACS Nano*, 2011, **5**, 3469-3474.
- (138) J. Han, L. Li and R. Guo, *Macromolecules*, 2010, **43**, 10636-10644.
- (139) H. G. Lemos, S. F. Santos and E. C. Venancio, *Synth. Met.*, 2015, **203**, 22-30.
- (140) P. Paulraj, N. Janaki, S. Sandhya and K. Pandian, *Colloids Surf., A*, 2011, **377**, 28-34.
- (141) H. Lin, J. Yang, J. Liu, Y. Huang, J. Xiao and X. Zhang, *Electrochim. Acta*, 2013, **90**, 382-392.
- (142) W. M. Lemke, R. B. Kaner and P. L. Diaconescu, *Inorg. Chem. Front.*, 2015, **2**, 35-41.
- (143) N. Ahmad and A. G. MacDiarmid, *Synth. Met.*, 1996, **78**, 103-110.
- (144) B. Yao, G. Wang, J. Ye and X. Li, *Mater. Lett.*, 2008, **62**, 1775-1778.
- (145) S. Ma, G. Song, N. Feng and P. Zhao, *J. Appl. Polym. Sci.*, 2012, **125**, 1601-1605.
- (146) C. Ge, X. Yang and B. Hou, *J. Coat. Technol. Res.*, 2012, **9**, 59-69.
- (147) P. R. Bidez III, S. Li, A. G. MacDiarmid, E. C. Venancio, Y. Wei, P. I. Lelkes, *J. Biomater. Sci., Polymer Ed.*, 2006, **17**, 199-212.
- (148) H. Kim, H. Hobbs, L. Wang, M. J. Rutten, C. C. Wamser, *Synth. Met.*, 2009, **159**, 1313-1318.
- (149) L. Wang, Y. Wu, B. Guo, P. X. Ma, *ACS Nano*, 2015, **9**, 9167-9179.
- (150) J. Zhang, K. Qiu, B. Sun, J. Fang, K. Zhang, H. El-Hamshary, S. S. Al-Deyab and X. Mo, *J. Mater. Chem. B*, 2014, **2**, 7945-7954.
- (151) G. R. Guillen, T. P. Farrell, R. B. Kaner and E. M. V. Hoek, *J. Mater. Chem.*, 2010, **20**, 4621-4628.
- (152) X. Huang, B. T. McVerry, C. Marambio-Jones, M. C. Y. Wong, E. M. V. Hoek and R. B. Kaner, *J. Mater. Chem. A*, 2015, **3**, 8725-8733.

(153) Z. Fan, Z. Wang, N. Sun, J. Wang and S. Wang, *J. Membr. Sci.*, 2008, **320**, 363-371.

(154) Y. Liao, X. Li, E. M. V. Hoek and R. B. Kaner, *J. Mater. Chem. A*, 2013, **1**, 15390-15396.